

**HOW ORGANISMS LACKING OXIDIZABLE LIPIDS UTILIZE LIPID  
PEROXIDATION FOR SIGNALING:  
LIPIDOMICS APPROACH**

by

Hsiu-Chi Ting

BS, National Taiwan University, Taiwan, 2008

MS, National Taiwan University, Taiwan, 2010

Submitted to the Graduate Faculty of  
the Graduate School of Public Health in partial fulfillment  
of the requirements for the degree of  
Doctor of Philosophy

University of Pittsburgh

2019

UNIVERSITY OF PITTSBURGH  
GRADUATE SCHOOL OF PUBLIC HEALTH

This dissertation was presented

by

**Hsiu-Chi Ting**

It was defended on

December 13, 2018

and approved by

Bruce R. Pitt, PhD, Professor  
Department of Environmental and Occupational Health  
Graduate School of Public Health, University of Pittsburgh

Hülya Bayır, MD, Professor  
Departments of Critical Care Medicine and Environmental and Occupational Health  
School of Medicine and Graduate School of Public Health, University of Pittsburgh

Joel S. Greenberger, MD, FACRO, FACR, Professor and Chairman  
Department of Radiation Oncology  
School of Medicine, University of Pittsburgh

**Dissertation Advisor:** Valerian E. Kagan, PhD, DSc, Professor and Vice Chairman  
Department of Environmental and Occupational Health  
Graduate School of Public Health, University of Pittsburgh

Copyright © by Hsiu-Chi Ting

2019

**HOW ORGANISMS LACKING OXIDIZABLE LIPIDS UTILIZE LIPID  
PEROXIDATION FOR SIGNALING:  
LIPIDOMICS APPROACH**

Hsiu-Chi Ting, PhD

University of Pittsburgh, 2019

**ABSTRACT**

Polyunsaturated lipids are lipids which contain two or more carbon-carbon double bonds in their constituent hydrocarbon chains. They also serve as excellent substrates for lipid peroxidation. However, the roles of lipid peroxidation and its associated enzymes in organisms lacking polyunsaturated fatty acids (PUFA) synthesis remain unclear. In this thesis, we studied 1) the function of the cardiolipin (CL) remodeling enzyme CL deacylase 1 (Cld1) in CL peroxidation in *Saccharomyces cerevisiae* (*S. cerevisiae*) and 2) the significance of pLoxA, a lipoxygenase (LOX) in *Pseudomonas aeruginosa* (*P. aeruginosa*), in triggering ferroptosis in host bronchial epithelial (HBE) cells.

In the first study, we detected oxidized CL (CLOx) and other oxidized PLs (PLOx) in both  $\Delta^{12}$ -desaturase-expressing WT and *cld1* $\Delta$  yeast. The higher molar ratio of CLOx than other PL and the absence of phosphatidylserine oxidation suggested the oxidation events occurred in the mitochondria. The loss of *cld1* elevated the levels of mono-hydroperoxy-CLs and decreased the chronological lifespan, mitochondrial membrane potential, and respiratory capacity of the yeast. We also found that CLOx is a preferred substrate for Cld1 *in vitro* compared to non-oxidized CLs. These data suggest CL remodeling is required to mitigate CL peroxidation. In the second study, we demonstrated pLoxA is required for *P. aeruginosa* to induce ferroptosis in HBE cells. We found that clinical *P. aeruginosa* isolate-induced ferroptosis correlated significantly with the

amount of pLoxA and its 15LOX activity. We found that pro-ferroptotic lipid signals 15-hydroperoxy-arachidonoyl phosphatidylethanolamines were elevated in both HBE cells treated with *P. aeruginosa* supernatants and in airway tissues from cystic fibrosis (CF) patients with *P. aeruginosa*. Computational studies showed that the catalytic site of LOX is highly conserved among species. The  $\alpha$ -helical-lid interaction of pLoxA facilitates AA-PE binding, resembling the function of the PE-binding protein (PEBP) in the PEBP-15LOX complex in mammalian cells. These data showed that *P. aeruginosa* hijacks host polyunsaturated PEs to induce ferroptosis in the bronchial epithelium.

For public health significance, the function of CL remodeling in mitigating CL peroxidation could contribute to the study of CL remodeling defects in Barth syndrome. The pLoxA-driven ferroptosis could be a potential therapeutic target against *P. aeruginosa*-associated diseases.

## TABLE OF CONTENTS

<b>ACKNOWLEDGEMENT</b> .....	<b>XVI</b>
<b>1.0 INTRODUCTION</b> .....	<b>1</b>
<b>1.1 OXYGEN AND REACTIVE OXYGEN SPECIES</b> .....	<b>1</b>
<b>1.2 UNESTERIFIED PUFA PEROXIDATION</b> .....	<b>2</b>
<b>1.3 PHOSPHOLIPID PEROXIDATION</b> .....	<b>5</b>
<b>1.4 OXIDIZED LIPID SIGNALING IN CELL DEATH</b> .....	<b>6</b>
<b>1.4.1 CLox and PSox in apoptosis</b> .....	<b>7</b>
<b>1.4.1.1 CL</b> .....	<b>7</b>
<b>1.4.1.2 CL metabolism and disease</b> .....	<b>7</b>
<b>1.4.1.3 CLox elicits apoptosis</b> .....	<b>9</b>
<b>1.4.1.4 PSox promotes apoptotic cell clearance</b> .....	<b>10</b>
<b>1.4.2 PEox in ferroptosis</b> .....	<b>10</b>
<b>1.5 SACCHAROMYCES CEREVISIAE</b> .....	<b>11</b>
<b>1.5.1 Lipidome</b> .....	<b>11</b>
<b>1.5.2 PUFA in yeast cell death</b> .....	<b>12</b>
<b>1.6 PSEUDOMONAS AERUGINOSA</b> .....	<b>12</b>
<b>1.6.1 Epidemiology</b> .....	<b>12</b>
<b>1.6.2 Cystic fibrosis</b> .....	<b>13</b>

1.6.3	Lipidome and lipid signaling in <i>P. aeruginosa</i> and other bacteria .....	14
1.7	HYPOTHESIS AND RATIONALE .....	15
1.8	SPECIFIC AIMS .....	18
2.0	RESULTS .....	19
2.1	GENETIC RE-ENGINEERING OF POLYUNSATURATED PHOSPHOLIPID PROFILE OF SACCHAROMYCES CEREVISIAE IDENTIFIES A NOVEL ROLE FOR CLD1 IN MITIGATING THE EFFECTS OF CARDIOLIPIN PEROXIDATION.....	19
2.1.1	ACKNOWLEDGEMENT.....	21
2.1.2	COPYRIGHT.....	22
2.1.3	NOTE.....	23
2.1.4	ABSTRACT .....	24
2.1.5	INTRODUCTION .....	26
2.1.6	MATERIALS AND METHODS.....	29
2.1.6.1	Strains, Media, and Growth Conditions .....	29
2.1.6.2	Construction of Plasmids and Expression of Yeast His <sub>6</sub> -tagged Cld1 in <i>S. cerevisiae</i> .....	30
2.1.6.3	Purification of His <sub>6</sub> -tagged Cld1 .....	30
2.1.6.4	Synthesis of CLs .....	31
2.1.6.5	Chronological Lifespan.....	31
2.1.6.6	Spotting Assay .....	32
2.1.6.7	Real-Time Quantitative PCR (RT-qPCR) Analysis .....	32
2.1.6.8	Synthesis of Mito-AAPH .....	32

2.1.6.9	Mito-AAPH Treatment.....	33
2.1.6.10	Determination of mitochondrial membrane potential (MMP).....	33
2.1.6.11	Respiration measurements.....	34
2.1.6.12	Statistical Analysis .....	34
2.1.6.13	LC/MS assessment of phospholipids .....	34
2.1.7	RESULTS.....	36
2.1.7.1	Expression of the <i>H. brasiliensis</i> $\Delta^{12}$ -desaturase alters the molecular speciation of CL in <i>S. cerevisiae</i> cells .....	36
2.1.7.2	$\Delta^{12}$ -desaturase expression leads to accumulation of CL <sub>ox</sub> .....	41
2.1.7.3	Detection of other oxidized phospholipids in $\Delta^{12}$ -desaturase-expressing-WT cells.....	45
2.1.7.4	$\Delta^{12}$ -desaturase expression results in an increased sensitivity to mitochondria-targeted lipid peroxidation .....	52
2.1.7.5	<i>cld1</i> $\Delta$ cells that express $\Delta^{12}$ -desaturase exhibit decreased levels of PUFA-CLs including TLCL but increased levels of specific peroxidized CL species.....	55
2.1.7.6	Cld1 mitigates the effects of CL peroxidation .....	60
2.1.8	DISCUSSION.....	63
2.2	<i>PSEUDOMONAS AERUGINOSA</i> UTILIZES HOST POLYUNSATURATED PHOSPHATIDYLETHANOLAMINES TO TRIGGER THEFT-FERROPTOSIS IN BRONCHIAL EPITHELIUM.....	69
2.2.1	ACKNOWLEDGEMENT .....	71
2.2.2	COPYRIGHT.....	72

<b>2.2.3</b>	<b>NOTE.....</b>	<b>73</b>
<b>2.2.4</b>	<b>ABSTRACT .....</b>	<b>74</b>
<b>2.2.5</b>	<b>INTRODUCTION .....</b>	<b>75</b>
<b>2.2.6</b>	<b>MATERIALS AND METHODS.....</b>	<b>77</b>
<b>2.2.6.1</b>	<b>Reagents. ....</b>	<b>77</b>
<b>2.2.6.2</b>	<b>Cell Culture. ....</b>	<b>77</b>
<b>2.2.6.3</b>	<b>Bacterial strains.....</b>	<b>78</b>
<b>2.2.6.4</b>	<b><i>P. aeruginosa</i> ICU respiratory isolates.....</b>	<b>78</b>
<b>2.2.6.5</b>	<b><i>loxA::Tn</i> Complementation.....</b>	<b>78</b>
<b>2.2.6.6</b>	<b>Abiotic biofilm and supernatant collection.....</b>	<b>81</b>
<b>2.2.6.7</b>	<b>Biotic biofilm assay. ....</b>	<b>84</b>
<b>2.2.6.8</b>	<b>Knock-down (KD) of <i>ACSL4</i> and <i>LPCAT3</i>.....</b>	<b>84</b>
<b>2.2.6.9</b>	<b>Live-cell imaging. ....</b>	<b>84</b>
<b>2.2.6.10</b>	<b>Western blotting.....</b>	<b>85</b>
<b>2.2.6.11</b>	<b>Arachidonic acid supplementation.....</b>	<b>86</b>
<b>2.2.6.12</b>	<b>Cell death assay. ....</b>	<b>87</b>
<b>2.2.6.13</b>	<b>Cell death induced by genetically manipulated pLoxA.....</b>	<b>87</b>
<b>2.2.6.14</b>	<b>Ferroptosis induced by exogenous 15-HOO-AA-PE.....</b>	<b>88</b>
<b>2.2.6.15</b>	<b>GSH measurements.....</b>	<b>88</b>
<b>2.2.6.16</b>	<b>Assessment of pyocyanin. ....</b>	<b>89</b>
<b>2.2.6.17</b>	<b>AA and AA-PE docking to pLoxA.....</b>	<b>89</b>
<b>2.2.6.18</b>	<b>Sequence alignment, generation of sequence similarity map and phylogenetic tree construction.....</b>	<b>89</b>

2.2.6.19	Gaussian Network Model (GNM) and Anisotropic Network Model (ANM) analyses for protein dynamics. ....	90
2.2.6.20	Expression and purification of pLoxA. ....	90
2.2.6.21	pLoxA antibody purification. ....	90
2.2.6.22	Liposome preparation. ....	91
2.2.6.23	Oxidation of AA and AA-PE by <i>P. aeruginosa</i> supernatant or pLoxA in a model system. ....	91
2.2.6.24	Determination of pLoxA activity in <i>P. aeruginosa</i> clinical isolates. ....	92
2.2.6.25	Redox phospholipidomics. ....	92
2.2.6.26	Analysis of AA and its oxidation products. ....	93
2.2.6.27	Statistical analysis. ....	93
2.2.6.28	Study approval. ....	94
2.2.7	RESULTS. ....	94
2.2.7.1	Biofilm-producing prokaryote <i>P. aeruginosa</i> utilizes pLoxA to induce ferroptotic death in HBE cells. ....	94
2.2.7.2	pLoxA generated 15-HOO-AA-PE act as pro-ferroptotic signals in HBE cells. ....	102
2.2.7.3	Computational analysis identifies evolutionarily conserved specific features of pLoxA required for AA-PE oxidation. ....	114
2.2.7.4	Redox phospholipidomics reveals elevated levels of 15-HOO-AA-PE in airway tissues of <i>P. aeruginosa</i> infected patients with cystic fibrosis. ....	122

2.2.7.5	High prevalence of pLoxA in ferroptosis-inducing clinical isolates of <i>P. aeruginosa</i> from persistent lower respiratory tract infection patients..	128
2.2.8	Discussion .....	129
3.0	SUMMARY AND FUTURE DIRECTIONS.....	133
	BIBLIOGRAPHY.....	137

## LIST OF TABLES

Table 1. The absolute amounts of oxidized phospholipids and their relative content (mol%) normalized to either the amounts of total phospholipids or the amounts of individual phospholipid class in desaturase ( <i>desa</i> )-expressing WT cells. ....	51
Table 2. Bacterial strains, plasmids, and primers used for <i>loxA</i> complementation study. ....	80
Table 3. PE-OX species identified in Human Bronchial Epithelial (HBE) cells treated with <i>P. aeruginosa</i> hyper-biofilm mutant ( $\Delta$ <i>wspF</i> ) supernatant. ....	108
Table 4. Identification of PE-OX species in CF lung samples infected with <i>P. aeruginosa</i> . ....	126
Table 5. Identification of Pathogenic bacteria present in CF lung samples. ....	127

## LIST OF FIGURES

Figure 1. CL biosynthesis and remodeling in <i>S. cerevisiae</i> .....	37
Figure 2. CL species synthesized in empty vector (EV)- and $\Delta^{12}$ -desaturase (desa)-expressing WT cells.....	40
Figure 3. Peroxidized CL (CL <sub>OX</sub> ) in desa-expressing WT cells. ....	42
Figure 4. Quantitative assessment of individual (A) PG and (B) PC molecular species in WT and <i>cld1</i> $\Delta$ yeast cells expressing desa. ....	43
Figure 5. Phosphatidylglycerol (PG) in EV- and desa-expressing WT cells.....	44
Figure 6. Heat maps of (A) PG and PG <sub>OX</sub> , (B) PC and PC <sub>OX</sub> , (C) PE and PE <sub>OX</sub> , (D) PS in WT cells expressing empty vector (EV) or desaturase (desa). ....	47
Figure 7. PC and PC <sub>OX</sub> species produced in EV- and desa-expressing WT cells.....	48
Figure 8. PE and PE <sub>OX</sub> species produced in EV- and desa-expressing WT cells.....	49
Figure 9. PS species synthesized in EV- and desa-expressing WT cells.....	50
Figure 10. Effect of mito-AAPH on EV- and desa-expressing WT cells. ....	54
Figure 11. CL profile analysis of desa-expressing WT and <i>cld1</i> $\Delta$ yeast cells.....	57
Figure 12. Heat maps of CL molecular species in <i>cld1</i> $\Delta$ cells expressing empty vector ( <i>cld1</i> $\Delta$ +EV) or desaturase ( <i>cld1</i> $\Delta$ +desa). ....	58
Figure 13. CL and CL <sub>OX</sub> in desa-expressing WT and <i>cld1</i> $\Delta$ yeast cells.....	59

Figure 14. Cld1 exhibits greater affinity for oxidized than non-oxidized CL in vitro and its expression is increased by supplementation of H <sub>2</sub> O <sub>2</sub> . .....	61
Figure 15. Analysis of chronological lifespan and mitochondrial functions of desa-expressing yeast cells. ....	62
Figure 16. Cell death induced by $\Delta$ wspF supernatant is not affected by presence of bacteria in the supernatant. ....	83
Figure 17. pLoxA is required for <i>P. aeruginosa</i> supernatant induced ferroptosis. ....	97
Figure 18. <i>P. aeruginosa</i> supernatant induced cell death is rescued by ferrostatin-1. ....	99
Figure 19. pLoxA is required for <i>P. aeruginosa</i> supernatant induced ferroptosis. ....	100
Figure 20. <i>P. aeruginosa</i> supernatants generate pro-ferroptotic hydroperoxy-lipid signals in HBE cells. ....	105
Figure 21. Cell death induced by $\Delta$ wspF supernatants. ....	107
Figure 22. Identification of di-oxygenated PE species in HBE cells exposed to supernatants obtained from $\Delta$ wspF mutants. ....	109
Figure 23. Identification of tri-oxygenated PE species in HBE cells exposed to supernatants obtained from $\Delta$ wspF mutants. ....	110
Figure 24. <i>P. aeruginosa</i> induced ferroptosis is affected by manipulations of phospholipids in HBE cells. ....	111
Figure 25. <i>P. aeruginosa</i> induced ferroptosis is affected by manipulations of (phospho)lipids in HBE cells. ....	113
Figure 26. Evolutionary analysis of LOX sequences. ....	117
Figure 27. Evolutionary analysis and computational modeling of pLoxA sequence and structure. ....	119

Figure 28. Evolutionary analysis of lipoxygenases (comparable to pLoxA) among bacteria. ...	120
Figure 29. Computational modeling of pLoxA structure and molecular dynamics. ....	121
Figure 30. <i>P. aeruginosa</i> clinical isolates from patients with persistent lower respiratory infection induce ferroptosis.....	123
Figure 31. Redox phospholipidomics reveals pro-ferroptotic oxygenated PE species in airway tissue samples from patients with cystic fibrosis (CF). ....	124

## **ACKNOWLEDGEMENT**

I would like to thank my graduate advisor Dr. Kagan for his great support and insightful guidance to my studies and projects in PhD training and my road on becoming an independent researcher. I would also like to thank my committee members, Dr. Hulya Bayır, Dr. Bruce Pitt and Dr. Joel Greenberger for their critical suggestions on my projects. I would also like to thank all the co-authors for their efforts and contributions.

None of the work contained in this thesis was done alone. I would like to thank Dr. Yulia Tyurina and Dr. Haider Dar for their experimental suggestions and academic discussion on these projects. I would also like to thank all lab members and classmates for their direct or indirect help.

Most importantly, I would like to thank my parents and family members for their endless love and support.

## 1.0 INTRODUCTION

### 1.1 OXYGEN AND REACTIVE OXYGEN SPECIES

Oxygen shapes the evolution of life by way of a double-edged sword. On the one hand, it sparked the evolution of aerobic respiration, allowing eukaryotes to generate ATP more efficiently than their ancestors that relied entirely on anaerobic respiration [1]. On the other hand, reactive oxygen species (ROS) are generated as a consequence when oxygen is reduced by the electrons leaking from the mitochondrial electron transport chain.

ROS, by definition, is a collective term for species derived from oxygen that are more reactive than oxygen itself [2]. It includes free radicals such as superoxide and hydroxyl radicals and non-radicals such as hydrogen peroxide and organic hydroperoxides [3]. ROS are generated endogenously by stepwise reduction of oxygen, which takes place in mitochondria, peroxisomes, the cell membrane, and the endoplasmic reticulum [4]. Superoxide anion is the first produced ROS from a one-step electron reduction of oxygen. Next, superoxide dismutase disproportionates superoxide anion to form hydrogen peroxide. Finally, hydrogen peroxide is either entirely reduced to water by a catalase and glutathione peroxidases or transformed into a strong oxidant, the hydroxyl radical, in the presence of transition metals [5]. ROS can be utilized in redox signaling if the basal level is maintained but toxic if not properly handled. Highly-reactive ROS attacks DNA [6], proteins [7] and lipids [8], which damages cellular structures and

functions. If the damage is unable to be repaired or is irreversible, it eventually leads to cell death.

## 1.2 UNESTERIFIED PUFA PEROXIDATION

Polyunsaturated fatty acids (PUFAs) are fatty acids that contain more than one double bond. In mammals, *de novo* biosynthesis of n-9 PUFAs starts from palmitic acid (PA, 16:0). The PA is converted into oleic acid (OA, 18:1) and is transformed into n-9 PUFAs via the activities of a series of elongases and desaturases. However, mammals are not able to synthesize n-3 and n-6 PUFAs due to the lack of  $\Delta^{12}$ - and  $\Delta^{15}$ -desaturases, which are present in plants. Therefore, mammals obtain linoleic acid (LA, 18:2) and  $\alpha$ -linolenic acid (ALA, 18:3) from plants for n-3 and n-6 fatty acid biosynthesis [9]. PUFAs are further incorporated into glycerophospholipids to form polyunsaturated PLs, which regulate membrane fluidity [10] and lipid signaling [11].

Despite the essential roles of PUFAs in cell physiology, PUFAs are the main substrates in lipid peroxidation because their bis-allylic hydrogens are easily extracted by oxidants. Lipid radicals formed in this step are stabilized by a conjugated dienes structure. The lipid peroxidation of PUFAs can be non-enzymatic or enzymatic. Non-enzymatic lipid peroxidation is initiated by the presence of oxygen and is facilitated by ferrous iron. Enzymatic lipid peroxidation can be catalyzed by lipoxygenases (LOXs)- a family of lipid peroxidation enzymes, which oxidize unesterified and esterified PUFAs [12].

Non-enzymatic unesterified PUFA peroxidation starts from the abstraction of the bis-allylic hydrogens of PUFAs by oxidants, including hydroperoxyl radicals and hydroxyl radicals. Then lipid radicals propagate to react with oxygen to form lipid peroxy radicals, which abstract

hydrogen from other PUFAs to form new lipid radicals and lipid hydroperoxides. This free radical chain reaction propagates until two free radicals conjugate each other to terminate the reactions. Antioxidants can also terminate the reactions by donating a hydrogen atom to the lipid peroxy radicals [13]. The lipid peroxidation products can be decomposed to form the secondary products malondialdehyde (MDA) and 4-hydroxynonenal(4-HNE), which are strong electrophiles, and tend to react with protein, leading to oxidative damages and/or protein modification [14].

One of the enzyme groups that catalyzes lipid peroxidation is the LOX group. There are six functional LOXs in humans. Among them, 15LOXs are the enzymes which are capable of catalyzing both unesterified and esterified PUFA peroxidation. 15LOXs contain three members: human 15-lipoxygenase-1 (15LOX1) (mouse leukocyte-type 12LOX) encoded by ALOX15 (alox15 in mouse), human 15-lipoxygenase-2 (15LOX2) (mouse 8LOX) encoded by ALOX15B (alox15b in mouse), and epidermis-type lipoxygenase encoded by ALOXE3 (aloxe3 in mouse). The X-ray crystal structure of human 15LOX1 and 15LOX2 showed that they contain two domains: a  $\beta$ -barrel domain and a catalytic domain. The  $\beta$ -barrel domain is responsible for membrane binding, and the catalytic domain is responsible for the coordination of the catalytic iron by His residues and the C-terminus Ile residue. The positional specificity of the oxygenation reaction is determined by its fatty acid substrate and the volume of the binding pocket [15, 16].

Mechanistically, the activation of ferrous LOXs to ferric LOXs initiates the LOX-catalyzed oxygenation of fatty acids. First, the bis-allylic hydrogen atom of a PUFA is abstracted as a proton, forming a lipid radical, and the resulting electron is tunneled to the ferric iron that is reduced to the ferrous iron. Next, the lipid radical is rearranged and stabilized by a conjugated double bond. Subsequently, the lipid radical reacts with molecular oxygen to form a lipid peroxy radical. Then, the lipid peroxy radical is reduced by an electron from the ferrous iron to form a lipid peroxy

anion. In this step, the ferrous iron is re-oxidized to the ferric iron. Finally, the lipid peroxy anion is protonated, creating a lipid hydroperoxide [17].

The main PUFA substrate of 15LOX1 and 15LOX2 is arachidonic acid (AA) but also LA. Human 15LOX1 produces products of 15-HpETE/12-HpETE in a 9:1 ratio, but the corresponding ratio in mice is 1:4. Human 15LOX2 produces almost completely 15-HpETE whereas mouse 8LOX produces 8-HpETE. Epidermis-type LOX in humans and mice uses 12-HpETE to generate hepoxilins [18].

LOXs are also found in plants, fungi, and bacteria [19, 20]. *P. aeruginosa* expresses secreted LOX isoform (pLoxA), which shares 25% and 31% of sequence identity to 15LOX1 and 15LOX2, respectively. It is structurally different from the mammalian LOXs. A pLoxA polypeptide folds into a single domain, which lacks the  $\beta$ -barrel domain that exists in the mammalian LOXs. But pLoxA contains a helical lid that regulates the substrate accessibility. The substrate binding pocket in pLoxA contains two sub-cavities and a lobby: one sub-cavity where catalytic iron is located, which accommodates the sn-1 fatty acid, and another sub-cavity that does not have direct access to the catalytic iron, which accommodates the sn-2 fatty acid, and the polar head of PLs arrested in the lobby [21]. Non-heme iron is coordinated by His, Asn, and Ile residues [21]. The substrate specificity of pLoxA has been reported in different studies. In Deschamp's study the preferred unesterified PUFA substrate is AA, and its main products are 15-(S)-H(p)ETE and a minute amount of 9-, and 11-H(p)ETE. The reaction with LA generates predominantly 13-H(p)ODE and a relatively lesser amount of 9-H(p)ODE [22]. In Banthiya's study, the preferred unesterified PUFA substrate is 8,11,14-eicosatrienoic acid (20:3), and the position of oxygenation is at carbon 15. The reaction with LA generates oxygenated products at carbon 13 [21].

### 1.3 PHOSPHOLIPID PEROXIDATION

The mechanistic studies of unesterified lipid peroxidation and its secondary metabolites has been intensely studied since the 1940s, but the knowledge of phospholipid peroxidation was still limited until the late 1980s due to the limitation of available methodology. The application of fast atom bombardment (FAB) and, subsequently, electrospray ionization (ESI) in mass spectrometry enabled the analysis of less volatile biomolecules and reduced thermal degradation, thus expanding the knowledge of phospholipid peroxidation by structural identification.

One of the ways to form PLox is by re-esterifying oxidized PUFAs (PUFAox) into PLs [23-26]. However, similar to the PUFA peroxidation, polyunsaturated PLs themselves can be the targets for lipid peroxidation. Notably, there are three enzymes that are capable of directly catalyzing polyunsaturated PL peroxidation: 15LOX1, 15LOX2, and cytochrome C (cyto C).

The activity of 15LOX1 that generates hydroperoxy PC has been first described in rabbit reticulocytes [27], where the products 12- and 15-HpETE-esterified PC were detected [28]. Later, the activity of 15LOX1 toward PC was found in cell-free human polymorphonuclear leukocytes [29]. Direct oxidation by 15LOX1 forms oxidized phosphatidylethanolamine (PEox) containing 15-H(p)ETE in monocytes activated by interleukin-4 and ionophore [30]. In addition, human 15LOX2 is another LOX family member which is capable of directly oxidizing various AA-PLs to form 15-H(p)ETE-PLs [31, 32]. Recently, we discovered that PE binding protein-1 (PEBP1), which allosterically facilitates the accommodation of AA-PE at the catalytic site of 15LOXs [33]. It is also reported that pLoxA exhibits PL oxygenase activity, and PE is the preferred substrate. The reaction with 1-palmitoyl-2-linoleoyl-PE preponderantly generates 13-(S)-H(p)ODE [21, 34]. Recently, one study found that pLoxA preferentially utilizes PE for lipid

peroxidation, and its main products were determined to be 15-H(p)ETE- and 15-H(p)ODE-containing PE in the biological membranes of erythrocytes and cultured lung epithelial cells [35].

Hydroperoxy-PLs can further transform into other types of oxidized PLs without enzymatic participation. First, additional oxidation generates PLox with various functional groups, such as hydroperoxides, hydroxides, keto- and epoxy-groups in a variety of combinations. Second, via intramolecular cyclization, rearrangement, and oxidation, isoprostanes, isolevuglandins, isothroboxanes, and isofurans can be formed. Third, oxidative fragmentation generates PLox containing a combination of hydroxyl, carbonyl, carboxyl, and furan groups [36, 37].

#### **1.4 OXIDIZED LIPID SIGNALING IN CELL DEATH**

Both PUFAox and PLox act as signaling molecules: PUFAox are essential lipid mediators, which bind to specific GPCRs and mediate inflammatory responses [38]. The secondary products of lipid peroxidation malondialdehyde (MDA) and 4-hydroxy-2-nonenal (4-HNE) are electrophiles that form adducts with proteins [14]. Oxidized phosphatidylcholines (PCox) modulate inflammation, intracellular signaling, blood coagulation, platelets activation, vascular smooth muscle phenotype, angiogenic activities, and cell adhesion [36, 39]. Additionally, oxidized lipids are essential signals in cell death. Three PLox have been reported actively participated in the cell death process: (1) oxidized CL (CLOx) and oxidized phosphatidylserine (PSox) in apoptosis, and (2) oxidized PE (PEox) in ferroptosis.

## **1.4.1 CLox and PSox in apoptosis**

### **1.4.1.1 CL**

CL is a dimeric anionic PL which contains one glycerol backbone, two phosphate groups and four fatty acyl chains, which can be conceptualized as two phosphatidic acids connected by a glycerol molecule. It is almost exclusively found in the mitochondrial inner membrane. This results its asymmetrical abundance in mitochondria. CL is less abundant compared to other PL classes in mitochondria (around 2-3 mol %) but highly abundant in the mitochondrial inner membrane (up to 20 mol %). The abundance of CL among tissue varies. It is the most abundant in the heart (10% in bovine heart tissue) and the skeletal muscle but present ubiquitously in all mammalian tissues [40]. The diversity of CL is tissue-dependent: in the mammalian heart, muscles, and liver the most abundant CL species is symmetric tetralinoleoyl CL [41]. However, in the mammalian brain CLs are highly asymmetric, containing abundant PUFAs [42-44]. CL is also found in prokaryotes but the fatty acyls are markedly different. CLs in prokaryotes contain shorter, saturated, monounsaturated, and odd-number fatty acids but in eukaryotes they contain longer-chain polyunsaturated residues [45]. It has been demonstrated that CL participates in various cellular functions including bioenergetics [46], mitochondrial dynamics [47], cell cycle progression [48], cellular aging [49], mitophagy [50, 51], lipid mediator generation [44], and apoptosis [52, 53].

### **1.4.1.2 CL metabolism and disease**

Two routes of CL metabolism have been identified in mitochondria: biosynthesis and remodeling. In the biosynthesis route, phosphatidic acid (PA) is catalyzed by the CDP-diacylglycerol (CDP-DAG) synthase activity of TAM41, forming CDP-DAG [54, 55]. The next

few enzymatic steps generate two intermediates phosphatidylglycerophosphates and phosphatidylglycerol (PG), and in a final step CL is formed by CL synthase (Crd) [56]. The CL formed in the biosynthesis route is termed “immature CL” as it contains mostly saturated fatty acyl chains. The immature CL undergoes remodeling to form “mature CL”, which is more unsaturated [56]. Remodeling of CL in yeast is catalyzed by two key enzymes: CL-specific deacylase 1 (Cld1) and tafazzin (Taz1). To be specific, Cld1 deacylates CL with a preference for palmitic acid (16:0) and stearic acid (18:0) [57] to form monolyso-CL (MLCL), and Taz1 functions as a transacylase to reacylate unsaturated fatty acids to MLCL forming mature CL [58]. Notably, it is suggested that tafazzin alone is competent for CL remodeling, and other enzymes are found to contribute to the CL remodeling such as Acyl-CoA:lysocardiolipin acyltransferase-1 (ALCAT1) and MLCL acyltransferase-1 (MLCAT1) [59].

Cld1 was first identified in 2009 and its phospholipase activity is very specific to CL [60]. This enzyme has no homolog in higher eukaryotes but its function, to remove acyl chains from CL, is similar to mammalian calcium-independent phospholipase A<sub>2</sub>γ [61]. Cld1 is associated with the inner leaflet of the mitochondrial inner membrane and responsible for the entry step of CL remodeling [62]. The mutant yeast lacking *cld1* was found to be normal with respect to growth, oxidative phosphorylation, and mitochondrial morphology [63].

The mutation of the gene that encodes tafazzin causes Barth syndrome (BTHS), an X-linked recessive disorder that is associated with cardiomyopathy, skeletal myopathy, neutropenia, and organic aciduria [64, 65]. The frequency of BTHS is estimated to be 1 in 300,000 to 400,000 [66]. As a loss in the final step of the CL remodeling pathway, BTHS patients accumulate MLCL and are devoid of tetralinoleoyl CL [67, 68]. The ratio of MLCL to CL is suggested to be a diagnostic marker for BTHS [69]. Notably, the deletion of *cld1* in yeast

could rescue the defection of the growth, lifespan, and respiration in the *taz1* mutant, suggesting that the deleterious effect caused by the loss of *taz1* is due to the increase in the ratio of MLCL to CL and not the decrease in CL unsaturation [70].

#### **1.4.1.3 CLox elicits apoptosis**

CL oxidation is a critical event in early apoptosis, and cyt C is responsible for this reaction. Cyt C has been known to be an electron carrier between mitochondrial Complex III and IV. It also acts as a superoxide scavenger. In apoptotic events, cyt C is an essential initiator of caspase cascades by binding to apoptosis protease-activating factor, Apaf-1, and facilitates the the formation of apoptosomes. Previous studies have shown that the peroxidase activity of cyt C is required for early apoptotic events [53]. Cyt C is capable of directly oxidizing anionic phospholipids, including CL and PS [71, 72]. At the onset of apoptosis, the externalization of CLs to the outer leaflet of the inner mitochondrial membrane allows the interactions with the intramembranous cyt C. Cyt C changes its conformation and switches its mode of electron transfer to peroxidase activity by interacting with CLs. In the presence of H<sub>2</sub>O<sub>2</sub>, cyt C acquires the ability to oxidize CLs with the formation of hydroperoxy- and hydroxy-CLs [72]. Linoleoyl CLs are preferentially oxidized by cyt c *in vitro* and *in vivo* [73-76]. Next, the decreased affinity of cyt C to CLox results in the release of cyt C into the cytoplasm through the pores in the mitochondrial outer membrane. It has been suggested that the interaction of CLox and Bcl-2 proteins increases the mitochondrial outer membrane permeabilization and facilitates the release of pro-apoptotic factors [71].

#### **1.4.1.4 PSox promotes apoptotic cell clearance**

In normal cells, PS mainly resides in the inner leaflet of plasma membrane [77]. In apoptotic cells PS is externalized to the cell surface and serves as an efferocytotic signal for the clearance of apoptotic cells by macrophages [78, 79]. In fact, PS oxidation is not required for phagocytosis. However, clearance of apoptotic cells by phagocytosis becomes more effective when PSox is externalized on the cell surface [80]. During apoptosis, cyt C is responsible for the oxidation of not only CL but for PS as well [81]. The release of cyt C from mitochondria is critical for the PS oxidation and its subsequent appearance on the cell surface during apoptosis [82].

#### **1.4.2 PEox in ferroptosis**

Ferroptosis is a newly-documented cell death program initially described as being iron-dependent and lipid ROS-driven. It is morphologically, biochemically, and genetically distinct from other forms of cell death [83]. The ferroptotic inducer erastin inhibits system Xc<sup>-</sup> and abrogates cystine import and inhibits glutathione biosynthesis [83, 84]. Another ferroptotic inducer RSL3 is a direct inhibitor of glutathione peroxidase 4 (GPX4), the only enzyme that has been known so far to reduce hydroperoxy-PLs utilizing glutathione as a cofactor [84]. Selenium is required for GPX4 because it is used for the regeneration of a functional GPX4 after reactions with lipid hydroperoxides [85]. Vitamin E homologues (tocopherols and tocotrienols) prevent ferroptosis by binding to the catalytic sites of 15LOX [86]. Another study showed that, once bound, the endogenous metabolite of vitamin E,  $\alpha$ -tocopherol hydroquinone, reduces the non-heme active ferric iron to ferrous ion [87]. ACSL4 and LPCAT3 are positive regulators of ferroptosis. The former catalyzes the formation of polyunsaturated fatty acyl-CoA (with the preference for AA), and the latter catalyzes the formation of PE/PC from lyso-PE/PC (with the

preference of polyunsaturated fatty acyl-CoA) [88, 89]. In our previous study, hydroperoxy arachidonoyl and adrenoyl PE were identified as unique ferroptotic signals by quantitative redox lipidomics, reverse genetics and bioinformatics and systems biology [90]. Recently, PE-binding protein 1 (PEBP1) has been shown to change the substrate specificity of 15LOX from fatty acids to PLs [91]. Ferroptosis inhibitors, ferrostatin-1s and liproxstatin protect the liver, brain, kidney, and heart from ischemic injury in mouse models [92]. The protective role of these inhibitors is also shown in Parkinson's disease [93], Alzheimer's disease [94], traumatic [95] and hemorrhagic brain injury [96], ischemia-reperfusion kidney injury [97], acute renal failure [98], acetaminophen-induced primary hepatocyte cell death [99], and hemochromatosis [100]. Several other metabolic and signaling pathways have been shown to impact ferroptosis including PI3K [101], Nrf2 [102], p53[103-106], mevalonate pathways [107] and BRCA1-associated protein 1[108].

## 1.5 *SACCHAROMYCES CEREVISIAE*

### 1.5.1 Lipidome

The lipidome of the yeast *Saccharomyces cerevisiae* has been reported in several studies [109, 110]. The most prominent characteristics of the *S. cerevisiae* lipidome is the lack of PUFA due to the presence of only one  $\Delta^9$ -desaturase encoded by *ole1* [111]. Therefore, the yeast generates minimal lipid peroxidation [112]. However, in other strains of yeast such as *Saccharomyces bayanus*, *Kluyveromyces thermotolerans*, *Pichia angusta*, and *Yarrowia lipolytica*, PUFA-containing glycerophospholipids are detected [113], which makes lipid peroxidation possible.

### 1.5.2 PUFA in yeast cell death

The uptake of PUFA from the environment enriches the yeast lipidome with PUFA. PUFA can be toxic to the yeast under certain circumstances. One study showed that PUFA, including OA, LA and linolenic acid, are not toxic to wild-type yeast but rather induce mitochondrial necrosis in yeast with triacylglycerol biosynthesis defects [114]. Another study showed that LA induced cell density-dependent apoptosis and also increased the MDA [115]. The effect of PUFA supplementation on the yeast survival is also exposure-dependent. PUFA enrichment protects the yeast from lipophilic organometal toxicity [116] and increases the yeast's ability to tolerate alkaline pH [117], but sensitizes the yeast to copper and cadmium toxicity [118, 119].

The expression of exogenous desaturases enriches yeast with PUFA species [120-124]. Heterogeneous expression of plant  $\Delta^{12}$ -desaturase in yeast used in this thesis had no adverse effects on the yeast but it sensitized the yeast to oxidative stress, which results in cell death [125]. However, another study which expressed an exogenous fungi desaturase in yeast with a different genetic background results in a PUFA-producing strain with low viability [126].

## 1.6 *PSEUDOMONAS AERUGINOSA*

### 1.6.1 Epidemiology

The Gram-negative bacterium *P. aeruginosa* is an opportunistic pathogen that is normally found in the environment, e.g. soil, water, and other moist locations. French pharmacist Carle Gessard first isolated it in 1882 from bluish-green pus [127]. The colonization of *P. aeruginosa* in healthy

adults is not common, and its prevalence of colonization is about 0-2% for the skin, 0-3% for the nasal mucosa, 0-6.6% for the throat, and 2.6-24% for the fecal samples [128]. To date, *P. aeruginosa* is one of the important pathogens that causes community- and nosocomial-acquired infections [129]. *P. aeruginosa* is the sixth most common opportunistic hospital pathogen reported by the National Health Care Safety Network (approximately 7.3%) [130]. It is the second most common pathogen isolated from patients with hospital-acquired pneumonia, healthcare-associated pneumonia, and ventilator-associated pneumonia (VAP, approximately 16.5%) [131]. *P. aeruginosa* causes the highest mortality in VAP, up to 30% [132]. It is also the most common multidrug-resistant Gram-negative pathogen leading to VAP [133].

### **1.6.2 Cystic fibrosis**

Cystic fibrosis (CF) is an autosomal recessive genetic disorder caused by the mutation of the gene encoding the CF transmembrane conductance regulator (CFTR) protein. The dysfunction of this protein interferes with the ion balance in airways and leads to an accumulation of mucus that hampers the mucociliary clearance [134]. Other factors that shape the pathological courses of CF include the abnormal structure of microbiota changes, the acidic environment, and airway inflammation in CF patients [135]. *P. aeruginosa* is the most common pathogen found in adult CF to date (over 70%) and the most important contributor to CF morbidity and mortality [136, 137].

### 1.6.3 Lipidome and lipid signaling in *P. aeruginosa* and other bacteria

Gram-negative bacteria contain two membranes, the inner membrane and the outer membrane, with a solvent-filled periplasm between the two membranes. The outer membrane contains mostly glycolipids and lipopolysaccharides while the inner membrane contains glycerophospholipids. Like other Gram-negative bacteria, the major glycerophospholipid classes in *P. aeruginosa* are PE, PG, and CL [138, 139]. Most prokaryotes do not synthesize PUFA except for some marine bacteria such as *Shewanella* species [140, 141].

PUFA can be imported from the environment and incorporated into glycerophospholipids. The effect of unsaturated fatty acids on bacteria can be beneficial or detrimental. It has been reported that PUFA supplementation to *P. aeruginosa* and the pathogenic *Vibrio* species affects the bacterial growth, membrane permeability, biofilm formation, and the resistance of antimicrobial peptides [142, 143]. Unsaturated fatty acid supplementation promotes motility in *Proteus mirabilis* and virulent gene expression in *Staphylococcus aureus*, *Listeria monocytogenes*, and *P. aeruginosa* [144-147]. However, some other reports have shown that PUFAs inhibit bacterial growth in *P. aeruginosa*, *Helicobacter pylori*, and *Neisseria gonorrhoeae* [148-150].

Lipid is an essential factor contributing to bacterial growth, infection, and antimicrobial resistance. For example, phosphatidylcholine (PC) is usually absent in most prokaryotes but is present in the Gram-negative bacteria *Brucella abortus*. PC is an essential nutrient for this particular bacterium grown in minimal medium and essential to its virulence [151]. CL synthesis and outer membrane localization are essential to the virulence of *Shigella flexneri* [152] and *Salmonella Typhimurium* [153]. PS and phosphatidylinositol, which are present in mucus or on

the cell surface, facilitate *P. aeruginosa* binding and contribute to its initial colonization [154]. PL aminoacylation is used by bacteria to induce antimicrobial resistance [155, 156].

Some studies have shown *P. aeruginosa* can trigger lipid peroxidation. For instance, nosocomial *P. aeruginosa* isolates can directly induce the production of MDA in PUFA-infused red blood cells [157]. Another study reported MDA increases in the *P. aeruginosa*-infected septic rat and the serum of *P. aeruginosa*-infected patients [158]. An earlier finding also reported that *P. aeruginosa* metabolizes arachidonic acid, however, the products and the enzyme responsible were not identified [159]. Fewer studies have been conducted on the role of lipid peroxidation in *P. aeruginosa*. The lipoxin synthase activity of pLoxA suggests that *P. aeruginosa* can downregulate host inflammatory responses via lipid peroxidation [21]. Another recent study showed that *P. aeruginosa* secretes epoxide hydrolase cystic fibrosis transmembrane conductance regulator inhibitory factor (Cif) to promote airway inflammation by interfering proresolving functions of lipoxins [160]. Notably, a recent study has showed that the organic hydroperoxide resistance enzymes, which are Cys-based, lipoyl-dependent peroxidases, are involved in the *P. aeruginosa* response to fatty acid hydroperoxides, implying a potential mechanism to combat lipid peroxidation [161].

## 1.7 HYPOTHESIS AND RATIONALE

PUFAs are the essential substrates for lipid peroxidation, whereby the oxidized lipid products are utilized as signaling molecules in mammalian cells. However, PUFAs are not synthesized endogenously in many organisms, including most of the prokaryotes and the eukaryotic yeast *S. cerevisiae*. Instead, these organisms obtain PUFAs from the environment, and interestingly, they

express enzymes that regulate oxidized lipids. These observations suggest that lipid peroxidation possesses significant functions in these organisms. However, the exact functions of the oxidized lipids and how the associated enzymes regulate them in these organisms are still not fully understood.

In yeast, CL that is synthesized *de novo* undergoes remodeling [56]. Previous studies in yeast have shown that un-remodeled and remodeled CLs are functionally indistinguishable [63], and the deletion of *cld1* can rescue the defects caused by the loss of the *taz1* [70]. Therefore, it raises the question of why cells remodel CL. Notably, the expression of *cld1* is upregulated in the stationary phase, which is in an active respiratory condition [70]. The expression of *cld1* is also regulated by the respiratory transcription factors Hap2 and Mig1 [70]. Based on these studies we hypothesized that one possible function of CL remodeling is to remove CLox products, which are formed during respiration and have been shown to be required for the early onset of apoptosis in mammalian cells. It has been known that *S. cerevisiae* expressing *H. brasiliensis*  $\Delta^{12}$ -desaturase synthesizes PUFAs and exhibits sensitivity to oxidants [125]. However, the effects of  $\Delta^{12}$ -desaturase expression on CL biosynthesis, remodeling, and peroxidation has not been explored quantitatively.

*P. aeruginosa*, a prokaryote which does not synthesize oxidizable PUFA-lipids, expresses pLoxA [20]. Previous reports have shown that PE is a preferred phospholipid substrate for pLoxA [21, 34]. Structurally, pLoxA possesses a spacious catalytic lobby for the accommodation of PE [21]. In addition, an endogenous non-PUFA-PE has also been co-crystallized with pLoxA [162]. Indeed, *P. aeruginosa* utilizes host-derived PUFAs as substrates to form PUFAox, which potentially modulate inflammation and host immune responses [21, 160]. However, the role of oxidized PE catalyzed by pLoxA in pathogen-host interactions

remains unclear. Recently, 15-hydroperoxy-AA-PE generated by 15LOXes in mammalian cells have been shown to be signals for ferroptotic cell death. Thus, based on these recent discoveries, we hypothesized that *P. aeruginosa* can oxidize AA-PE in host cells via pLoxA and induce ferroptosis by hijacking the mammalian PUFA-PE and death program.

## 1.8 SPECIFIC AIMS

The overall goal of this project is to investigate the roles of lipid peroxidation for signaling and its regulatory enzymes in organisms lacking PUFA synthesis.

The specific aims of the project are:

- 1) To characterize phospholipids and oxidized phospholipids in  $\Delta^{12}$ -desaturase-expressing *cld1* $\Delta$  and wild-type yeast by mass spectrometry.
- 2) To investigate the role of CL remodeling as a potential mechanism for the removal of CLox species.
- 3) To test the hypothesis that *P. aeruginosa* utilizes pLoxA to induce ferroptosis in host cells thereby generating pro-ferroptotic lipid signals.
- 4) To study the clinical significance of pLoxA in *P. aeruginosa*.

## 2.0 RESULTS

### 2.1 GENETIC RE-ENGINEERING OF POLYUNSATURATED PHOSPHOLIPID PROFILE OF SACCHAROMYCES CEREVISIAE IDENTIFIES A NOVEL ROLE FOR CLD1 IN MITIGATING THE EFFECTS OF CARDIOLIPIN PEROXIDATION

Published in:

*Biochimica et Biophysica Acta (BBA) - Molecular and Cell Biology of Lipids*

Volume 1863, Issue 10, October 2018, Pages 1354-1368

Wenjia Lou\*, Hsiu-Chi Ting\*, Christian A. Reynolds\*, Yulia Y. Tyurina, Vladimir A. Tyurin, Yiran Li, Jiajia Ji, Wenxi Yu, Zhuqing Liang, Detcho A. Stoyanovsky, Tamil S. Anthonymuthu, Michael A. Frasso, Peter Wipf, Joel S. Greenberger, Hülya Bayır, Valerian E. Kagan, and Miriam L. Greenberg

Department of Biological Sciences, Wayne State University, Detroit, Michigan, United States; Department of Environmental and Occupational Health, Center for Free Radical and Antioxidant Health, Radiation Oncology, Chemistry, Critical Care Medicine, Pharmacology and Chemical Biology, University of Pittsburgh, Pittsburgh, Pennsylvania, United States; Laboratory of

Navigational Redox Lipidomics, and Department of Human Pathology, IM Sechenov Moscow  
State Medical University, Moscow, Russian Federation

\* Corresponding authors

### **2.1.1 ACKNOWLEDGMENT**

The plasmids pYES2-EV and pYES2-desa used in this study were kindly given by Dr. Ana Cipak Gasparovic from the Rudjer Boskovic Institute in Zagreb, Croatia.

Funding: This work was supported by the National Institutes of Health [U19AI068021, HL117880, HL114453, NS076511, NS061817], the Barth Syndrome Foundation Barth Syndrome Foundation of Canada, Association Barth France as well as Human Frontier Science Program.

## 2.1.2 COPYRIGHT

This document is copyright free for educational and scientific development.

Permission was granted for the use of parts from:

Genetic re-engineering of polyunsaturated phospholipid profile of *Saccharomyces cerevisiae* identifies a novel role for Cld1 in mitigating the effects of cardiolipin peroxidation. Wenjia Lou, Hsiu-Chi Ting, Christian A. Reynolds, Yulia Y. Tyurina, Vladimir A. Tyurin, Yiran Li, Jiajia Ji, Wenxi Yu, Zhuqing Liang, Detcho A. Stoyanovsky, Tamil S. Anthonymuthu, Michael A. Frasso, Peter Wipf, Joel S. Greenberger, Hülya Bayir, Valerian E. Kagan, and Miriam L. Greenberg. *Biochimica et Biophysica Acta (BBA) - Molecular and Cell Biology of Lipids* Volume 1863, Issue 10, October 2018, Pages 1354-1368

Document with permission is on file with Hsiu-Chi Ting

### 2.1.3 NOTE

Corresponding authors: Miriam L. Greenberg, E-mail: [mgreenberg@wayne.edu](mailto:mgreenberg@wayne.edu), Phone: (313) 577-5202, Address: Department of Biological Sciences, 4105 Biological Sciences Building, 5047 Gullen Mall, Detroit, MI 48202. Valerian E. Kagan, E-mail: [kagan@pitt.edu](mailto:kagan@pitt.edu), Phone: (412) 624-9479, Address: 130 DeSoto Street, Parran Hall, Room 4120, Pittsburgh, PA 15213.

#### 2.1.4 ABSTRACT

Cardiolipin (CL) is a unique phospholipid localized almost exclusively within the mitochondrial membranes where it is synthesized. Newly synthesized CL undergoes acyl remodeling to produce CL species enriched with unsaturated acyl groups. Cld1 is the only identified CL specific phospholipase in yeast and is required to initiate the CL remodeling pathway. In higher eukaryotes, peroxidation of CL, yielding CL<sub>OX</sub>, has been implicated in the cellular signaling events that initiate apoptosis. CL<sub>OX</sub> can undergo enzymatic hydrolysis, resulting in the release of lipid mediators with signaling properties. Our previous findings suggested that CLD1 expression is upregulated in response to oxidative stress, and that one of the physiological roles of CL remodeling is to remove peroxidized CL. To exploit the powerful yeast model to study functions of CLD1 in CL peroxidation, we expressed the *H. brasiliensis*  $\Delta^{12}$ -desaturase gene in yeast, which then synthesized PUFAs that are incorporated into CL species. Using LC-MS based redox phospholipidomics, we identified and quantified the molecular species of CL and other phospholipids in *cld1Δ* vs. WT cells. Loss of CLD1 led to a dramatic decrease in chronological lifespan, mitochondrial membrane potential, and respiratory capacity; and increased levels of mono-hydroperoxy-CLs, particularly among the highly unsaturated CL species, including tetralinoleoyl-CL. In addition, purified Cld1 exhibited a higher affinity for CLO<sub>x</sub>, and treatment of cells with H<sub>2</sub>O<sub>2</sub> increased CLD1 expression in the logarithmic growth phase. These data suggest that CLD1 expression is required to mitigate oxidative stress. The findings from this study contribute to our overall understanding of CL remodeling and its role in mitigating oxidative stress.

Keywords: cardiolipin, remodeling, yeast, polyunsaturated fatty acid (PUFA), lipid peroxidation, mass spectrometry (MS), Cld1

### 2.1.5 INTRODUCTION

The dimeric mitochondrial phospholipid cardiolipin (CL) is most abundant in the mammalian heart, where it was first discovered [163]; however, it is present in nearly all mammalian tissues and throughout the eukaryotic kingdom [164]. The cellular and subcellular functions of CL have been studied for decades using the powerful yeast genetic model, *Saccharomyces cerevisiae* [165]. Yeast genes encoding the CL biosynthetic enzymes (Fig. 1) have been identified, and well-characterized mutants are available for each step of the pathway, enabling *in vivo* studies of CL function that are not easily carried out in mammalian cells [166]. The yeast model has, thus, been pivotal in demonstrating the critical role of CL in mitochondrial bioenergetics [167-171], mitochondrial protein import [168, 172], mitochondrial dynamics [173, 174], cell cycle progression [48], cellular aging [49], and mitophagy [51] among other essential functions.

CL that is synthesized *de novo* undergoes remodeling, in which it is deacylated to mono-lyso-CL (MLCL), which is reacylated by the transacylase, tafazzin, thus forming CL species that are more unsaturated [60, 64]. Polyunsaturated tetralinoleoyl-CL (TLCL) is the major CL species detected in human and other mammalian heart, skeletal muscle and liver cells [64]. Despite the obvious energetic expenditures required for the biosynthesis of a unique homo-acylated TLCL, the physiological significance of TLCL remains unclear. It is absent from cells of patients with Barth syndrome (BTHS), an X-linked recessive disorder associated with variable cardiomyopathy, skeletal myopathy, neutropenia, and organic aciduria [64, 65]. BTHS is caused by mutations in the *TAZ* gene that codes for tafazzin [175]. Accordingly, BTHS patient cells accumulate MLCL and are devoid of TLCL, owing to a loss in the final step of the CL remodeling pathway [176]. In yeast, unremodeled and remodeled CL are thought to be

functionally indistinguishable [63], and deletion of the CL-specific phospholipase, *Cld1*, was found to rescue the defects caused by loss of the CL-transacylase, *Taz1* [70]. This raises the question of why cells remodel CL, and how CL enriched with PUFAs are functionally distinct from those containing saturated or mono-unsaturated fatty acyl CL species. Recent studies indicate that peroxidation of CL is a powerful cell signaling event that can initiate apoptosis [73, 75, 177-180]. Furthermore, the enzymatic hydrolysis of oxidized CL ( $CL_{OX}$ ), leading to the release of lipid mediators, may have diverse signaling properties [71, 98]. In the wild, yeast cells proliferate in diverse environments [181-184], from which PUFAs may be readily incorporated into CL. We previously reported that yeast cells supplemented with PUFAs linoleic acid (C18:2) or arachidonic acid (C20:4) readily incorporate these fatty acids into CL [57]. Cipak and co-workers demonstrated that *S. cerevisiae* cells expressing the *H. brasiliensis*  $\Delta^{12}$ -desaturase synthesize PUFAs and exhibit sensitivity to oxidative stress [125, 185]. However, the effect of  $\Delta^{12}$ -desaturase-expression on CL biosynthesis and remodeling or CL peroxidation has not been explored.

In the current study, multiple species of  $CL_{OX}$ , including mono-hydroperoxy-CL and di-hydroperoxy-CL, were also detected in these cells. Further, oxidized species of two additional phospholipids abundant in mitochondria, phosphatidylcholine (PC) and phosphatidylethanolamine (PE), were also detected. However, the oxidized form of phosphatidylserine (PS), which is lacking from mitochondria, was not detected. Thus, our findings suggest that yeast cells synthesizing PUFAs generate  $CL_{OX}$  species within the mitochondria. We compared the CL profiles of  $\Delta^{12}$ -desaturase-expressing WT and *cld1* $\Delta$  cells.  $\Delta^{12}$ -Desaturase-expressing *cld1* $\Delta$  cells contain increased levels of mono-hydroperoxy-CLs, particularly among the highly unsaturated CL species, including TLCL. Furthermore, we

observed that *CLDI* expression is upregulated in response to treatment with H<sub>2</sub>O<sub>2</sub>, and purified Cld1 protein exhibits higher activity towards hydroperoxy-TLCL than non-peroxidized TLCL. The presence of PUFA-containing CL and the production of CL<sub>OX</sub> were not associated with major growth defects under optimum conditions. Interestingly, loss of *CLDI* in  $\Delta^{12}$ -desaturase-expressing cells led to decreased chronological lifespan. These results suggest a novel role for Cld1 and CL remodeling in mitigating the effects of oxidative stress and CL peroxidation. Importantly, these findings provide a powerful genetic model that can be exploited to elucidate mechanisms underlying the generation and function of CL peroxidation.

## 2.1.6 MATERIALS AND METHODS

### 2.1.6.1 Strains, Media, and Growth Conditions

The *S. cerevisiae* strain used in this work is BY4741(*MATa his3 $\Delta$  1 leu2 $\Delta$  0 met15 $\Delta$  0 ura3 $\Delta$  0*). Plasmids pYES2-EV and pYES2-*desa* were kindly given by Dr. Ana Cipak Gasparovic (Rudjer Boskovic Institute, Zagreb, Croatia). Expression of the  $\Delta^{12}$ -desaturase is controlled by a Gal promoter and is induced by growth on galactose-containing medium. Complex medium contained yeast extract (1%), peptone (2%), and glucose (2%) (YPD). The solid medium contained agar (2%) in addition to the ingredients mentioned above. Synthetic complete (SC) *ura*- medium contained adenine (20.25 mg/liter), histidine (20 mg/liter), arginine (20 mg/liter), lysine (200 mg/liter), leucine (60 mg/liter), methionine (20 mg/liter), tryptophan (20 mg/liter), threonine (300 mg/liter), all the essential components of yeast nitrogen base without amino acids (Difco), 0.2% ammonium sulfate, and glucose/galactose (2%). Yeast strains were grown at 30°C. *E. coli* strain DH5- $\alpha$  was used for plasmid maintenance and amplification. Bacteria were grown at 37°C in LB medium (0.5% yeast extract, 1% tryptone, 1% NaCl), supplemented with ampicillin (100  $\mu$ g/mL) for selection purposes. For growth on plates, media were supplemented with 1.5 and 2% agar for *E. coli* and yeast, respectively. Growth in liquid cultures was monitored spectrophotometrically. For lipidomic analysis, cells were harvested and centrifuged at 4 °C (4,300 rpm, 5 min). The supernatant was discarded, and glass beads (0.3g) were added to the centrifuge tubes. Samples were vortexed (5 X 1 min intervals) and centrifuged again at 4 °C (4,300 rpm, 5 min). Supernatants were collected and frozen at -80 °C for lipidomic analysis.

### 2.1.6.2 Construction of Plasmids and Expression of Yeast His<sub>6</sub>-tagged Cld1 in *S. cerevisiae*

To construct a His<sub>6</sub>-tagged *CLD1* overexpression plasmid, a 1373-bp sequence containing the entire open reading frame without stop codon of *CLD1* was amplified from yeast genomic DNA using an EcoRI-tagged forward primer *CLD1\_EcoRI\_F3* (5'-TGATTAATAAGAATTCAACACAATGTTCAAGTCAACTTTAAACTC-3') and an XbaI-tagged reverse primer *CLD1\_XbaI\_R3* (5'-ATTTTGAGATTCTAGATATTTTTTGCATTTCTTTTCG-3'). The PCR products were purified using the Wizard SV gel and PCR clean-up system (Promega). The purified DNA fragments were ligated into the pYES2/CT cut with *EcoRI* and *XbaI* downstream of the GAL1 promoter. All the plasmids were amplified and extracted using standard protocols. The plasmids were transformed into yeast strains using a one-step transformation protocol.

### 2.1.6.3 Purification of His<sub>6</sub>-tagged Cld1

*S. cerevisiae* BY4741 was used to express the recombinant His<sub>6</sub>-tagged Cld1. Cells were grown at 30 °C in synthetic complete raffinose medium lacking uracil. Galactose (2%) was used to induce overexpression of the recombinant protein. Cell extracts were prepared by disrupting cells with glass beads (0.5 mm diameter), vortexing for 5 min intermittently. The disruption buffer contained 50 mM Tris-Cl (pH 8.0) and 300 mM NaCl. Protease inhibitor was added to the disruption buffer before breaking the cells. His<sub>6</sub>-tagged Cld1 was purified with Millipore® PureProteome nickel magnetic beads following manufacturer's instructions. Millipore® UFC503024 Amicon® Ultra-0.5 centrifugal filter concentrator (30 KD) was used to concentrate the protein and remove imidazole. Protein concentration was determined with BIO-RAD DC protein assay kit using bovine serum albumin as the standard.

#### **2.1.6.4 Synthesis of CLs**

Commercially available CLs: 1,1',2,2'-Tetramyristoyl-CL (TMCL, CL (14:0)<sub>4</sub>); 1,1',2,2'-Tetralinoleoyl-CL (TLCL, CL (18:2)<sub>4</sub>) and 1,2-Dioleoyl-sn-glycerol-3-phosphocholine (DOPC) were purchased from Avanti Polar Lipids Inc. (Alabaster, AL). 1,1',2,2'-Tetrapalmitoyl-CL and (TPCL, CL (16:0)<sub>4</sub>) was synthesized and purified as previously described [35]. Hydroperoxy-TLCL (TLCL-OOH, CL(18:2)<sub>3</sub>/18:2-OOH) was prepared in soybean lipoxygenase-catalyzed reaction (Cayman Chemical Company, Ann Arbor, MI) in 50 mM HEPES buffer, containing 100 μM DTPA. To prevent the conversion of hydroperoxy-groups to secondary products during incubation, HEPES buffer was saturated with oxygen. After CL oxygenation, the crude product was purified by HPLC. Internal MLCL (14:0)<sub>3</sub> and reference standards MLCL (16:0)<sub>3</sub> and MLCL (18:2)<sub>3</sub> were prepared from the respective CLs by a PLA2 (porcine pancreatic, Sigma) driven reaction as described by Kim and Hoppel [186] with slight modifications.

#### **2.1.6.5 Chronological Lifespan**

Yeast chronological lifespan was determined by survival of non-dividing cells in a prolonged stationary culture [187]. A protocol modified from the one previously described [188] was followed to assess the chronological lifespan. In brief, individual colonies were inoculated in 5 mL of SC galactose medium and incubated overnight. The cultures were then diluted in 50 mL of SC galactose medium, and cells were allowed to grow until saturation during the first 24 hours. At this time, cells stopped dividing and reached a maximum number. Viability was considered to be 100% at this time, and viable cells were measured by counting colonies that were formed following dilution and plating on YPD plates. Viable cells were measured every day in the same volume of cell culture and the percentage of cells that formed colonies on day one was determined.

#### 2.1.6.6 Spotting Assay

Cells were pre-cultured in SC galactose medium to the early stationary growth phase at 30 °C and washed with sterile water. 2.5 µL aliquots of a series of 10-fold dilutions of 0.5 units of A<sub>550</sub> cells were spotted onto the indicated plates and incubated at 30 °C for 3 days.

#### 2.1.6.7 Real-Time Quantitative PCR (RT-qPCR) Analysis

Cells were grown to the indicated growth phase and harvested at 4 °C. Total RNA was extracted and purified using the RNeasy Mini Plus kit (Qiagen, Valencia, CA). Complementary DNA (cDNA) was synthesized using the first strand cDNA synthesis kit (Roche Applied Science) according to the manufacturer's manuals. RT-qPCRs were performed in a 20 µL volume using Brilliant III Ultra-Faster SYBR Green qPCR Master Mix (Agilent Technologies, Santa Clara, CA). Triplicates were included for each reaction. The primers for *CLDI* and *ACT1* RT-qPCR are described previously [70]. RNA levels were normalized to *ACT1*. Relative values of mRNA transcripts were shown as fold change relative to indicated controls.

#### 2.1.6.8 Synthesis of Mito-AAPH

**2-[(E)-(2-Amino-2-imino-1,1-dimethyl-ethyl)azo]-2-methyl-propanamide hydrochloride (2; yield, 82%):** In ice-cold methanol (100 mL), 2,2'-azobis-2-methyl-propanimidamide (AAPH; 2,2'-azobis-2-methyl-propanimidamide, **1**; 1 g; 3.7 mmol) was neutralized with NaOH (0.3 g; 7.4 mmol). The solvent was rotor-evaporated (25 °C; 10 torr) and the crystals formed were suspended in chloroform (100 mL). Undissolved **1** and NaCl were filtered off. Rotor-evaporation of the filtrate afforded **2** (0.6 g; 3 mmol), which was used immediately for the preparation of **5**.

**(4-Chloro-4-oxo-butyl)-triphenyl-phosphonium bromide (4; yield, 65%):** 3-carboxypropyl(triphenyl)phosphonium bromide (**3**, 1 g; 2.3 mmol) was dissolved in chloroform (50 mL) containing thionyl chloride (3 g; 25 mmol) and dimethylformamide (DMF; 0.05 g; 0.68 mmol), and the reaction solution was refluxed for 4 hours. The volume of the solvent was reduced to ~ 5 mL (rotor-evaporation; 25 °C; 150 torr) and trituration with n-hexane afforded **4** (0.68 g), which was dried under vacuum (40 °C; 10 torr) for 1 hour.

**[2-[(E)-[2-Imino-1,1-dimethyl-2-(4-triphenylphosphaniumylbutanoylamino)ethyl]azo]-2-methyl-propanimidoyl]ammonium chlorobromide (5; yield 45%):** Chloroform (50 mL) containing **2** (0.5 g; 2.5 mmol) and **4** (1.12 g; 2.5 mmol) was incubated for 24 hours at 0 °C. Thereafter, the solvent was rotor-evaporated (20 °C; 10 torr) and the dry residue was redissolved in minimal volume of ethanol. Trituration of the solution with diethyl ether afforded **5** (0.69 g), which was filtered and dried under vacuum (20 °C; 1 torr) for 30 min. ESI MS calculated for the triphenylphosphonium cation of **5** ( $C_{30}H_{38}N_6OP^+$ ), 529.64; found, 529.80.

#### 2.1.6.9 Mito-AAPH Treatment

Mito-AAPH was diluted with ethanol to make a 50 mM stock. For the spotting assay, 50  $\mu$ M Mito-AAPH was directly spread on the plate before the experiment. For liquid culture, 50  $\mu$ M Mito-AAPH was added at log phase ( $A_{550} \approx 0.5$ ).

#### 2.1.6.10 Determination of mitochondrial membrane potential (MMP)

Cells were grown in SC Gal Ura- medium to log phase and incubated with 500 nM TMRM for 30 min at 30°C. Cells were washed, resuspended in warm medium and divided in half. One group was treated with 6  $\mu$ M FCCP and the other group was untreated. The TMRM fluorescence

intensity was determined in 30,000 cells from each group using a LSR II flow cytometer in the Wayne State University Microscopy, Imaging and Cytometry Resources Core. Median fluorescence intensity was calculated after correcting for background TMRM fluorescence (values obtained after treatment with FCCP) using FlowJo v10.2.

#### **2.1.6.11 Respiration measurements**

Oxygen consumption rate (ORC) of intact yeast cells was analyzed via the polarographic method in a closed 500  $\mu$ L chamber equipped with a micro Clark-type oxygen electrode (Oxygraph Plus System, Hansatech Instruments) at 30°C. Yeast cells were grown in synthetic complete medium until log phase. Cells were mixed in fresh medium with a cell density normalized to a protein concentration of 0.5 mg/mL followed by the measurement of respiration. KCN (0.2 mM) was added at the end of the experiment to inhibit cytochrome c oxidase, to correct for cytochrome c oxidase-independent oxygen utilization. Oxygen consumption was recorded on a computer and analyzed with Oxygraph plus software. Oxygen consumption rate (ORC) is defined as consumed O<sub>2</sub> (nmol)/min/total protein (mg).

#### **2.1.6.12 Statistical Analysis**

The results are presented as mean  $\pm$  S.D. values from at least three experiments, and statistical analyses were performed by paired/unpaired Student's t-test. The statistical significance of differences was set at  $p < 0.05$ .

#### **2.1.6.13 LC/MS assessment of phospholipids**

Lipids were extracted from cells, and the LC/MS analysis of phospholipids was performed as previously described [57]. Briefly, phospholipids were analyzed in negative mode using a

Dionex Ultimate™ 3000 RSLCnano system coupled online to a Q-Exactive hybrid quadrupole-orbitrap mass spectrometer (ThermoFisher Scientific, San Jose, CA). Lipids were separated on a normal phase column (Silica Luna 3 μm, 100A, 150x2 mm, (Phenomenex, Torrance CA)) with flow rate 0.2 mL/min using gradient solvents containing 5 mM CH<sub>3</sub>COONH<sub>4</sub> (A – *n*-hexane:2-propanol: water, 43:57:1 (v/v/v) and B - *n*-hexane:2-propanol: water, 43:57:10 (v/v/v)). MS lipid standards used in this study were from Avanti polar lipids (Alabaster, AL). Analysis of LC-MS data was performed using software package Compound Discoverer™ (ThermoFisher Scientific) with an in-house generated analysis workflow and peroxidized phospholipid database.

## 2.1.7 RESULTS

### 2.1.7.1 Expression of the *H. brasiliensis* $\Delta^{12}$ -desaturase alters the molecular speciation of CL in *S. cerevisiae* cells

Yeast cells that are not supplemented with exogenous fatty acids produce only saturated and  $\Delta^9$ -mono-unsaturated fatty acyl residues, and cannot synthesize PUFAs [57]. To construct a yeast model with PUFA-containing CL, we expressed the *H. brasiliensis*  $\Delta^{12}$ -desaturase gene in yeast [125] and established its effect on the phospholipidome of these cells. As described in Figure 1, yeast readily produce 16:0-CoA and 18:0-CoA, which can be converted to 16:1-CoA and 18:1-CoA via endogenous  $\Delta^9$ -desaturase activity. These acyl-CoA species can be incorporated into phosphatidic acid (PA) and used in the *de novo* synthesis of CL via the CL synthase (Crd1) - catalyzed reaction to form nascent CL, which contains predominately saturated fatty acyl chains [189-192]. Nascent CL is deacylated by the phospholipase, Cld1, to form monolysocardiolipin (MLCL) [60, 62]. The transacylase, Taz1, utilizes donor phospholipids, particularly PC and PE, to acylate MLCL to form CL, with the concomitant formation of lyso-PC (LPC) and lyso-PE (LPE) [58, 193]. Multiple cycles of deacylation-reacylation lead to the synthesis of mature CL containing mainly unsaturated acyl chains [58, 193]. As we showed previously, Cld1 has a greater affinity for C16- than for C18-containing acyl chains [57]. Accordingly, the predominant CL species detected in yeast contain C18 acyl chains.

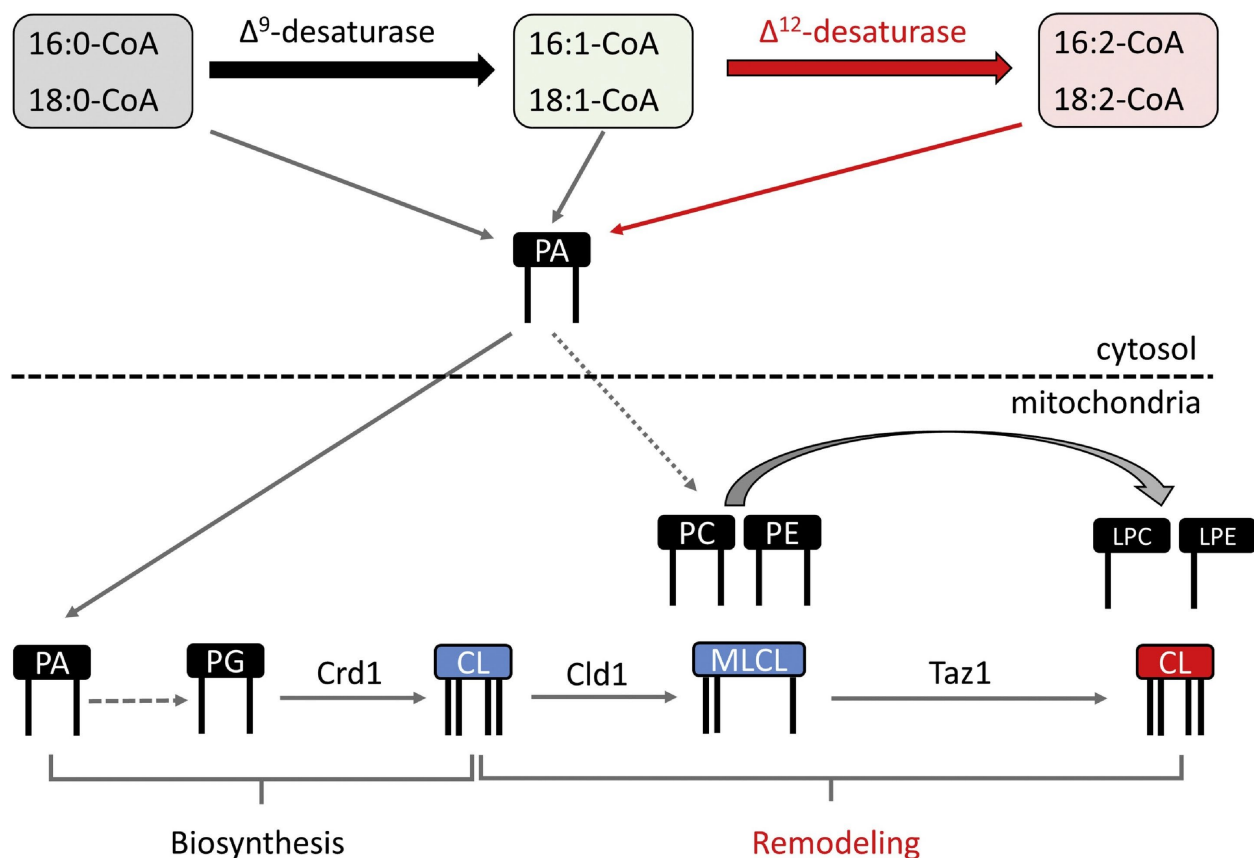
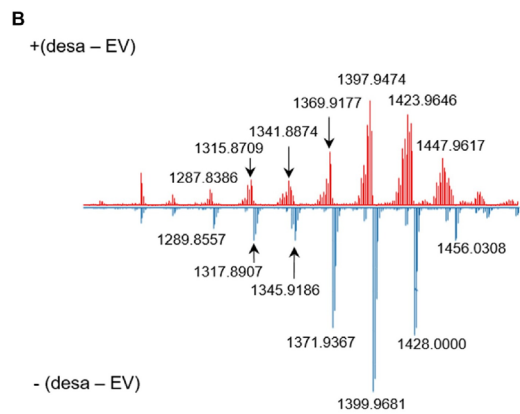
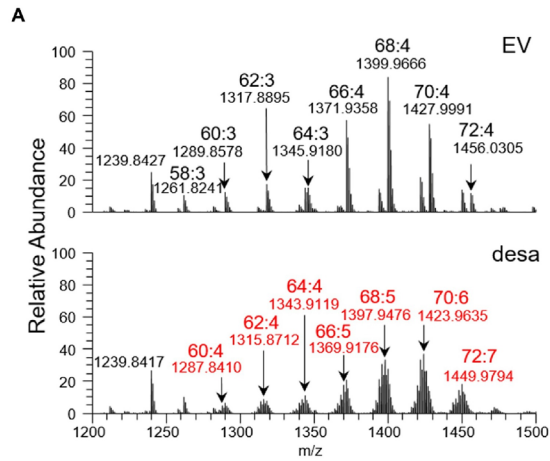


**Figure 1. CL biosynthesis and remodeling in *S. cerevisiae*.**

Yeast cells readily produce 16:0-CoA and 18:0-CoA, which can be converted to 16:1-CoA and 18:1-CoA via endogenous  $\Delta^9$ -desaturase activity. 16:1-CoA and 18:1-CoA can be further converted to 16:2-CoA and 18:2-CoA by the expressed  $\Delta^{12}$ -desaturase. All available acyl-CoA species can be incorporated into phosphatidic acid (PA) and used in the de novo synthesis of CL via CL synthase (Crd1). Newly synthesized CL contains predominantly saturated fatty acyl chains. Nascent CL may undergo Cld1-catalyzed deacylation to form mono-lyso-CL (MLCL). The transacylase, Taz1, utilizes donor phospholipids, particularly phosphatidylcholine (PC) and phosphatidylethanolamine (PE), to reacylate MLCL to CL, accompanied by the formation of the hydrolysis products of PC and PE, lyso-PC (LPC) and lyso-PE (LPE). PC and PE are also synthesized from PA. Multiple cycles of deacylation-reacylation generate CL that contains mainly unsaturated acyl chains.

The expression of  $\Delta^{12}$ -desaturase results in the production of 16:2-CoA and 18:2-CoA, which are incorporated into CL through *de novo* synthesis or via CL remodeling. As shown in Figure 2A expression of the  $\Delta^{12}$ -desaturase caused dramatic changes in CL composition. Wild-type (WT) yeast cells expressing empty vector (EV) have predominantly species containing

saturated or mono unsaturated fatty acyls such as CL64:3, CL66:4, CL68:4, CL70:4 and CL72:4, while WT cells expressing the  $\Delta^{12}$ -desaturase contained predominantly CL66:5, CL68:5, CL70:6 and CL72:7. The appearance of PUFA-CL species are readily observed in differential LC-MS spectra obtained by subtracting the spectrum corresponding to EV-expressing WT cells from the spectrum of  $\Delta^{12}$ -desaturase-expressing WT cells (red spectrum). Similarly, the loss of saturated and mono-unsaturated CL is apparent when subtracting the spectrum of  $\Delta^{12}$ -desaturase-expressing WT cells from EV-expressing WT cells (blue spectrum) (Figure 2B). The quantitative assessment of individual CL species indicates that  $\Delta^{12}$ -desaturase expression resulted in the production of multiple PUFA-containing CL species and a concomitant reduction in the abundance of CL species containing saturated or monounsaturated fatty acids (Figure 2C and 2D).

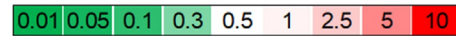


**C**

CN:DB	m/z	EV	desa
58:1	1265.8557	0.07	0.05
58:2	1263.8401	0.49	0.36
58:3	1261.8232	1.00	1.04
58:4	1259.8109	N.D.	0.10
60:1	1293.8858	0.15	0.13
60:2	1291.8707	0.78	0.42
60:3	1289.8565	1.62	0.73
60:4	1287.8397	N.D.	0.55
60:5	1285.8236	N.D.	0.28
60:6	1283.8084	N.D.	0.12
60:7	1281.7919	N.D.	0.02
62:1	1321.9158	0.16	0.09
62:2	1319.9010	0.98	0.38
62:3	1317.8873	2.17	0.86
62:4	1315.8702	N.D.	0.99
62:5	1313.8544	N.D.	0.83
62:6	1311.8392	N.D.	0.43
62:7	1309.8231	N.D.	0.14
62:8	1307.8076	N.D.	0.06
64:1	1349.9414	0.08	0.03
64:2	1347.9317	0.66	0.21
64:3	1345.9171	1.99	0.65
64:4	1343.9023	1.93	1.17
64:5	1341.8854	N.D.	0.94
64:6	1339.8704	N.D.	0.67
64:7	1337.8538	N.D.	0.29
64:8	1335.8385	N.D.	0.20

CN:DB	m/z	EV	desa
66:1	1377.9709	0.08	0.04
66:2	1375.9621	0.55	0.25
66:3	1373.9466	3.43	0.96
66:4	1371.9334	6.88	2.13
66:5	1369.9165	N.D.	1.76
66:6	1367.9009	N.D.	1.13
66:7	1365.8856	N.D.	0.63
66:8	1363.8699	N.D.	0.29
68:2	1403.9929	0.62	0.25
68:3	1401.9769	4.51	1.05
68:4	1399.9643	9.77	2.66
68:5	1397.9465	N.D.	3.20
68:6	1395.9307	N.D.	2.98
68:7	1393.9163	N.D.	2.01
68:8	1391.9010	N.D.	0.77
70:2	1432.0255	0.28	0.05
70:3	1430.0070	2.68	0.44
70:4	1427.9964	6.08	1.40
70:5	1425.9774	N.D.	2.49
70:6	1423.9619	N.D.	3.43
70:7	1421.9481	N.D.	3.18
70:8	1419.9327	N.D.	1.56
72:3	1458.0362	0.59	0.06
72:4	1456.0287	1.30	0.22
72:5	1454.0082	N.D.	0.53
72:6	1451.9918	N.D.	1.13
72:7	1449.9793	N.D.	1.63
72:8	1447.9638	N.D.	1.28

pmol/nmol PLs



N.D. - not detected

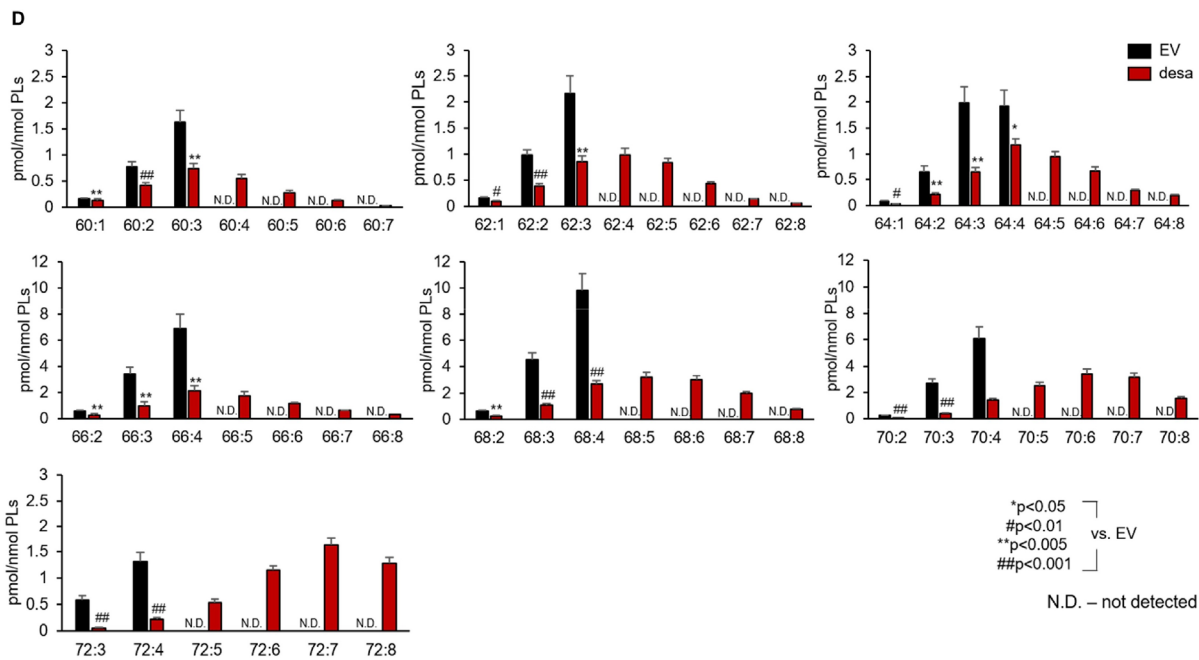


**Figure 2. CL species synthesized in empty vector (EV)- and  $\Delta^{12}$ -desaturase (desa)-expressing WT cells.**

Typical mass spectra of CL obtained from wild-type (WT) yeast cells expressing the empty vector (EV) (upper panel) or desa (lower panel). Major CL molecular species are identified as: CL58:3 (m/z 1261.8241); CL60:3 (m/z 1289.8578); CL62:3 (m/z 1317.8895); CL64:3 (m/z 1345.9180); CL66:4 (m/z 1371.9358); CL68:4 (m/z 1399.9666); CL70:4 (m/z 1427.9991); CL72:4 (m/z 1456.0305); CL60:4 (m/z 1287.8410); CL62:4 (m/z 1315.8712); CL64:4 (m/z 1343.9119); CL66:5 (m/z 1369.9176); CL68:5 (m/z 1397.9476); CL70:6 (m/z 1423.9635); CL72:7 (m/z 1449.9794). (B) A differential mass spectra of CL species were obtained to highlight individual CL species that were increased [+(desa-EV)] or decreased [-(desa-EV)] by the expression of desa. (C) Heat map of CL quantified from WT yeast cells expressing EV or desa. (D) Quantitative assessment of individual CL molecular species in WT cells expressing the EV or desa.

### 2.1.7.2 $\Delta^{12}$ -desaturase expression leads to accumulation of CLO<sub>x</sub>

The accumulation of CLO<sub>x</sub> was readily observed in WT cells expressing  $\Delta^{12}$ -desaturase (Figure 3A-C). Mono-hydroperoxy-CL and di-hydroperoxy-CL species were observed in these cells. As anticipated, oxidized CL species were not detected in EV-expressing WT cells. Oxidized MLCL species were not found, but oxidized PG, particularly PG 36:4+2[O], was readily detectable in the  $\Delta^{12}$ -desaturase-expressing-WT cells (Figure 6A). The accumulated CLO<sub>x</sub> could be synthesized from either pre-oxidized PG (containing peroxidized fatty acid residues) (Figure. 4 and Figure. 5) or generated from oxidizable PUFA-CL species via direct peroxidation or via reacylation with the transfer of peroxidized PUFA residues.

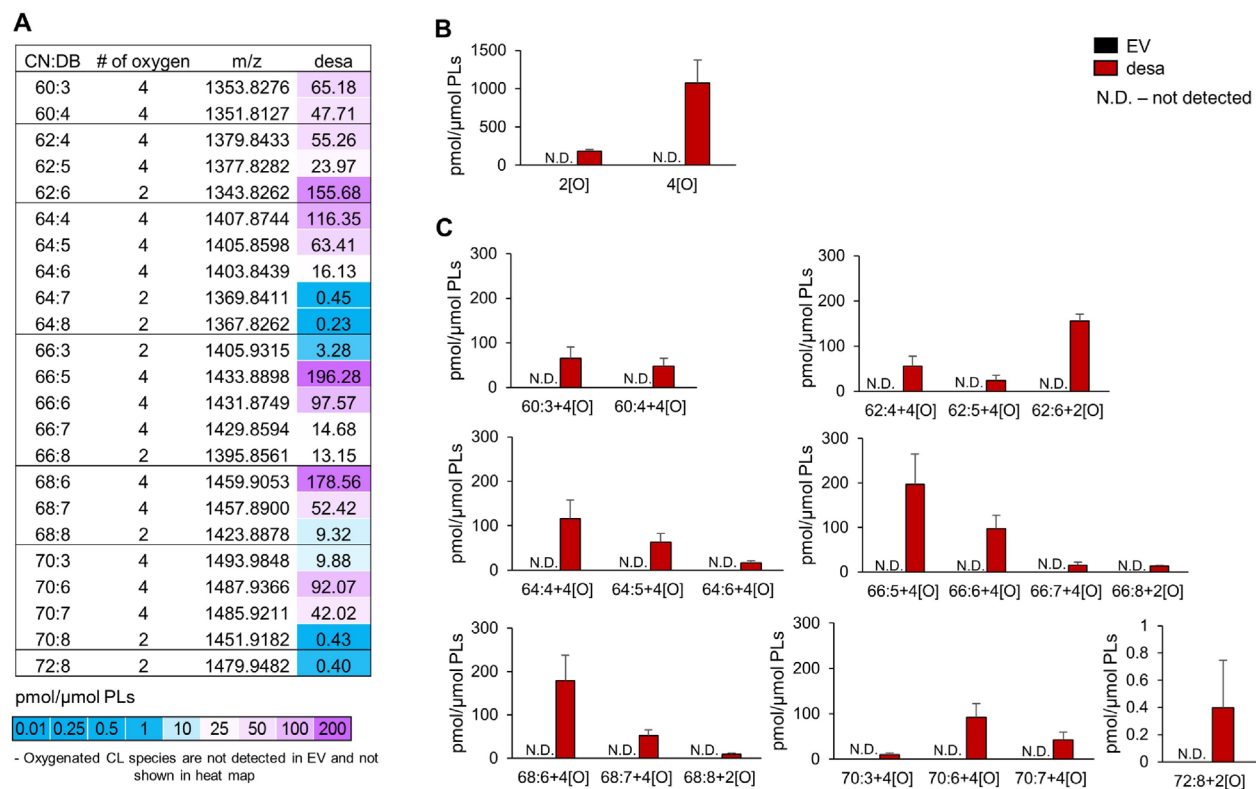


**Figure 3. Peroxidized CL (CLO<sub>x</sub>) in desa-expressing WT cells.**

(A) Heat map of CLO<sub>x</sub>. (B) Quantitative assessment of total CLO<sub>x</sub>. (C) Quantitative assessment of individual CLO<sub>x</sub> molecular species.

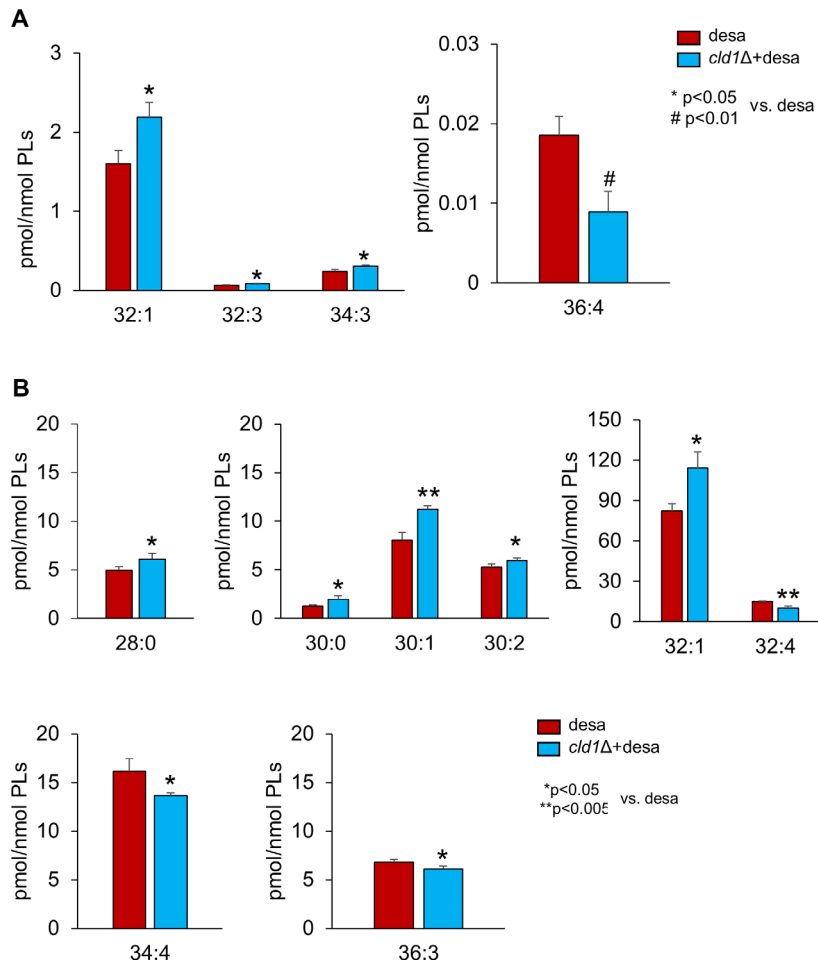


**Figure 4. Quantitative assessment of individual (A) PG and (B) PC molecular species in WT and *cld1Δ* yeast cells expressing *desa*.**

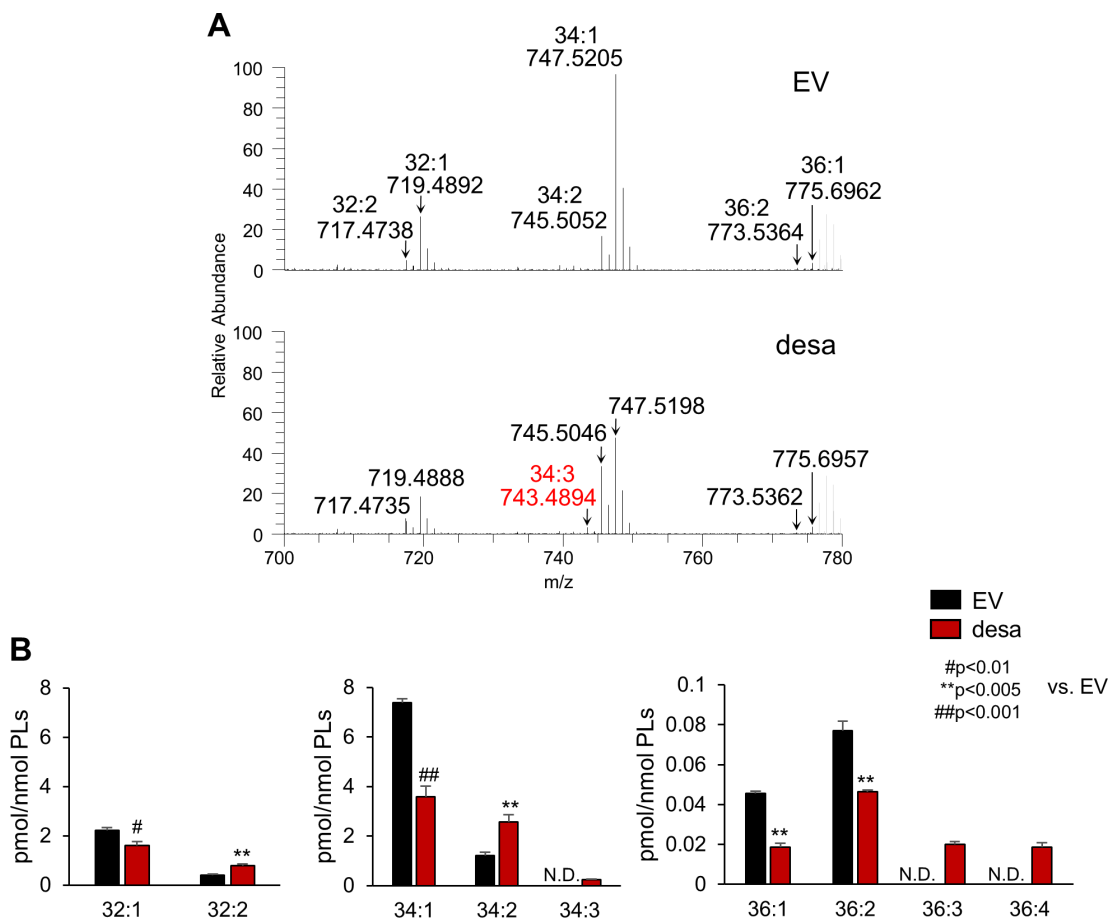


**Figure 5. Phosphatidylglycerol (PG) in EV- and desa-expressing WT cells.**

(A) Typical mass spectra of PG obtained from WT yeast cells expressing EV (upper panel) or desa (lower panel). Major PG molecular species identified as: PG32:1 (m/z 719.4892); PG32:2 (m/z 717.4738); PG34:1 (m/z 747.5205); PG34:2 (m/z 745.5052); PG34:3 (m/z 743.4894); PG36:1 (m/z 775.5520) and PG36:2 (m/z 773.5364). (B) Quantitative assessment of individual PG species.

Fragmentations of non-peroxidized PUFA-CL, including 16:2 and 18:2 fatty acids, were found in our analysis, but the structural information related to the location of dienes was not available. In yeast, exogenous plant  $\Delta^{12}$ -desaturase utilized 16:1-CoA and 18:1-CoA that were generated by endogenous  $\Delta^9$ -desaturase as substrates [125], indicating that the location of dienes are at position 9 and position 12 in the 18:2 and 16:2 aliphatic chain. In addition, the fragmentations of CL mono-hydroperoxides and di-hydroperoxides were examined to precisely identify CL peroxidation and locate the oxygen within the species. However, the fragmentations were not able to be detected due to insufficient levels of CL peroxidation products (the ratio of oxidized CL in the analysis was about 0.13 mol% of total phospholipids and 2.5 mol% of non-oxidized CL). In fact, the position of oxygen in CL monohydroperoxides and di-hydroperoxides was already identified via mass spectrometry in previous studies when the CL peroxidation was performed *in vitro*. Previously, the position of oxygen was structurally identified in CL generated from TLCL incubated with cyt C and H<sub>2</sub>O<sub>2</sub>, in which hydroperoxidation at position 9 and position 13 was detected [76]. In addition, soybean lipoxygenase incubated with CL specifically generated 13-hydroperoxy-CL and very low amount of 9-hydroperoxy-CL [194]. Recently, Shu-Ping Hui and coworkers identified the position of oxygen in CL mono-hydroperoxides generated from oxidation of commercial bovine heart CL and HepG2 lipid extracts treated with CuSO<sub>4</sub>/H<sub>2</sub>O<sub>2</sub>, showing that the oxygen atom was located at position 13 of linoleoyl chain [195]. However, the location of oxygens of CL peroxidation occurring within cells is still unknown. Further investigation is needed.

### **2.1.7.3 Detection of other oxidized phospholipids in $\Delta^{12}$ -desaturase-expressing-WT cells**

The effects of  $\Delta^{12}$ -desaturase expression on PC (Figure 6B and Figure 7), PE (Figure 6C and Figure 8), and PS (Figure 6D and Figure 9) were determined. All phospholipids analyzed in

these cells contained C16:2 and/or C18:2 fatty acyl chains. Oxidized species of PC (PC<sub>OX</sub>) and PE (PE<sub>OX</sub>) were detected in  $\Delta^{12}$ -desaturase-expressing cells. Interestingly, however, oxidized PS (PS<sub>OX</sub>) species were not found. Given that PC and PE species are enriched within mitochondrial membranes while PS species contribute minimally to the mitochondrial phospholipidome [196, 197], this finding suggests that phospholipid peroxidation observed in  $\Delta^{12}$ -desaturase-expressing cells likely occurs within the mitochondrial subcellular compartment. This conclusion is further supported by the comparative data on the absolute amounts of oxidized phospholipids and their relative content (mol %) normalized to either total amounts of all phospholipids or the amounts of individual phospholipid classes (Table 1). The results show that the total oxidized phospholipid species constituted ~1% of the total PLs whereby PC<sub>OX</sub> products were the most abundant. Notably, the content of CL<sub>OX</sub> constituted ~2.5% of the CL species, compared to the levels of PC<sub>OX</sub> and PE<sub>OX</sub>, which were ~1.1% and 0.9% as normalized to PC and PE, respectively.

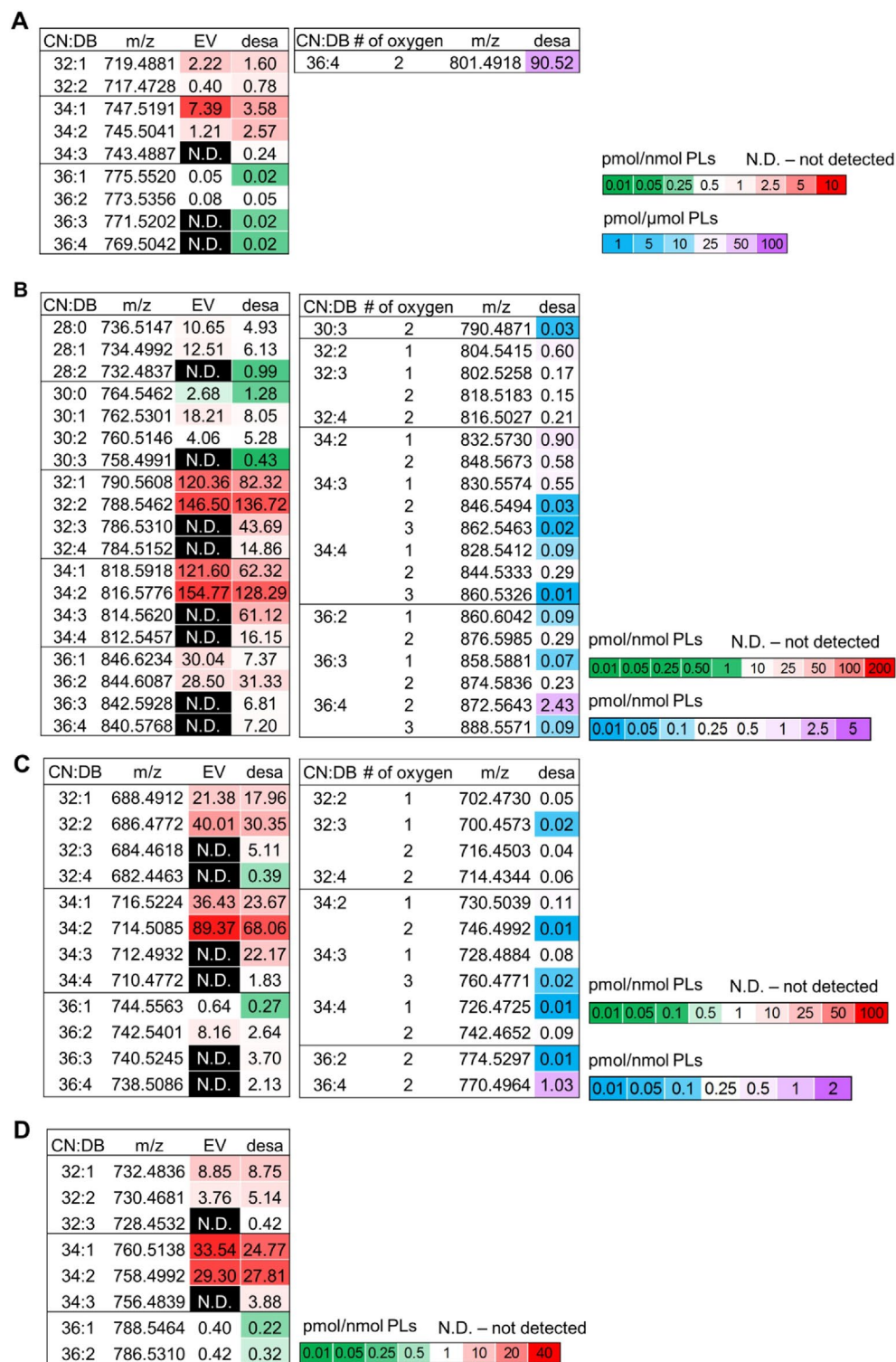


**Figure 6. Heat maps of (A) PG and PGox, (B) PC and PCox, (C) PE and PEox, (D) PS in WT cells expressing empty vector (EV) or desaturase (desa).**

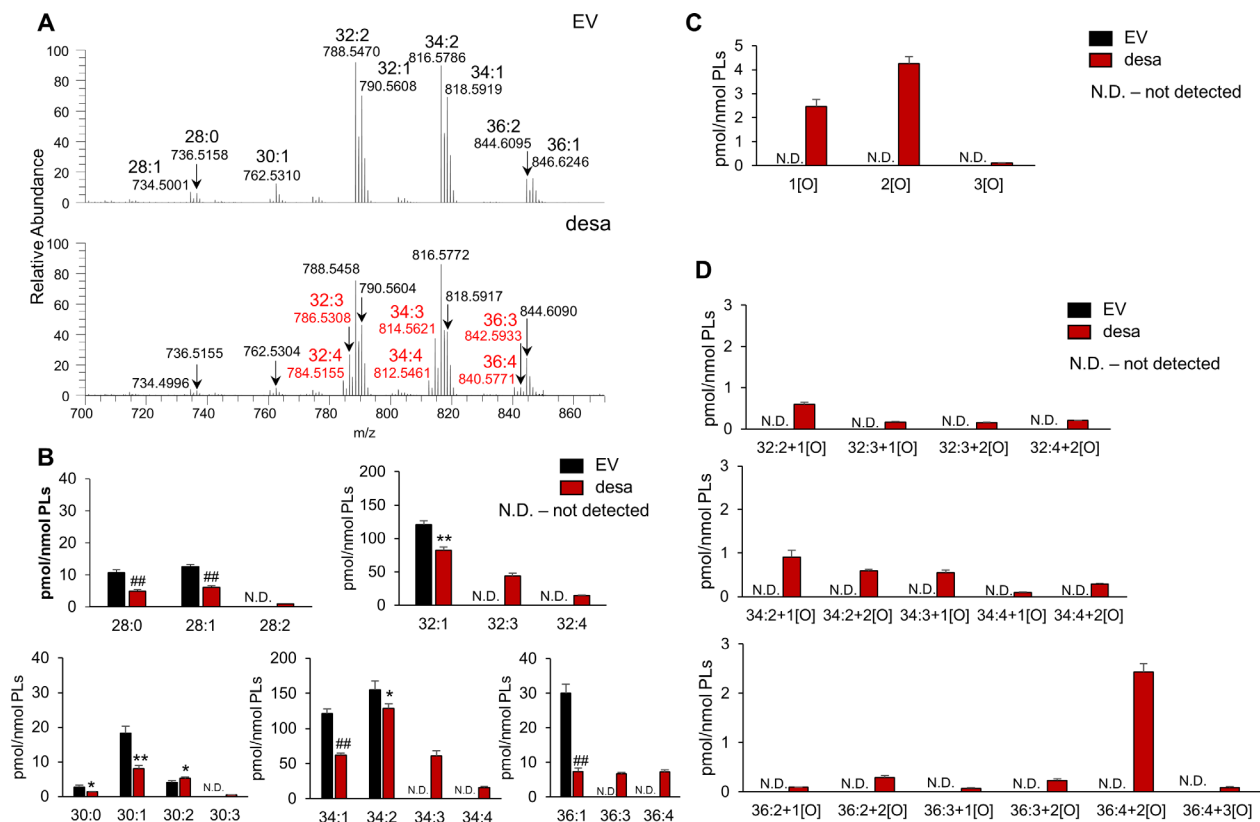


**Figure 7. PC and PCox species produced in EV- and desa-expressing WT cells.**

Typical mass spectra of PC obtained from WT yeast cells expressing EV (upper panel) or desa (lower panel). Major PC molecular species are identified as: PC28:0 (m/z 736.5158); PC28:1 (m/z 734.5011); PC30:1 (m/z 762.5310); PC32:1 (m/z 790.5608); PC32:2 (m/z 788.5470); PC32:3 (m/z 786.5308); PC32:4 (m/z 784.5155); PC34:1 (m/z 818.5919); PC34:2 (m/z 816.5786); PC34:3 (m/z 814.5621); PC34:4 (m/z 812.5461); PC36:1 (m/z 846.6246); PC36:2 (m/z 844.6095); PC36:3 (m/z 842.5933); PC36:4 (m/z 840.5771). (B) Quantitative assessment of individual PC species in EV- and desa-expressing WT cells. Quantitative assessment of (C) PC with one, two and three oxygen and (D) individual PC<sub>OX</sub> molecular species in EV- and desa-expressing WT cells.

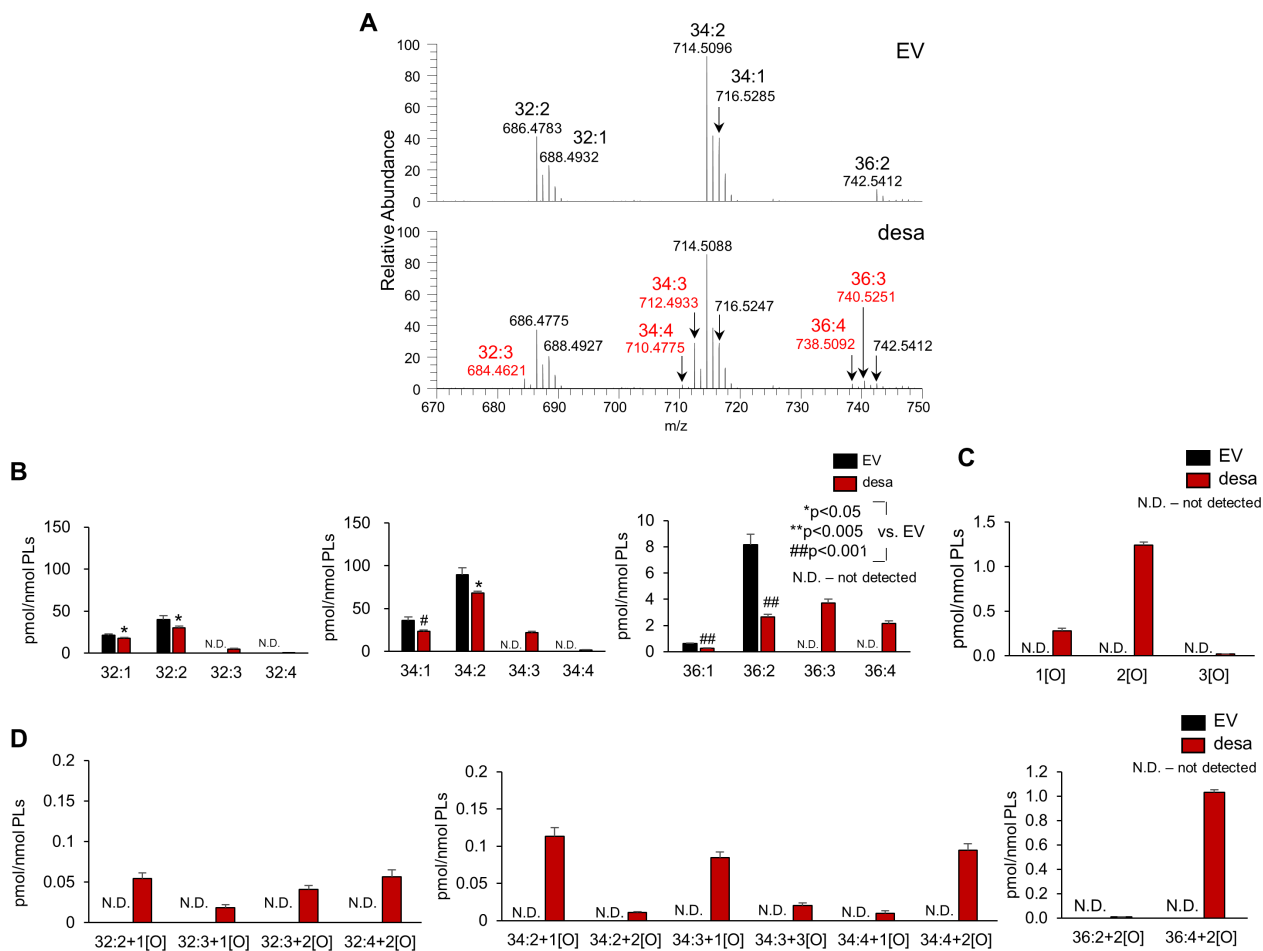


**Figure 8. PE and PEO<sub>x</sub> species produced in EV- and desa-expressing WT cells**

Typical mass spectra of PE obtained from WT yeast cells expressing EV (upper panel) or desa (lower panel). Major PE molecular species are identified as: PE<sub>32:1</sub> (m/z 688.4932); PE<sub>32:2</sub> (m/z 686.4783); PE<sub>32:3</sub> (m/z 684.4621); PE<sub>34:1</sub> (m/z 716.5285); PE<sub>34:2</sub> (m/z 714.5096); PE<sub>34:3</sub> (m/z 712.4933); PE<sub>34:4</sub> (m/z 710.4775); PE<sub>36:2</sub> (m/z 742.5412); PE<sub>36:3</sub> (m/z 740.5251); PE<sub>36:4</sub> (m/z 738.5092). (B) Quantitative assessment of individual PE species in EV- and desa-expressing WT cells. Quantitative assessment of (C) PE with one, two and three oxygen and (D) individual PEO<sub>x</sub> molecular species in EV- and desa-expressing WT cells.

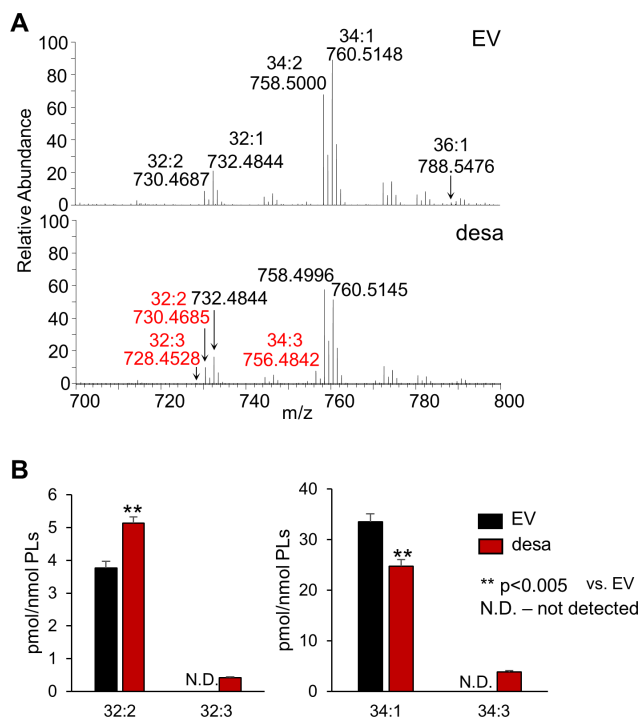


**Figure 9. PS species synthesized in EV- and desa-expressing WT cells.**

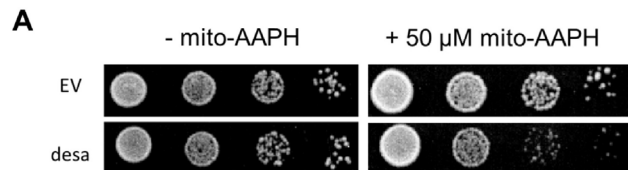
(A) Typical mass spectra of PS obtained from WT yeast cells expressing EV (upper panel) or desa (lower panel). Major PS molecular species are identified as: PS32:1 (m/z 732.4844); PS32:2 (m/z 730.4685); PS32:3 (m/z 728.4528); PS34:1 (m/z 760.5148); PS34:2 (m/z 758.5000); PS34:3 (m/z 756.4842); PS36:1 (m/z 788.5476). (B) Quantitative assessment of individual PS species in EV- and desa-expressing WT cells.

**Table 1. The absolute amounts of oxidized phospholipids and their relative content (mol%) normalized to either the amounts of total phospholipids or the amounts of individual phospholipid class in desaturase (desa)-expressing WT cells.**

<b>PL class</b>	<b># of PLox</b>	<b>mol% to total PLs</b>	<b>mol% to individual PL class</b>
<b>CL</b>	23	0.13	2.49
<b>PC</b>	19	0.68	1.08
<b>PE</b>	12	0.15	0.85
<b>PG</b>	2	0.01	0.13
<b>PS</b>	0	0	0

#### **2.1.7.4 $\Delta^{12}$ -desaturase expression results in an increased sensitivity to mitochondria-targeted lipid peroxidation**

We next used a mitochondria-targeted azo-initiator of peroxy radicals, mito-AAPH, to examine how CL peroxidation and growth are affected in  $\Delta^{12}$ -desaturase-expressing WT cells. We determined that  $\Delta^{12}$ -desaturase-expressing WT cells exhibit increased sensitivity to mito-AAPH (Figure 10A). As mito-AAPH partitions into mitochondria, it spontaneously decomposes at a constant rate to generate carbon-centered radicals, which, in aerobic conditions, are converted into peroxy radicals that stimulate lipid peroxidation [198]. Exposure to mito-AAPH resulted in increased generation of specific mono-hydroperoxy-CL species, including CL62:6+2[O], CL64:8+2[O], CL66:7+2[O], CL66:8+2[O], CL68:8+2[O], and CL72:8+2[O] (Figure 10B). PC36:4+2[O] (Figure 10C), PE32:4+2[O], PE34:4+2[O] (Figure 10D), and PG36:4+2[O] (Figure 10E) were also increased. CL66:7+2[O] and PE34:3+2[O] were found only in desaturase-expressing WT cells exposed to mito-AAPH. Oxidized MLCL and PS were not found in desaturase-expressing WT cells exposed to mito-AAPH. These results suggest that the increased mitochondrial lipid peroxidation contributes to the overall growth defects observed in the  $\Delta^{12}$ -desaturase-expressing WT cells.

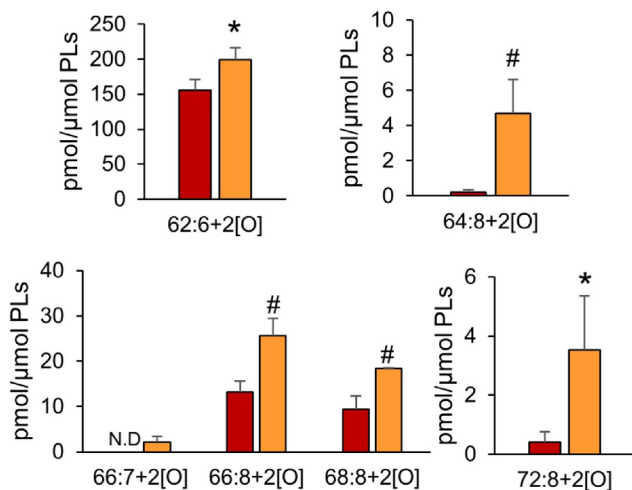


**B**

(CN:DB)	# of oxygen	m/z	desa	desa+mito-AAPH
62:6	2	1343.8271	155.68	198.84
64:8	2	1367.8271	0.23	4.69
66:7	2	1397.8725	N.D.	2.15
66:8	2	1395.8561	13.15	25.65
68:8	2	1423.8887	9.32	18.44
72:8	2	1479.9491	0.40	3.52

0.01 0.05 0.1 0.25 0.5 1 10 25 50 100 200

pmol/ $\mu$ mol PLs

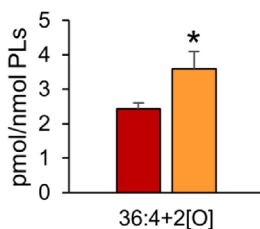


**C**

CN:DB	# of oxygen	m/z	desa	desa+mito-AAPH
36:4	2	872.5652	2.43	3.59

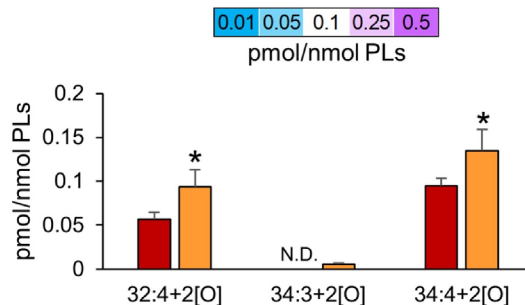
0.01 0.05 0.1 0.25 0.5 1 2.5 5

pmol/nmol PLs



**D**

CN:DB	# of oxygen	m/z	desa	desa+mito-AAPH
32:4	2	714.4343	0.06	0.09
34:3	2	744.4805	N.D.	0.01
34:4	2	742.4652	0.09	0.14

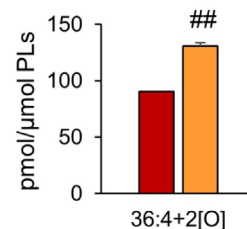


**E**

CN:DB	# of oxygen	m/z	desa	desa+mito-AAPH
36:4	2	801.4918	90.52	130.99

1 5 10 25 50 100 150

pmol/ $\mu$ mol PLs



■ desa    ■ desa+mito-AAPH

\*p<0.05  
#p<0.01  
\*\*p<0.005  
##p<0.001

vs. desa

N.D. – not detected

**Figure 10. Effect of mito-AAPH on EV- and desa-expressing WT cells.**

(A) Serial 10-fold dilutions of cells were spotted on SC medium containing 2% galactose as carbon source. Mito-AAPH was spread on the plates immediately before spotting. Plates were incubated at 30°C for 3 days. (B) Heat map and quantitative assessment of individual CL<sub>OX</sub> molecular species in WT cells expressing  $\Delta^{12}$ -desaturase (desa) treated with or without mito-AAPH. (C) Heat map and quantitative assessment of individual PC<sub>OX</sub> molecular species in WT cells expressing desa treated with or without mito-AAPH. (D) Heat map and quantitative assessment of individual PE<sub>OX</sub> molecular species in WT cells expressing desa treated with or without mito-AAPH. (E) Heat map and quantitative assessment of individual PG<sub>OX</sub> molecular species in WT cells expressing desa treated with or without mito-AAPH.

### **2.1.7.5 *cdl1*Δ cells that express Δ<sup>12</sup>-desaturase exhibit decreased levels of PUFA-CLs including TLCL but increased levels of specific peroxidized CL species**

We have previously shown that expression of *CLDI* is highest when cells are actively respiring [70]. These conditions lead to increased generation of ROS and a pro-oxidant environment conducive to enhanced PUFA lipid peroxidation. Increased *CLDI* in these conditions suggests the possibility that Cld1 deacylates peroxidized CL, in which case the loss of *CLDI* would lead to increased content of peroxidized CL. To investigate the role of Cld1 in deacylating peroxidized CL, we expressed the Δ<sup>12</sup>-desaturase in *cdl1*Δ cells.

In *cdl1*Δ +desa, (Figure 11A), the LC-MS spectrum contained the signals from CL species formed through the biosynthesis. By subtracting this spectrum from the spectrum corresponding to the WT cells expressing Δ<sup>12</sup>-desaturase we obtained the differential LC-MS spectrum (Figure 11B) where the increasing red signals correspond to the remodeling products whereas the decreasing blue signals are derived from the substrates of remodeling pathway. In other words, CL species containing saturated and monounsaturated acyl chains were susceptible to remodeling, and the remodeling process yielded CL species with polyunsaturated fatty acyls. Quantitatively, these data are summarized in the heat-map (Figure 11C and Figure 12). PUFA-containing CL species were detected in the Δ<sup>12</sup>-desaturase-expressing *cdl1*Δ cells, likely because some incorporation of PUFA into CL occurs via *de novo* CL biosynthesis. Peroxidized CL species were also detected in *cdl1*Δ cells expressing Δ<sup>12</sup>-desaturase. Surprisingly, although Δ<sup>12</sup>-desaturase-*cdl1*Δ cells had decreased total levels of peroxidizable CL (Figure 11D), they contained significantly more CL<sub>OX</sub> species within PUFA-CL species (CL64:7, CL64:8, CL66:7, CL66:8, CL68:7, CL68:8, CL70:8, and CL72:8) (Figure 13A-B). Notably, mono-hydroperoxy-

CLs were mainly found in *cld1* $\Delta$  (Figure 13A-B), whereas di-hydroperoxy-CLs were predominately generated in WT cells (Figure 13A).

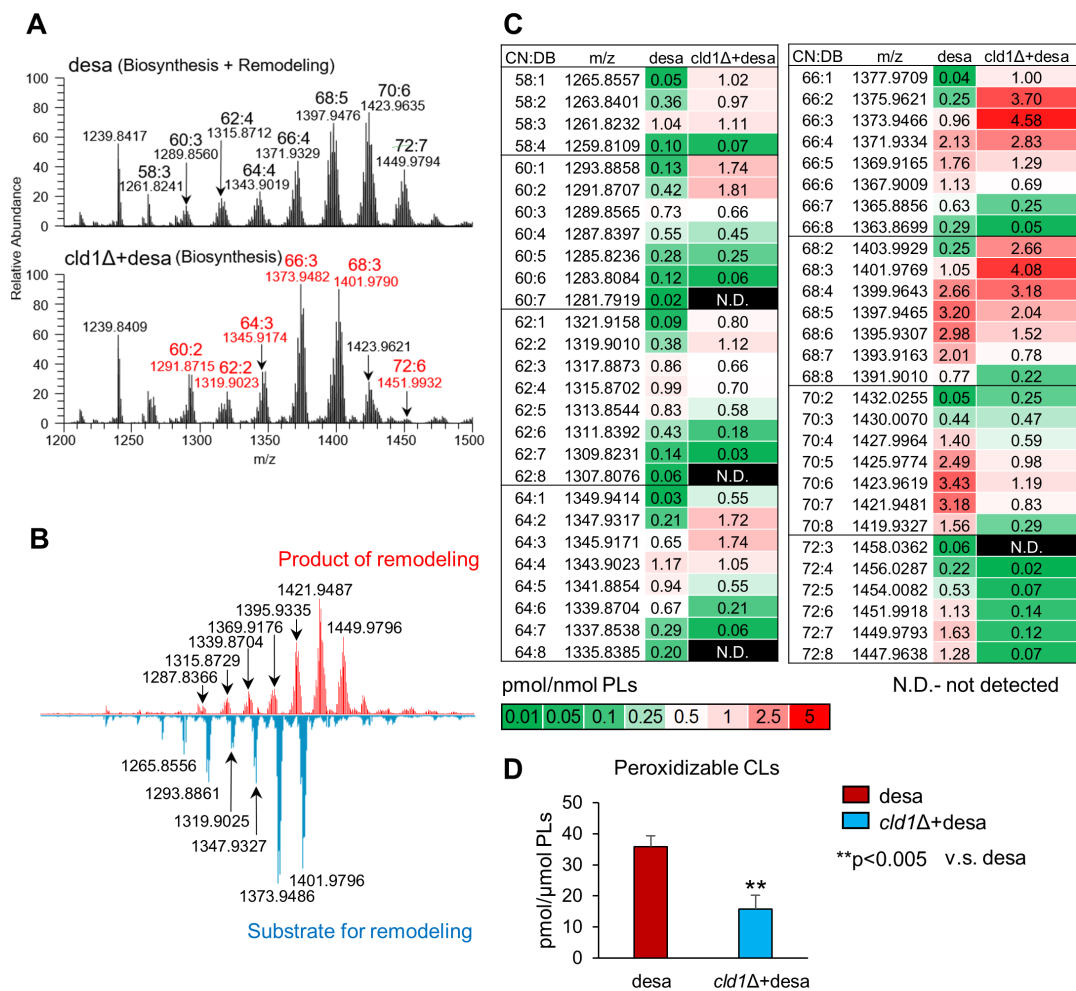


**Figure 11. CL profile analysis of *desa*-expressing WT and *cld1Δ* yeast cells.**

(A) Typical mass spectra of CL species obtained from WT cells expressing desaturase (*desa*) and *cld1Δ* cells expressing *desa* (*cld1Δ+desa*). (B) Differential mass spectral analysis of CL profiles highlights individual CL species that were increased (product of remodeling) or decreased (substrate for remodeling) by the deletion of *CLDI*. Major CL molecular species are identified as: CL60:3 (m/z 1289.8560); CL62:4 (m/z 1315.8712); CL64:4 (m/z 1371.9014); CL66:4 (m/z 1371.9329); CL70:6 (m/z 1423.9635); CL72:7 (m/z 1449.9794); CL60:2 (1291.8715); CL62:2 (m/z 1319.9023); CL66:3 (m/z 1373.9482); CL68:3 (m/z 1401.9790); CL72:6 (m/z 1451.9932). (C) Heat map of CL molecular species of WT or *cld1Δ* cells expressing *desa*. (D) Quantitative assessment of peroxidizable CLs in *desa*-expressing WT and *cld1Δ* yeast cells.

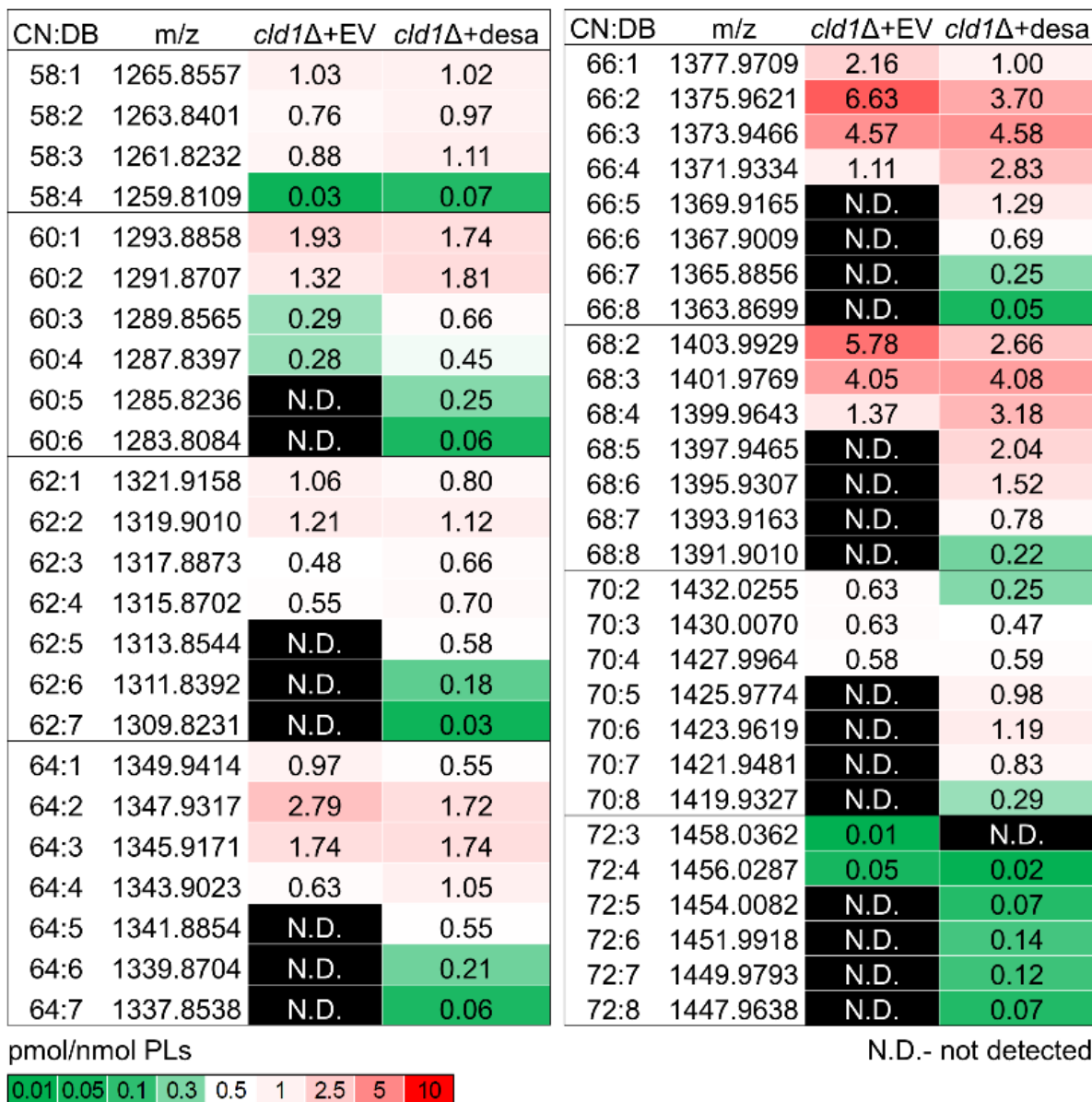


**Figure 12.** Heat maps of CL molecular species in *cld1Δ* cells expressing empty vector (*cld1Δ+EV*) or desaturase (*cld1Δ+desa*).

**A**

CN:DB	# of oxygen	m/z	desa	<i>cld1Δ</i> +desa
60:3	4	1353.8276	65.18	0.86
60:4	4	1351.8127	47.71	N.D.
62:4	4	1379.8433	55.26	1.85
62:5	4	1377.8282	23.97	N.D.
62:6	2	1343.8262	155.68	174.35
64:4	4	1407.8744	116.35	36.15
64:5	4	1405.8598	63.41	1.87
64:6	4	1403.8439	16.13	0.28
64:7	2	1369.8411	0.45	51.30
64:8	2	1367.8262	0.23	40.00
66:3	2	1405.9315	3.28	5.48
66:5	4	1433.8898	196.28	5.33
66:6	4	1431.8749	97.57	3.68
66:7	2	1397.8716	N.D.	91.36
66:7	4	1429.8594	14.68	1.46
66:8	2	1395.8561	13.15	95.41
68:6	4	1459.9053	178.56	3.90
68:7	2	1425.9031	N.D.	36.50
68:7	4	1457.8900	52.42	4.60
68:8	2	1423.8878	9.32	51.64
70:3	4	1493.9848	9.88	N.D.
70:6	4	1487.9366	92.07	0.25
70:7	4	1485.9211	42.02	0.61
70:8	2	1451.9182	0.43	78.85
72:8	2	1479.9482	0.40	164.76

pmol/μmol PLs

N.D. – not detected



**B**

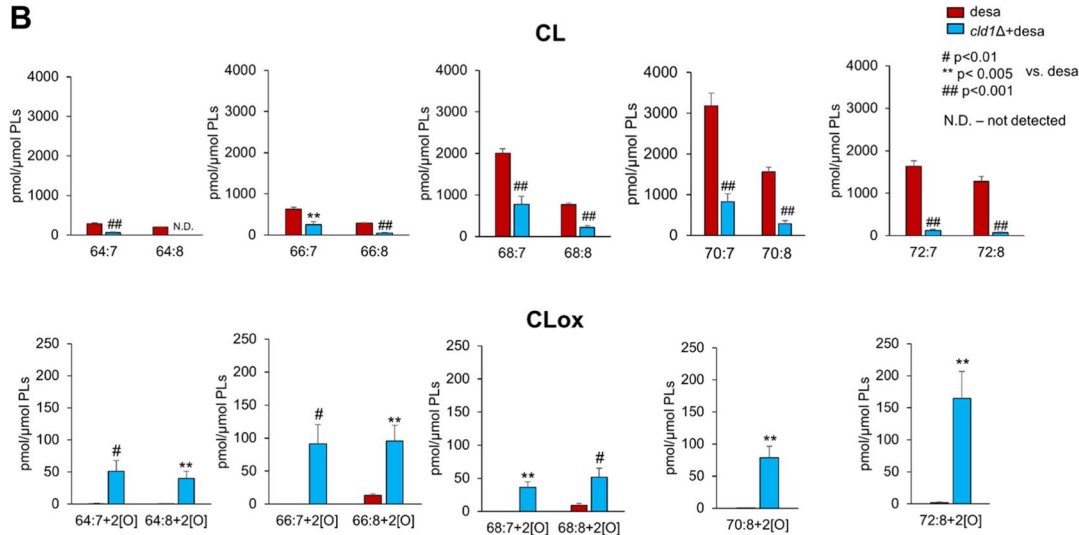


**Figure 13. CL and CLOx in *desa*-expressing WT and *cld1Δ* yeast cells.**

(A) Heat map of CLOx molecular species of WT or *cld1Δ* yeast cells expressing *desa* (B) Quantitative assessment of specific CL and mono-hydroperoxy-CL species (with 7 or 8 double bonds) including tetralinoleoyl-CL (TLCL) in *desa*-expressing WT and *cld1Δ* yeast cells.

### 2.1.7.6 Cld1 mitigates the effects of CL peroxidation

As both non-oxidized as well as peroxidized PUFA-CL species may be hydrolyzed by Cld1, we performed *in vitro* experiments which showed that Cld1 exhibits greater affinity for the latter than for the former (Figure 14A-D). Incubation of DOPC/CL (16:0)<sub>4</sub>; DOPC/CL (18:2)<sub>4</sub> and DOPC/CL (18:2)<sub>3</sub>/18:2-OOH liposomes with Cld1 isolated from *S. cerevisiae* resulted in the accumulation of two molecular species of MLCL respectively. The signals at m/z 1113.7 and 1185.7 corresponded to 16:0/16:0/16:0 and 18:2/18:2/18:2 molecular species. Quantitatively, the larger signals were formed from TPCL and TLCL-OOH respectively and a much weaker signal (also at m/z 1185.7) from TLCL (Fig. 14B). These data indicate that CL (18:2)<sub>4</sub> was a relatively “poor” substrate for Cld1, whereas both CL (16:0)<sub>4</sub> and CL (18:2)<sub>3</sub>/18:2-OOH were readily hydrolyzed by the enzyme (Fig. 14B). We have previously shown that *CLDI* expression is increased during respiratory growth and regulated by the HAP complex [70]. It is plausible that increased *CLDI* expression during respiratory growth mitigates the effects of superoxide anions and their dismutation product H<sub>2</sub>O<sub>2</sub> generated by respiratory complex III. This would likely contribute to the enhanced peroxidation of CL. Consistent with this possibility, WT cells treated in the log phase with H<sub>2</sub>O<sub>2</sub> for 1 hr exhibited a 2-fold increase in *CLDI* expression (Figure 14E). The chronological life span of *cld1Δ* was dramatically decreased by expression of Δ<sup>12</sup>-desaturase (Figure 15A), while the lifespan of wt cells expressing the Δ<sup>12</sup>-desaturase was not affected. Interestingly, while desaturase expression increased the mitochondrial membrane potential and respiratory capacity in wt cells, the mitochondrial membrane potential and respiratory capacity in *cld1Δ* cells were decreased (Figure 15B-C). Taken together, these findings support a role for Cld1 in mitigating the effects of CL peroxidation.

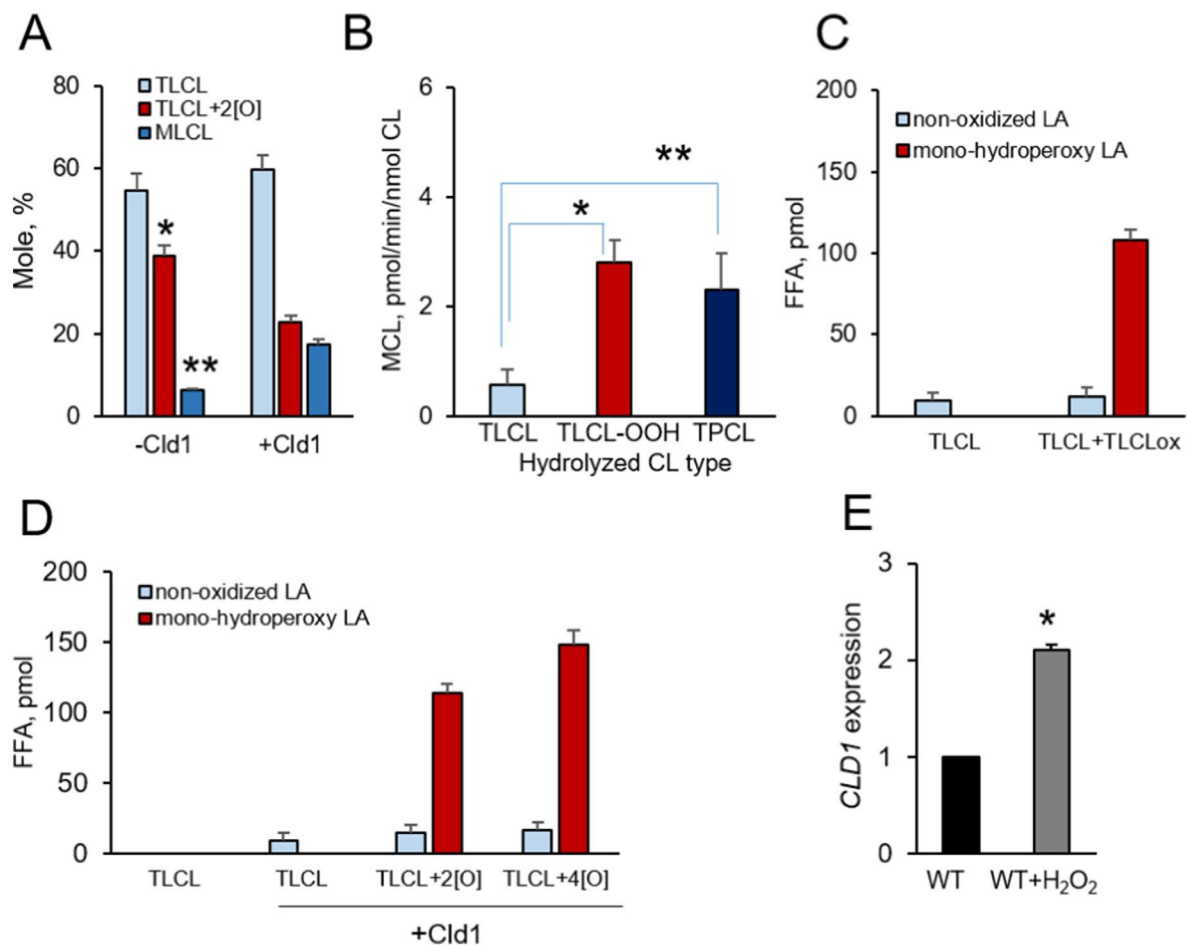


**Figure 14. Cld1 exhibits greater affinity for oxidized than non-oxidized CL in vitro and its expression is increased by supplementation of H<sub>2</sub>O<sub>2</sub>.**

(A) A mixture of 10  $\mu$ M CL that contains TLCL and oxidized TLCL (TLCL<sub>OX</sub>) in HEPES buffer pH 7.4 was incubated at 37 °C for 45 min with Cld1. Total TLCL was extracted by the Folch procedure, and TLCL, TLCL<sub>OX</sub>, and MLCL were quantified by LC-MS. Hydrolysis of CL<sub>OX</sub> was evident by an accumulation of MLCL and concomitant reduction of CL<sub>OX</sub>. n=3, \*p = 0.020, and \*\*p= 0.007, respectively. (B) Liposomes containing DOPC and CL (10  $\mu$ M, 1:1) - DOPC/TPCL; DOPC/TLCL and DOPC/TLCL-OOH were prepared by sonication (Ultrasonic Homogenizer 4710 series, Cole-Parmer Instrument Co., Chicago, IL) and treated with Cld1 (0.5  $\mu$ g of protein) in 50 mM HEPES at pH 7.4, containing 100  $\mu$ M DTPA for 20 min at 37 °C. After extraction, CL hydrolysis was detected by reduction of CL content and accumulation of MCL: ((16:0)<sub>4</sub>  $\rightarrow$  (16:0)<sub>3</sub>; (18:2)<sub>4</sub>  $\rightarrow$  (18:2)<sub>3</sub> and (18:2)<sub>3</sub>/(C18:2-OOH)  $\rightarrow$  (18:2)<sub>3</sub>). n=3, \*p = 0.030, and \*\*p= 0.027, respectively. (C) Isolated Cld1 was incubated with TLCL or with mixture of TLCL + TLCL<sub>OX</sub> (ratios 1:1). (D) Isolated Cld1 was incubated with TLCL, TLCL containing one mono-hydroperoxy-linoleic acid (LA) residue (TLCL+2[O]), or TLCL containing two mono-hydroperoxy-LA residues (TLCL+4[O]). In the presence of CL<sub>OX</sub> (TLCL+2[O] or TLCL+4[O]) Cld1 generated significantly increased free mono-hydroperoxy-LA (m/z 311) than non-oxidized-LA (m/z 279). (E) WT cells were grown to the mid-logarithmic phase and treated with 1 mM H<sub>2</sub>O<sub>2</sub> for 1 hour. Analyses *CLD1* expression in H<sub>2</sub>O<sub>2</sub>-treated cells and non-treated cells was determined using RT-qPCR. \*p = 0.050 vs WT.

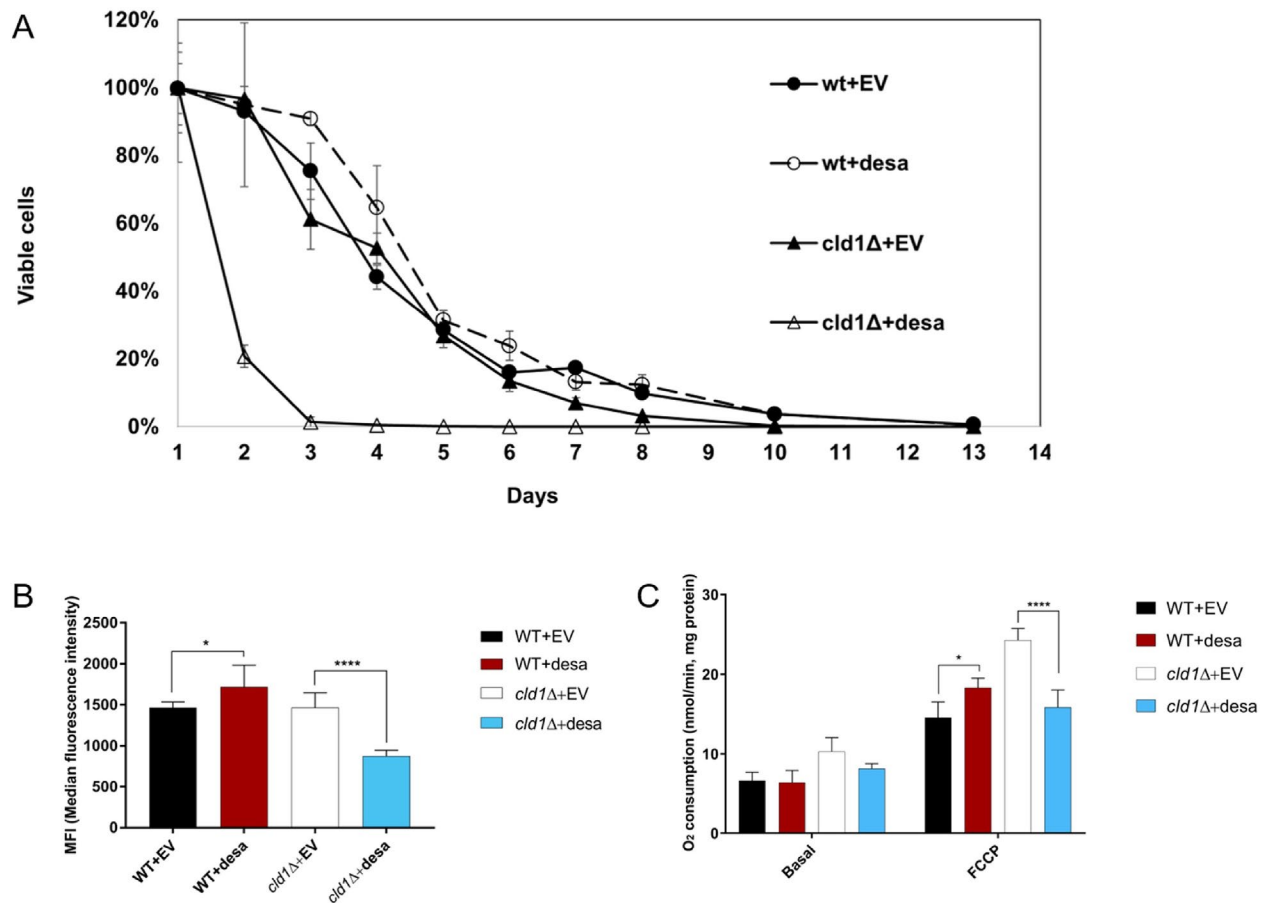


**Figure 15. Analysis of chronological lifespan and mitochondrial functions of desa-expressing yeast cells.**

(A) The chronological lifespan of WT and *cld1Δ* yeast cells expressing desa or EV. The data depicted are representative of three experiments. (B) Mitochondrial membrane potential is increased in WT+desa but reduced in *cld1Δ*+desa. Membrane potential of growing cells was determined by fluorescence quantification of the membrane potential dependent dye TMRM. (C) Mitochondrial respiratory capacity is decreased in *cld1Δ* +desa compared with *cld1Δ*+EV. Cells were grown in synthetic complete medium with galactose as carbon source. Respiration of intact cells was analyzed via the polarographic method. \* $p < 0.05$  versus control ( $n=3$ ).

## 2.1.8 DISCUSSION

This study demonstrates for the first time that  $\Delta^{12}$ -desaturase expression in yeast promotes the formation of PUFA-containing CL species that are readily peroxidized *in vivo* without any prooxidant stimulation. To date, the study of processes governing CL peroxidation and the various cellular signaling functions of CL<sub>OX</sub> and CL<sub>OX</sub>-derived lipid mediators has not been possible using yeast model systems. We have confirmed that 16:2-CoA and 18:2-CoA produced by yeast expressing the  $\Delta^{12}$ -desaturase are incorporated into CL. This likely occurs, in part, during *de novo* synthesis of CL from PUFA-containing PG and CDP-diacylglycerol by CL synthase, with subsequent enrichment of CL with PUFA occurring during CL remodeling.

This is the first study to identify a role for Cld1 in mitigating the effects of CL peroxidation. Previously, we determined that deletion of *CLDI* rescues the respiratory growth defect of tafazzin deficient yeast cells, indicating that an increased MLCL/CL ratio, not a decrease in CL containing unsaturated fatty acyl chains, is detrimental to tafazzin deficient cells [70]. Similarly, a study by Baile and colleagues illustrated that unremodeled and remodeled CL are functionally indistinguishable in yeast [63]. An interesting question arises from these observations: why do yeast require CL remodeling if there is no adaptive advantage of accumulating CL dominated by unsaturated fatty acyl chains? A clue to answering this question comes from our current findings, which indicate that expression of *CLDI* is increased in response to respiratory growth conditions, and this increase is mediated by the HAP and Mig1 transcriptional factors. Baile and coworkers revealed that Cld1 protein level and function are decreased when cells are grown on glucose and increased when grown on the non-fermentable

carbon source, lactate [62]. They observed that CL remodeling is regulated by carbon source and mitochondrial membrane potential. Mitochondria are the major producer of cellular ROS, and CL-hydroperoxides are known to reduce oxidative metabolism by inactivating complex IV [199]. Similarly, respiratory chain defects have been shown to increase ROS production and decrease the membrane potential [200, 201]. These findings support a model in which decreased membrane potential resulting from the accumulation of CL-hydroperoxides serves as a signal to activate CL remodeling. This model is further supported by the notion that CL remodeling may function to remove peroxidized fatty acyl residues from CL, thereby mitigating the downstream consequences of mitochondrial CL-hydroperoxide accumulation, possibly including mitophagy or apoptosis. In mammalian cells, Liu et al. demonstrated that iPLA2 $\gamma$ , a gene product whose function is analogous to Cld1, as the major enzyme responsible for deacylation of oxidized aliphatic chains from CL [202]. Deletion of iPLA2 $\gamma$  results in the accumulation of peroxidized CL in mouse mitochondria when subjected to oxidative stress. However, it is unclear if this model applies to yeast cells because the loss of *cld1* does not cause any detectable functional defects [63]. CL-hydroperoxides are not produced in either WT or *cld1* $\Delta$  cells unless PUFA is supplied in the growth medium or an exogenous-desaturase is expressed [57]. WT yeast cells readily incorporate PUFA into CL, which suggests that CL enriched with PUFA may influence cellular function in *S. cerevisiae*.

In the current study, we used  $\Delta^{12}$ -desaturase-expressing cells to study the functions of Cld1 and CL remodeling in the presence of PUFA-containing CL and reveal that loss of Cld1 causes an accumulation of CL<sub>OX</sub> species among the C18:2-containing-CL and decreased chronological lifespan. These results suggest that Cld1 is involved in removing C18:2-hydroperoxide acyl moieties from CL<sub>OX</sub> species. This is supported by the demonstration that

purified Cld1 has a higher affinity for peroxidized (C18:2)<sub>4</sub>CL than non-peroxidized (C18:2)<sub>4</sub>CL. This may explain the previous observation that *CLDI* expression is upregulated during the stationary phase and that *CLDI* upregulation is respiration dependent [70]. Consistent with this model, H<sub>2</sub>O<sub>2</sub> treatment, which leads to increased oxidative stress, upregulates *CLDI* expression.

In the current study, we found that  $\Delta^{12}$ -desaturase-expressing WT cells exhibit increased sensitivity to mito-AAPH, and treatment with mito-AAPH was associated with an increase in C18:2-containing-CL<sub>OX</sub> species. Increased sensitivity to lipid peroxidation was previously reported using this genetic yeast model [185]. However, our comprehensive lipidomics approach provides compelling evidence to implicate mitochondrial redox reactions and CL peroxidation in contributing to the growth defects observed in  $\Delta^{12}$ -desaturase-expressing WT cells. Excessive generation of CL<sub>OX</sub> in response to mitochondrial oxidative stress likely contributes to the small but significant growth defect observed under these conditions.

The absence of oxidized PS supports a model of mitochondria-localized phospholipid peroxidation. PS species are confined almost exclusively to the cell membrane and secretory vesicles [203]. Although PS is imported into mitochondrial membranes, its intra-mitochondrial transport is linked to enzymatic conversion to PE by PS decarboxylase [204-206]. Thus, the relative abundance of PS within the mitochondrial membranes is minimal when compared to PG, PC and PE [203]. Peroxidation of CL, PG, PC, and PE but not PS suggests that phospholipid peroxidation observed in  $\Delta^{12}$ -desaturase-expressing cells likely occurs within the mitochondrial subcellular compartment. In yeast, beta-oxidation exclusively occurs in the peroxisome, but in mammalian cells, it occurs within both mitochondria and peroxisome. To be specific, short chain fatty acids (C6-C20) are degraded by mitochondrial beta-oxidation, but long chain fatty acid (>C20) are oxidized in the peroxisome. Hydrogen peroxide resulting from oxygen in the first

step of beta-oxidation is the major source of ROS in the peroxisome. Mitochondria, especially the electron transport chain, have long been considered the major source of ROS, including superoxide radicals, hydrogen peroxide, and hydroxyl radicals [207]. In mammalian cells, ROS are predominantly generated from Complex I and Complex III, while in *Saccharomyces cerevisiae* ROS are generated only by Complex III due to the lack of Complex I [208, 209]. Indeed, hydrogen peroxide can easily permeate through the membrane, and peroxisomal catalase deletion in *Saccharomyces cerevisiae* leads to a high level of intracellular hydrogen peroxide [210]. It is possible that ROS generated from peroxisomes contribute to mitochondrial CL peroxidation, and PC/PE peroxidation in yeast. However, the exact contribution of this “trans-organellar” process is not well-understood. The yeast cells used during this study were in stationary phase, during which respiratory activity is relatively high. Respiration takes place in mitochondria, suggesting that the ROS-mediated oxidation of CL, PC, and PE is primarily of mitochondrial origin.

While substantial evidence exists to link the accumulation of mitochondrial hydroperoxy-CLs with cytotoxicity and apoptosis, the precise catalyst of CL peroxidation remains to be fully elucidated. CL peroxidase activity of cytochrome C (cyt C) has been identified as the primary enzymatic mechanism leading to the accumulation of CL<sub>OX</sub> in mammalian mitochondria [53, 81]. Thus, it is tempting to speculate that cyt C is responsible for peroxidation of CL in yeast mitochondria. This is compatible with the indications of the less stringent barrier and easier activation of yeast vs. mammalian cyt C into a peroxidase [211, 212]. Importantly, cyt C does not exhibit appreciable peroxidase activity toward phospholipid species other than CL [213]. Our findings in the  $\Delta^{12}$ -desaturase-expressing WT cells indicate that yeast mitochondria readily accumulate oxidized species of PC and PE, which suggests that enzymatic peroxidation by cyt C

may not be the sole mechanism contributing to the formation of oxidized phospholipids in yeast mitochondria. In mammalian cells, 15-lipoxygenase (15LOX) enzymes are major catalysts of PE peroxidation that participate in ferroptotic cell death [214]. As 15LOX enzymes have not been identified in the yeast genome, the catalysts of phospholipid peroxidation in yeast cells remain to be identified.

Mammalian cells effectively reduce hydroperoxy-phospholipids to hydroxy-phospholipids via a glutathione peroxidase 4 (GPX4)-dependent enzymatic mechanism [214, 215]. However, the yeast glutathione peroxidase enzymes appear to be incapable of reducing hydroperoxy-phospholipids. The predominant accumulation of hydroperoxy-CL, hydroperoxy-PC, and hydroperoxy-PE species in the absence of corresponding hydroxy-phospholipids is indicative of relative inefficiency of this pathway in yeast. *S. cerevisiae* has three glutathione peroxidase enzymes encoded by *GPX1*, *GPX2*, and *GPX3*, all of which are believed to have hydroperoxy-phospholipid reducing glutathione-dependent peroxidase activity. While the loss of *GPX1/2/3* confers sensitivity to supplementation with linolenate [216, 217], our findings in the  $\Delta^{12}$ -desaturase-expressing WT cells indicate that yeast glutathione peroxidase enzymes do not readily reduce endogenously produced hydroperoxy-phospholipids *in vivo*. Given the recently established role of GPX4 in thwarting ferroptotic programmed death via reduction of hydroperoxy-phospholipid [84, 98, 214], it is interesting to speculate if this newly discovered cell death program can be realized in yeast cells [218].

CL peroxidation provides a critical signal for the initiation of apoptosis [81, 219, 220], and therapeutic reduction of CL peroxidation is being explored to treat human diseases associated with apoptosis [221-223]. Hydrolysis of CL<sub>ox</sub> likely serves as a key mitochondrial source of oxidized fatty acid lipid signaling molecules [44]. The expression of exogenous

desaturase enzymes in yeast has variable effects on cellular function and viability depending on the yeast strain, and growth conditions used [125, 126, 185, 224]. Johansson and co-workers observed severe growth defects in cells expressing both  $\Delta^{12}$  and  $\Delta^6$ -desaturase enzymes [126]. Cipak and co-workers report distinct effects of  $\Delta^{12}$ -desaturase expression depending on the yeast strain used [125, 185, 224]. The current study is the first to perform unbiased lipidomic analysis of yeast cells expressing an exogenous desaturase enzyme. Our findings indicate that CL<sub>OX</sub> is readily detected in  $\Delta^{12}$ -desaturase-expressing yeast under normal growth conditions, suggesting that CL peroxidation may occur in the absence of cytotoxic stressors. The  $\Delta^{12}$ -desaturase-expressing yeast provides a powerful tool for the study of CL peroxidation and CL<sub>OX</sub> signaling. Future studies will explore potential inducers of CL peroxidation as well as functions of CL<sub>OX</sub> using this model system.

**2.2 PSEUDOMONAS AERUGINOSA UTILIZES HOST POLYUNSATURATED  
PHOSPHATIDYLETHANOLAMINES TO TRIGGER THEFT-FERROPTOSIS IN  
BRONCHIAL EPITHELIUM.**

Published in:

*The Journal of Clinical Investigation* 2018;128(10):4639–4653

Haider H. Dar, Yulia Y. Tyurina, Karolina Mikulska-Ruminska, Indira Shrivastava, Hsiu-Chi Ting, Vladimir A. Tyurin, James Krieger, Claudette M. St. Croix, Simon Watkins, Erkan Bayir, Gaowei Mao, Catherine Ambruster, Alexandr Kapralov, Hong Wang, Mathew R. Parsek, Tamil S. Anthonymuthu, Abiola F. Ogunsola, Becca A. Flitter, Cody J. Freedman, Jordan R. Gaston, Ted Holman, Joseph M. Pilewski, Joel S. Greenberger, Rama K. Mallampalli, Yohei Doi, Janet S. Lee, Ivet Bahar, Jennifer Bomberger, Hülya Bayır and Valerian E. Kagan

Department of Environmental and Occupational Health and Center for Free Radical and Antioxidant Health, Departments of Computational and System Biology, Cell Biology, Critical Care Medicine, Microbiology and Molecular Genetics, Biostatistics, Medicine, Radiation Oncology, Chemistry, Pharmacology and Chemical Biology, University of Pittsburgh, Pittsburgh University of Pittsburgh, Pittsburgh, PA, USA; Institute of Physics, Nicolaus Copernicus University, Torun, Poland; Department of Microbiology, School of Medicine, University of Washington, Seattle, USA; Department of Chemistry and Biochemistry, University of California, Santa Cruz, CA, USA; Medical Specialty Service Line, Veterans Affairs Pittsburgh Healthcare

System, Pittsburgh, PA, USA; Laboratory of Navigational Redox Lipidomics, Institute of Regenerative Medicine, IM Sechenov Moscow State Medical University, Russian Federation.

### **2.2.1 ACKNOWLEDGEMENT**

This work was supported by NIH (U19AI068021, HL114453-06, NS076511, NS061817, HL136143, and HL086884) and by Russian academic excellence project "5-100."

## 2.2.2 COPYRIGHT

This document is copyright free for educational and scientific development.

Permission was granted for the use from:

*Pseudomonas aeruginosa* utilizes host polyunsaturated phosphatidylethanolamines to trigger theft-ferroptosis in bronchial epithelium. Haider H. Dar, Yulia Y. Tyurina, Karolina Mikulska-Ruminska, Indira Shrivastava, Hsiu-Chi Ting, Vladimir A. Tyurin, James Krieger, Claudette M. St. Croix, Simon Watkins, Erkan Bayir, Gaowei Mao, Catherine Ambruster, Alexandr Kapralov, Hong Wang, Mathew R. Parsek, Tamil S. Anthonymuthu, Abiola F. Ogunsola, Becca A. Flitter, Cody J. Freedman, Jordan R. Gaston, Ted Holman, Joseph M. Pilewski, Joel S. Greenberger, Rama K. Mallampalli, Yohei Doi, Janet S. Lee, Ivet Bahar, Jennifer Bomberger, Hülya Bayır and Valerian E. Kagan. *The Journal of Clinical Investigation* 2018;128(10):4639–4653

Document with permission is on file with Hsiu-Chi Ting

### 2.2.3 NOTE

Corresponding Authors: Hülya Bayır, Department of Environmental and Occupational Health, Public Health Building, 130 De Soto St, Pittsburgh, PA 15261. USA. Phone: 412.692.5164. Email: [bayihx@ccm.upmc.edu](mailto:bayihx@ccm.upmc.edu). Valerian E. Kagan, Department of Environmental and Occupational Health, Public Health Building, 130 De Soto St, Pittsburgh, PA 15261. USA. Phone: 412.624.9700. Email: [kagan@pitt.edu](mailto:kagan@pitt.edu)

#### 2.2.4 ABSTRACT

Ferroptosis is a death program executed via selective oxidation of arachidonic acid-phosphatidylethanolamines (AA-PE) by 15-lipoxygenases. In mammalian cells and tissues, ferroptosis has been pathogenically associated with brain, kidney, liver injury/diseases. We discovered that a prokaryotic bacterium, *Pseudomonas aeruginosa* (*P. aeruginosa*), that does not contain AA-PE, can express lipoxygenase (pLoxA), oxidize host AA-PE to 15-hydroperoxy-AA-PE (15-HOO-AA-PE) and trigger ferroptosis in human bronchial epithelial cells. Clinical *P. aeruginosa* isolates from patients with persistent lower respiratory tract infections induced ferroptosis dependently on the level and enzymatic activity of pLoxA. Redox phospholipidomics revealed elevated levels of oxidized AA-PE in airway tissues from patients with cystic fibrosis (CF) but not with emphysema or CF without *P. aeruginosa*. We believe that the evolutionarily conserved mechanism of pLoxA-driven ferroptosis may represent a potential therapeutic target against *P. aeruginosa*-associated diseases such as CF and persistent lower respiratory tract infections.

## 2.2.5 INTRODUCTION

Ferroptosis is a cell death program that is executed via activation of a selective enzymatic process of lipid peroxidation (LPO) catalyzed by 15-lipoxygenases (15LOX), dioxygenases for polyunsaturated fatty acids (PUFA), under conditions when hydroperoxy-phospholipids cannot be enzymatically inactivated by a specific seleno-peroxidase, glutathione peroxidase 4 (GPX4) [218, 225]. We recently identified the substrates and the products of this process as arachidonoyl (AA)-phosphatidylethanoamine(PE) and 15-hydroperoxy(HOO)-AA-PE, respectively (1, 3). We further discovered that two isoforms of mammalian 15LOX – 15LOX1 and 15LOX2 – form a complex with a scaffold protein, PE-binding protein 1 (PEBP1), that switches the substrate specificity of 15LOX from free AA to AA-PE [33]. While 15LOXes are widely represented in many eukaryotic cells [18, 19, 226], they were also found in prokaryotes, particularly in several genera of bacteria [227, 228]. Surprisingly, 15LOX was also detected in *Pseudomonas aeruginosa* (PA1169, hereafter referred to as pLoxA), an organism that lacks oxidizable PUFA-lipid substrates for 15LOX [20, 34]. Structural and computational studies established significant differences between the mammalian 15LOXes and pLoxA, including a more spacious catalytic “lobby” readily accommodating a bulky PE in the latter [21, 162]. Moreover, endogenous non-PUFA-PE was found to co-crystallize with the protein in spite of the fact that it is a very poor substrate for the enzyme [162].

In attempts to resolve this conundrum, we suggested that, as a bacterial pathogen, *P. aeruginosa* can oxygenate AA-PE in host cells and induce “theft-ferroptosis” by hijacking the mammalian PUFA-PE and death program. Here, we discovered that a biofilm producing mutant of *P. aeruginosa* is capable of inducing ferroptosis in human bronchial epithelial (HBE) cells via

enhanced expression of pLoxA and oxidation of host cell AA-PE to 15-HOO-AA-PE. Clinical *P. aeruginosa* isolates from persistent lower respiratory infection patients caused pLoxA-dependent ferroptosis of HBE cells. By employing global redox phospholipidomics, we further detected elevated levels of 15-HOO-AA-PE in airway tissues from patients with cystic fibrosis (CF) but not from patients with emphysema or CF without *P. aeruginosa* in airway cultures. Assuming that disruption of epithelial barrier and immune-regulatory functions are important for pathogenesis of *P. aeruginosa*-associated respiratory diseases we propose that pLoxA may represent a new therapeutic target.

## 2.2.6 MATERIALS AND METHODS

### 2.2.6.1 Reagents.

Minimal essential medium (MEM) (Thermo Fisher, 11095-080), Fetal calf serum (Gibco, 10437-028), Lysogeny broth (LB) (Sigma, L3152), z-VAD-fmk (Millipore, 627610), necrostatin-1s (BioVision, 2263), bafilomycin-A1 (Sigma-Aldrich, B1793), RSL3 (Selleck chemicals, S8155), ferrostatin-1 (Sigma-Aldrich, SML0583), PD146176 (4079-26-9) and ML351 (847163-28-4) (Cayman Chemicals), 1-stearoyl-2-arachidonoyl-sn-glycero-3-phosphoethanolamine (SAPE) (Avanti Polar Lipids, 850804), bovine serum albumin (BSA) (Sigma), Pierce 660 nm protein assay (Thermo Fisher Scientific, 22660), Pierce BCA protein assay kit (Thermo Fisher Scientific, 23225), MTT (Thermo Fisher, M6494), arabinose (Sigma, A3256), deoxycholic acid (Thermo Fisher, BP349), anti-GPx4 (rabbit monoclonal, abcam, ab125066), anti-ACSL4 (F-4) (mouse monoclonal, sc-365230), anti-LPCAT3 (goat polyclonal, sc-161831) from Santa Cruz, anti-actin (mouse monoclonal, Sigma-Aldrich, A3854, clone AC-15), anti-*Pseudomonas aeruginosa* PA-I galactophilic lectin polyclonal antibody (rabbit polyclonal, Mybiosource, MBS1495605), secondary antibodies, rabbit anti-mouse (A9044), goat anti-rabbit (A0545) and rabbit anti-goat (A5420) were from Sigma-Aldrich.

### 2.2.6.2 Cell Culture.

HBE cells (a human bronchial epithelial cell line originally established by Dr. Dieter Gruenert) were cultured in MEM (Thermo Fisher Scientific) supplemented with 10% fetal calf serum (Gibco), 50 Uml<sup>-1</sup> penicillin-streptomycin (Thermo Fisher Scientific), plasmocin (InvivoGen)

and L-glutamine (Thermo Fisher Scientific). HBE cells till passage 50 were used for experiments.

### **2.2.6.3 Bacterial strains.**

*P. aeruginosa* wild-type (MPAO1), *loxA::Tn* (*PA1169* transposon deletion mutant) (PW3111) and hyper-biofilm mutant (*ΔwspF*) strains were obtained from the *P. aeruginosa* transposon mutant library, The University of Washington (Seattle, WA) [229]. PAO1 isogenic strain, rugose small colony variant MJK8 and its *loxA* deleted strain MJK8 $\Delta$ *PA1169* (herein referred to as MJK8 $\Delta$ *loxA*) were generated as previously described [230].

### **2.2.6.4 *P. aeruginosa* ICU respiratory isolates.**

Tobramycin-resistant *P. aeruginosa* respiratory isolates from intensive care units were identified at the clinical microbiology laboratory of University of Pittsburgh Medical Center (IRB# PRO12060302) and name as TRPA0022-TRPA1122. For confirmation, the isolates were re-identified as *P. aeruginosa* using a commercial biochemical panel (API 20NE system, bioMerieux, Durham, NC). PA14 strain [231] is a reference clinical *P. aeruginosa* strain originally isolated from a burn patient and the fully sequenced genome of PA14 is publicly available.

### **2.2.6.5 *loxA::Tn* Complementation.**

PW3111 (MPAO1 *loxA::Tn*) was complemented with an arabinose-inducible promoter at the chromosomal attTn7 site as previously described using pUC18-miniTn7T-Gm-GW [232]. From genomic MPAO1 DNA, PA119 was amplified using primers attB5-RBS-*loxA*-F and attB2-*loxA*down-R (Table 2), which included the entire *loxA* coding region and introduced a synthetic

ribosomal binding site. The *loxA* amplicon was gel purified and recombined into pDONR221P5P2 (Table 2) using BP Clonase II (Invitrogen). The resulting entry vector, pENTR221L5L2::RBS-*PA1169*, was transformed into *E. coli* DH5 $\alpha$  and insertions were checked by PCR and Sanger sequencing (Eurofins) using primers M13F(-21) and M13R. We used Multisite Gateway Technology (Invitrogen) to recombine pENTR221L1L5r::*araC*-P<sub>BAD</sub> (the plasmid pENTR221L1L5r::*araC*-P<sub>BAD</sub> was a generous gift from Dr. Joe Harrison, Department of Biological Sciences, University of Calgary, Calgary, Canada) and pENTR221L5L2::RBS-*PA1169* with pUC18miniTn7T-Gm-GW, generating the complementation vector pUC18miniTn7T::P<sub>BAD</sub>-*PA1169*. The complementation vector was transformed into *E. coli* DH5 $\alpha$  and plasmids from transformants were sequenced using primers pBAD-F and pUC18BackboneR01. To complement PW3111, we electroporated pUC18miniTn7T::P<sub>BAD</sub>-*PA1169* and pTNS3 into PW3111. Transformants were selected on LB with 30  $\mu$ g/mL gentamycin and colony PCR was performed using primers P<sub>Tn7R</sub> and P<sub>glmSdown</sub> as previously described [232] to identify an insertion at the attTn7 site on the chromosome (Table 2). All the *E. coli* strains, plasmids and primers used for complementation studies are given in Table 2.

**Table 2. Bacterial strains, plasmids, and primers used for *loxA* complementation study.**

Strains	Characteristics	Reference
<i>E. coli</i> DH5 $\alpha$ (Zymo5a)	F- $\phi$ 80lacZ $\Delta$ M15 $\Delta$ (lacZYA-argF)U169 deoR nupG recA1 endA1 hsdR17(rK- mK+) phoA glnV44 (supE44) thi-1 gyrA96 relA1, $\lambda$ -	Zymo Research
<i>E. coli</i> DH5 $\alpha$ pENTR221L5 L2::RBS-PA1169	<i>E. coli</i> harboring pDONR221P5P2 with an attL flanked, 2,070 bp fragment encoding a 12 bp synthetic ribosomal binding site and the 2,058 bp <i>loxA</i> ORF from <i>P. aeruginosa</i> PAO1, KmR	This study
<i>E. coli</i> DH5 $\alpha$ pUC18miniTn 7T::PBAD-PA1169	<i>E. coli</i> harboring a suicide plasmid for inserting arabinose-inducible PA1169 onto the <i>P. aeruginosa</i> chromosome at the attTn7 site, GmR	This study
<i>P. aeruginosa</i> PW3111	MPAO1 with a transposon inserted into PA1169 ( <i>loxA</i> ::Tn)	[229]
<i>P. aeruginosa</i> PW3111 Tn7:PBAD- <i>loxA</i>	MPAO1 with a transposon inserted into PA1169 ( <i>loxA</i> ; PW3111) and complemented with arabinose-inducible <i>loxA</i> at attTn7 site, GmR	This study
Plasmids	Characteristics	
pUC18miniTn 7T-Gm-GW	pUC18-miniTn7T-Gm with a Gateway destination cloning site, ApR, GmR, CmR	[232]
pTNS3	helper plasmid encoding tnsABCD, ApR	[233]
pENTR221L1 L5r:araC-P <sub>BAD</sub>	pDONR221P1P5r with an attL-flanked, 1,192-bp fragment encoding the araC repressor and the P <sub>BAD</sub> promoter, KmR	[234]
pDONR221P5 P2	Multisite Gateway donor vector with attP5 and attP2 recombination sites, CmR, KmR	Invitrogen
pENTR221L5 L2::RBS-PA1169	pDONR221P5P2 with an attL flanked, 2,070 bp fragment encoding a 12 bp synthetic ribosomal binding site and the 2,058 bp <i>loxA</i> ORF from <i>P. aeruginosa</i> PAO1, KmR	This study
pUC18miniTn 7T::PBAD-PA1169	Suicide plasmid for inserting arabinose-inducible PA1169 onto the <i>P. aeruginosa</i> chromosome at the attTn7 site, GmR	This study
Primer	Sequence	Reference
attB5-RBS- <i>loxA</i> -F	ggggacaacttgtatacaaaagttgccag aggaggatattcATGAAACGCAGGAGTGTGC	This study
attB2- <i>loxA</i> down-R	ggggaccacttgtacaagaagctgggtaCGCCCCGTCTCTT TCTC	This study
M13F (-21)	GTAAAACGACGGCCAG	Eurofins
M13R	CAGGAAACAGCTATGAC	Eurofins
pBAD-F	ATGCCATAGCATT TTTATCC	This study
pUC18BackboneR01	GGCCGATTCATTAATGCAGC	This study
PTn7R	CACAGCATAACTGGACTGATTC	[232]
PglmS-down	GCACATCGGCGACGTGCTCTC	[232]

### 2.2.6.6 Abiotic biofilm and supernatant collection.

*P. aeruginosa* strains including the tobramycin resistant clinical isolates were grown overnight in LB at 37°C, 220 rpm. These overnight cultures were diluted in MEM medium (without phenol red), to OD<sub>600</sub> of 0.05 and plated in 96-well vinyl microtiter plates (100 µl per well) (Costar). Bacteria were grown for 24h at 37°C without agitation and the supernatant was collected by centrifugation at 4,000 rpm for 8 min and then frozen before further use in cell death and activity assays. For pLoxA activity assays and treatment of HBE cells, frozen supernatants were thawed and centrifuged at 4,000 rpm for 8 min and protein concentration was estimated by the BCA protein assay (Thermo Fisher Scientific). Supernatants were added to HBE cells containing fresh MEM medium and incubated for 20h followed by cell death assays. We believe this freeze-thaw step was sufficient to prevent survival of any bacteria in the supernatants (Figure 16). In all experiments, control is untreated HBE cells containing media only. Overnight cultures of MJK8 and MJK8 $\Delta$ loxA were re-suspended vigorously before measuring the OD<sub>600</sub>. CFU assay was performed to determine the number of bacteria/ml in the supernatants of *P. aeruginosa* WT,  $\Delta$ wspF and loxA::Tn strains. For this, the supernatants were serially diluted in MEM medium (without phenol red), plated on LB agar plates and incubated overnight at 37°C. For biofilm quantification, after the removal of supernatant, biofilms were washed using deionized water to remove non-adherent bacteria and stained with crystal violet (41%) for 15 min at room temperature. Samples were washed (3x) and biofilms were resuspended in 30% acetic acid and quantified at OD<sub>550</sub> as previously reported [235].

For pLoxA imaging, biofilms were grown on glass cover slips by placing the cover slip vertically in 12 well plates containing WT,  $\Delta$ wspF or loxA::Tn biofilm cultures. After incubation (37° C for 24h), the cover slips were washed with water (2 times) and fixed with

paraformaldehyde (2%) or glutaraldehyde (2.5%) for 30 min and then used for pLoxA staining or for SEM imaging.

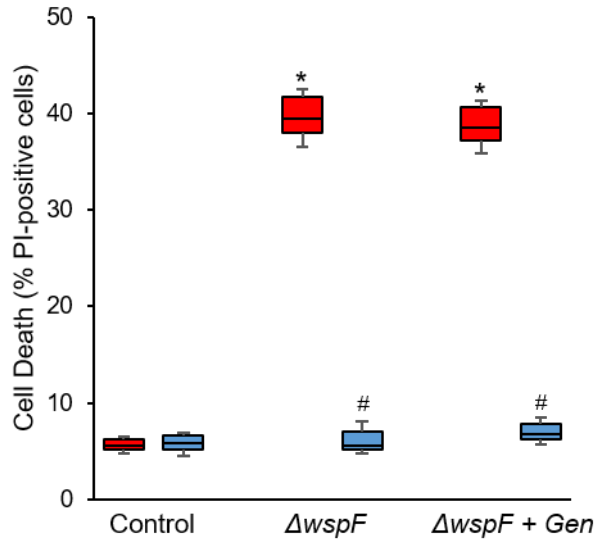


**Figure 16. Cell death induced by  $\Delta wspF$  supernatant is not affected by presence of bacteria in the supernatant.**

HBE cells were treated with  $\Delta wspF$  supernatant alone or with Gentamycin (20  $\mu\text{g/ml}$ ) in the presence or absence of ferrostatin-1(FER). Cells were incubated for 20h and then used for cell death analysis. Data represents mean $\pm$ s.d., \* $p < 0.05$  vs. Control; # $p < 0.05$  vs.  $\Delta wspF$  or  $\Delta wspF + Gen$ . N=3.

#### **2.2.6.7 Biotic biofilm assay.**

HBEs were enzymatically dissociated, expanded in growth media, and seeded onto Trans-well inserts and grown at the air-liquid interface for 7-10 days. Cultures were used when well polarized and differentiated [236]. Biotic biofilm assays were performed as follows: overnight culture of the  $\Delta wspF$  mutant strain *P. aeruginosa* was rinsed once and added to the apical surface of the epithelial cells in 500  $\mu$ l of MEM with 0.4% glutamine at a multiplicity of infection (MOI) of 25. After the 60 min bacterial attachment period, developing biofilms were treated with vehicle or ferrostatin-1 (0.2 and 1.0  $\mu$ M) for the subsequent 5h. At the end of this period, biofilms were removed with 0.1% Triton X-100 and live bacteria were plated in a CFU assay.

#### **2.2.6.8 Knock-down (KD) of *ACSL4* and *LPCAT3*.**

HBE cells were transfected with a mix of two Dicer-substrate short interfering RNAs (*DsiRNAs*) against *ACSL4* (mm.Ri.Acsl4.13. and mm.Ri.Acsl4.13.2) or On target plus SMART pool *LPCAT3* si-RNA (L-010273-01-0005., Dharmacon) or with negative control DsiRNA (51-01-14-04) (Integrated DNA Technology) using Lipofectamine 3000 (Life Technology) according to manufacturer's instructions. Efficiency of KD was determined by Western blotting using antibodies against ACSL4 (1:1,000) and LPCAT3 (1:500).

#### **2.2.6.9 Live-cell imaging.**

To visualize intracellular lipid-peroxidation, HBE cells were seeded in glass-bottomed (35 mm) tissue culture dishes (MatTek Corp., Ashland, MA) and after 48h, cells were pre-stained with Liperfluo (Djindo Molecular Technologies, Inc. Rockville, MD., 10  $\mu$ M) for 30 min, washed and then treated with supernatant collected under biofilm growth conditions from  $\Delta wspF$  strain or

with RSL3 (200 nM). The dish was inserted into a closed, thermo-controlled (37°C) stage top incubator (Tokai Hit Co., Shizuoka-ken, Japan) atop the motorized stage of an inverted Nikon TiE fluorescent microscope (Nikon Inc., Melville, NY) equipped with a 60X oil immersion optic (Nikon, CFI PlanFluor, NA 1.43) and NIS Elements Software. Liperfluo was excited using a Lumencor diode-pumped light engine (SpectraX, Lumencor Inc., Beaverton OR) and detected using an ORCA-Flash 4.0 sCMOS camera (HAMAMATSU Corporation, Bridgewater, NJ) and excitation and emission filters from Chroma Technology Corp. (Bellows Falls, VT). Data were collected every 5 minutes for 4 hours, on approximately 10-20 cells per stage position, with 10-15 stage positions in each of 3 separate experiments per condition. Data were analyzed using NIS Elements (Nikon Inc., Melville, NY).

To monitor cell death, HBE cells were seeded in glass-bottomed partitioned (35 mm) cell culture dishes (Griener Bio-One GmbH., Germany) and after 48h, cells were treated with *ΔwspF* supernatant in presence of Sytox Green and examined for 48h by live cell imaging. Data were collected every 30 min for 48h and analyzed by NIS Elements (Nikon Inc., Melville, NY).

#### **2.2.6.10 Western blotting.**

Total cell lysates were prepared after washing cells with PBS and then adding cell lysis buffer (25mM Tris-HCl, pH 7.5, 150 mM NaCl and 1% SDS) or RIPA buffer (Thermo Fisher Scientific) containing freshly added protease-phosphatase cocktail inhibitor mix (Thermo Fisher Scientific). Samples were boiled at 95°C for 10 min, sonicated to break down DNA. Total protein was estimated by Pierce BCA protein assay kit (23225) and diluted with 2X or 4X Laemmli buffer before loading in Tris-glycine gradient gels (8–16% Tris-Glycine Gels) (Life Technologies). Proteins were transferred to PVDF membrane (Biorad), blocked with milk (5%) in PBST (0.1% Tween) 1h, incubated with primary antibodies (1% BSA in PBST) overnight at

room temperature (RT), washed 3 times and incubated with secondary antibody (1 h) in blocking solution before developing with SuperSignal™ West Pico Chemiluminescent Substrate (Thermo Fisher Scientific).

For analysis of GPX4, HBE cells (80,000 cells per well) were seeded in 6-well plate and samples were collected after 20h of treatment. Quantification of the bands was performed using ImageJ software from NIH ([imagej.nih.gov/ij/](http://imagej.nih.gov/ij/)).

For pLoxA Western blotting, *P. aeruginosa* (WT,  $\Delta$ *wspF*, *loxA::Tn*), MJK8 (WT and MJK8 $\Delta$ *loxA*) and the clinical isolates were grown in biofilm conditions in 3 ml of MEM media or LB media for 24h. After centrifugation, pellet washed with PBS and then resuspended in RIPA lysis buffer or in Laemmli buffer (2X). Cells were lysed by freeze/thaw (3 cycles) and sonication (3 times, 10 sec on, 10 sec off). Supernatants were collected after centrifugation (10 min, 12,000 rpm) and amount of protein estimated as mentioned earlier. Samples in Laemmli buffer were boiled (10 min), sonicated and protein was estimated using Pierce 660 nm protein assay (Thermo Fisher Scientific). Equal amount of protein was loaded in Tris-glycine gradient gels and transferred to PVDF or nitrocellulose membranes (Biorad), blocked with BSA (2.5%) in PBST 2h and incubated with anti-pLoxA antibody (1:1,000) (in 1% BSA in PBST) overnight at RT. Blots were washed (3 times) and incubated for 1h with secondary antibody (1:2,000) in milk (5%) before developing. Bands were quantified by ImageJ software and recombinant pLoxA included in the gels was used to generate a standard curve and determine the amount of pLoxA in clinical isolates.

#### **2.2.6.11 Arachidonic acid supplementation.**

Arachidonic acid (AA) (Sigma-Aldrich, A0281) was added to HBE cells as reported previously [225]. Briefly, suspension of AA was incubated with fatty acid free bovine serum albumin (BSA

5%) to form a complex of AA with BSA. This soluble complex was added to and incubated with HBE cells overnight along with WT,  $\Delta wspF$  or  $loxA::Tn$  supernatants containing 10  $\mu$ g protein, before estimating the cell death by flow cytometry.

#### **2.2.6.12 Cell death assay.**

Propidium Iodide (PI) (Life Technology) staining was used to measure cell death using flow cytometry as described previously [225]. Briefly, HBE cells were plated in 24-well plate (12,000 – 15,000 cells/well). After 48h, cells in fresh media were incubated with *P. aeruginosa* supernatants containing 10  $\mu$ g of protein alone or with indicated treatments for 20h. Cells were trypsinized, centrifuged at 700 x g for 6 min and resuspended in PBS containing PI for 5 min on ice and then monitored by flow cytometry. The gate settings were chosen at 5% or less PI – positive cells for control samples. Annexin V-FITC (BioVision) staining and MTT (3-(4,5-dimethylthiazol-2-yl)-2,5-diphenyltetrazolium bromide) (Invitrogen) cell viability assay were used as described previously [225]. Cell death was calculated as per instructions of the manufacturer.

For ACSL4 and LPCAT3 KD samples, 12h after transfection, cells were seeded in 24 well plates (15,000 per well) and in 6-cm tissue culture dish. After 36h, cells were treated with  $\Delta wspF$  supernatant for 20h and cell death was analyzed by flow cytometry after staining with PI. Samples from 6-cm dish were used for western blotting.

#### **2.2.6.13 Cell death induced by genetically manipulated pLoxA**

Overnight culture of pLoxA deficient ( $loxA::Tn$  (PW3111)) and complemented (PW3111 Tn7::*loxA*) strains were re-inoculated at an OD<sub>600</sub> of 0.05 and grown in biofilm conditions in presence of 0.1% arabinose for 24h. Cultures were centrifuged and the pellet was washed with

PBS, then resuspended in PBS containing protease inhibitors. Cells were lysed by freeze/thaw method as mentioned earlier. Cell supernatants were collected after centrifugation (10 min, 12,000 rpm) and protein amount estimated by BCA protein assay (23225). Equal amount of protein (100  $\mu$ g) was incubated with SAPE (100  $\mu$ M), in 150 mM borate buffer (pH 9.0) containing 0.02% deoxycholate for 30 min at RT under constant supply of oxygen. The reaction mix was added to RSL3 (20 nM) pre-treated HBE cells (4h) with or without ferrostatin-1 and incubated for 2h in the absence of serum. Then serum was added back to the final concentration of 10% and the cells were incubated for 20h before cell death measurements.

#### **2.2.6.14 Ferroptosis induced by exogenous 15-HOO-AA-PE**

HBE cells were pre-treated with RSL3 (20 nM) for 4h and then incubated with 15-HOO-AA-PE (0.75  $\mu$ M) for 2h in the absence of serum. After adding back serum (10% final concentration), 15-HOO-AA-PE sensitized cells were then treated with equal amounts of supernatant (5  $\mu$ g) either from *loxA::Tn* or WT in the presence or absence of ferrostatin-1 and incubated overnight before cell death assays.

#### **2.2.6.15 GSH measurements.**

After incubations, cells were suspended in 80  $\mu$ l PBS, freeze/thawed at -80°C and mildly sonicated on ice. For GSH analysis (run in triplicates) 15  $\mu$ l of sample was incubated in PBS with 10 mM Thiol Fluorescent Probe IV (Millipore) for 15 min. Then fluorescence was measured with Cytation 5 imaging reader by using an excitation wavelength of 535 nm and an emission wavelength of 585 nm. Protein concentration was measured by Bradford Protein Assay (Bio-Rad).

#### **2.2.6.16 Assessment of pyocyanin.**

UV-Vis spectra of chloroform extracts from clinical isolates were performed in the range of 300-800 nm. The total concentration of pyocyanin was determined in chloroform extracts dried and re-dissolved in methanol by absorbance at 690 nm using molar extinction coefficients of 5816 [237].

#### **2.2.6.17 AA and AA-PE docking to pLoxA.**

Ligand docking has been performed using the SMINA package[238], which is customized to better support scoring function and high-performance energy minimization. The structure used for pLoxA was 4G32 [162]. Five runs each for AA and AA-PE were performed, and the top binding pose (lowest energy) was considered for statistical purposes.

#### **2.2.6.18 Sequence alignment, generation of sequence similarity map and phylogenetic tree construction.**

A multiple sequence alignment (MSA) of lipoxygenase domains was downloaded from the Pfam protein families database [239] and analyzed using ProDy [240]. The MSA was refined by removal of poorly aligned and highly similar sequences, resulting in a final alignment of 218 sequences that was more amenable to further analysis. This was followed by alignment and sorting of the sequences with MUSCLE [241, 242] and manually curated using UniPro UGENE [243]. The resulting alignment was then fed back into ProDy for additional analysis including production of the sequence identity matrix shown in Figure 25A.

### **2.2.6.19 Gaussian Network Model (GNM) and Anisotropic Network Model (ANM) analyses for protein dynamics.**

The analysis of ANM[244] and GNM[245] was done using the ProDY API. Identification of relative modes of motion along the principle mode was done using GNM. In this model, the positive (red) and negative (blue) regions indicate the structural regions which are subject to correlated (positive) or anticorrelated (negative) motions. The theory of GNM and ANM can be found in [244, 245] respectively. Movie was generated using the ANM implemented in the DynOmics server [246]. Structural visualization and analysis were performed using ProDy.

### **2.2.6.20 Expression and purification of pLoxA.**

pLoxA with a His<sub>6</sub> tag was purified using NTA-Ni affinity chromatography, as described previously [22, 33]. Briefly, pet151/His6-pLoxA plasmid containing *Escherichai coli* BL21 (DE3) was grown to OD<sub>600</sub> of 0.6 at 37 °C and induced by incubating the culture at low temperature (20°C) overnight. Pellet was collected by centrifugation (5,000 x g, 10 min), resuspended in buffer A (25 mM HEPES (pH 7.5), 150 mM NaCl) and sonicated to lyse the cells. Lysate was centrifuged at 40,000 x g for 25 min and the supernatant was loaded onto an NTA-Ni affinity column, washed with lysis buffer and the protein eluted with a gradient of 0 to 500 mM imidazole in buffer A. Fractions containing pLoxA were pooled together and preserved in 10% (v/v) glycerol and stored at -80°C for further use.

### **2.2.6.21 pLoxA antibody purification.**

pLoxA antibody against recombinant purified pLoxA was raised and purified from rabbit whole blood by Pocono Rabbit Farm and Laboratory as described previously [22]. Briefly, recombinant pLoxA (3mL of 2mg/mL) was immobilized using Pierce Aminolonk immobilization kit

following manufacturer's recommendations. After loading 4 mL of rabbit serum, column was washed with PBS (7 mL), 1M NaCl (1 mL) and PBS (7 mL) and finally eluted with glycine (6 mL). Fraction with more than 0.05 mg/mL of protein were pooled and stored at -80°C in presence of 10% glycerol.

#### **2.2.6.22 Liposome preparation.**

Liposomes of DOPC/SAPE (1:1) or DOPC/AA (1:10) were prepared using sonication method. Briefly, 1,2-dioleoyl-PC (DOPC) and 1-stearoyl-2-arachidonyl-PE (SAPE) (Avanti Polar Lipids Inc., Alabaster, AL), lipids were dried under nitrogen and resuspended in PBS (pH 7.4) prepared fresh under oxygen flow. Lipids were vortexed and then sonicated using Torbeo ultra cell disruptor (36180-series) with maximum power for 10 min on ice.

#### **2.2.6.23 Oxidation of AA and AA-PE by *P. aeruginosa* supernatant or pLoxA in a model system.**

Lipoxygenase activity of the *P. aeruginosa* supernatants (WT,  $\Delta wspF$  and  $loxA::Tn$ ) was assessed by formation of primary products of AA oxidation: 15-HpETE or PE (C18:0/15-HpETE) that were detected by reverse phase LC/MS. Briefly, supernatants were incubated with liposomes (DOPC/AA or DOPC/SAPE) in the presence of 0.5  $\mu$ M 15-HpETE, 100  $\mu$ M DTPA in 20 mM HEPES pH 7.4 at 37°C for 10 min. To prevent conversion of 15-HpETE to secondary products during incubation, HEPES buffer included 100  $\mu$ M DTPA (for transition metals chelation) that has been saturated with oxygen (before addition of supernatants or pLoxA). For oxidation of AA-PE with purified recombinant pLoxA, 400 nM of enzyme was incubated with DOPC/SAPE (1:1) liposomes along with 0.5  $\mu$ M 15-HpETE, 100  $\mu$ M DTPA in 20 mM HEPES

pH 7.4 at 37°C for 10 min. At the end of incubation AA and PE as well as their oxygenated products were extracted by Folch [247] procedure and analyzed by LC/MS.

#### **2.2.6.24 Determination of pLoxA activity in *P. aeruginosa* clinical isolates.**

Clinical isolates (50 µl) were mixed in 1:1 ratio with 20 mM HEPES buffer pH 7.4, containing 100 µM DTPA, 10 µM AA (arachidonic acid), 0.5 µM 15-HOO-AA-PE and incubated at 37 °C during 10 min. At the end of incubation AA and its oxygenated products were extracted by Folch procedure [247] and analyzed by LC/MS. The data were normalized to the amount of protein and represented as AA<sub>oxidation</sub> (pmol/min/µg of protein).

#### **2.2.6.25 Redox phospholipidomics.**

MS of PLs was performed on an Orbitrap<sup>TM</sup> Fusion<sup>TM</sup> Lumos<sup>TM</sup> mass spectrometer (ThermoFisher Scientific). Phospholipids were separated on a normal phase column (Luna 3 µm Silica (2) 100Å, 150 x 2.0 mm, (Phenomenex) at a flow rate of 0.2 mL/min on a Dionex Ultimate 3000 HPLC system at 35 °C. Gradient solvents A: propanol:hexane:water (285:215:5, v/v/v) and B: propanol:hexane:water (285:215:40, v/v/v) containing 10 mM ammonium acetate were used. The column was eluted for 0-23 min with a linear gradient from 10% to 32% B; 23-32 min from 32 to 65% B; 32-35 min from 65 to 100% B; 35-62 min held at 100% B; 62-64 min from 100% to 10% B followed by and equilibration from 64 to 80 min at 10% B. The instrument was operated with ESI probe in negative mode. Analysis of data was performed using software package Compound Discoverer<sup>TM</sup> (ThermoFisher Scientific) with an in-house generated analysis workflow and oxidized phospholipid database. Lipids were filtered by retention time and confirmed by fragmentation analysis.

#### **2.2.6.26 Analysis of AA and its oxidation products.**

AA and AAox were analyzed by LC/MS using Dionex Ultimate TM 3000 HPLC system coupled on-line to Q-Exactive hybrid quadrupole-orbitrap mass spectrometer (ThermoFisher Scientific, San Jose, CA) using a C18 column (Accliam PepMap RSLC, 0.3 mm x 15 cm, ThermoFisher Scientific). Gradient solvents (A: Methanol (20%)/Water (80%) (v/v) and B: Methanol (90%)/Water (10%) (v/v)) with 5 mM ammonium acetate were used. The column was eluted at a flow rate of 12  $\mu$ L/min using a linear gradient from 30% solvent B to 95% solvent B over 70 min, held at 95% B from 70 to 80 min followed by a return to initial conditions by 83 min and re-equilibration for an additional 7 min. Spectra were acquired in negative mode with the scan range of 150-600  $m/z$ , maximum injection time 100 ms and resolution of 1400,000. An isolation window of 1.0 Da was set for the MS and MS2 scans with an inclusion list of AA oxygenated products. Capillary spray voltage was set at 2.6 kV, and capillary temperature was 250°C. The S-lens Rf level was set to 60. Analytical data were acquired and analyzed using Xcalibur software.

#### **2.2.6.27 Statistical analysis.**

All the data are shown as means $\pm$ s.d. from at least three experiments (biological replicates) unless otherwise specified. Statistical analysis was performed using SPSS software 25 (IBM Corporation, Armonk, NY). One-way ANOVA followed by Fisher-LSD post-hoc analysis was used for multiple group comparisons. The threshold of significance was set at  $p < 0.05$ . Sample sizes (n) are indicated in the figure legends. In the box plots, the boundaries of the box represent 1<sup>st</sup> quartile (bottom boundary) and 3<sup>rd</sup> quartile (top boundary), the band represents the median, and the whiskers represent the maximum and minimum values.

For correlation analysis, first we checked if a Box-Cox transformation [248] was necessary to make the percent of ferroptotic cell death variable normally distributed, using

PROC TRANSREG in SAS 9.4 software (SAS Institute Inc. Cary, NC). It was found that the data could be regarded as normally distributed after being raised to the power of 0.25. We studied the effect of the following factors on the percent of ferroptotic cell death: pLoxA amount, pLoxA activities (15LOX activity and 5LOX activity), amount of pyocyanin in *P. aeruginosa* supernatants and GSH contents in HBE cells after treatments. First, the univariate effect of each factor was studied with the linear regression for the transformed percent of ferroptotic cell death. Variables from univariate models that had a p-value of less than 0.1 were considered for inclusion in the multivariate regression analysis. Then we performed the multivariate analysis, using the stepwise variable selection method to find a best linear regression model for this transformed endpoint. In the stepwise procedure, variables were removed from the model if the associated p-value was greater than 0.05. All p-values reported are two-sided.

#### **2.2.6.28 Study approval.**

All human samples were obtained from human volunteers who provided written informed consent prior to their participation in the study. All studies were approved by the Institutional Review Board (IRB) of the University of Pittsburgh (Pittsburgh, PA).

## **2.2.7 RESULTS**

### **2.2.7.1 Biofilm-producing prokaryote *P. aeruginosa* utilizes pLoxA to induce ferroptotic death in HBE cells**

Transition of *P. aeruginosa* from planktonic to biofilm growth is associated with an ~~sharp~~ increase in expression of its lipoyxygenase (*ploxA*) gene [22]. Given recent discovery of the leading role of human lipoyxygenases (15LOX1 and 15LOX2) in triggering ferroptotic cell death

program [33] we asked whether *P. aeruginosa* can induce ferroptosis in host HBE cells. Like many Gram-negative bacteria, *P. aeruginosa* produces and releases into the environment membrane vesicles containing many intracellular proteins, including pLoxA [249, 250]. These vesicles could be isolated as supernatants after centrifugation of growing cultures. Given the high prevalence of inactivating mutations of *wspF* gene in CF clinical isolates and its hyper-biofilm nature [230, 251, 252], we tested supernatant from  $\Delta$ *wspF* mutant of *P. aeruginosa* grown in biofilm conditions as inducer of ferroptosis in HBE target cells. Supernatants from the  $\Delta$ *wspF* mutant were significantly more efficient in inducing cell death preventable by a specific inhibitor of ferroptosis, ferrostatin-1, than WT supernatants (Figure 17A). Notably, the planktonic supernatants did not induce this type of cell death (Figure 18A). By employing several commonly used inhibitors of alternative cell death programs - z-VAD-fmk (for apoptosis) [105], necrostatin-1s (for necroptosis) [253] and bafilomycin-A1 (for autophagic death) [254] - we investigated the nature of the death pathway triggered by the  $\Delta$ *wspF* mutant (Figure 17B). In contrast to ferrostatin-1, none of the tested inhibitors revealed significant suppression of cell death induced by  $\Delta$ *wspF* supernatant as evidenced by PI, MTT and PI/Annexin V double staining assessments (Figure 17B and Figures 18B, C and D).

To test the involvement of pLoxA in ferroptotic death, we analyzed the level of the protein in lysates of WT,  $\Delta$ *wspF* and *loxA::Tn* (PW3111) *P. aeruginosa*. Expectedly,  $\Delta$ *wspF* mutant contained markedly higher levels of pLoxA than WT strain (Figure 19A). Similarly, larger amounts of pLoxA were found in biofilms formed by  $\Delta$ *wspF* mutant than by WT strain (Figure 17C). No detectable signals were found in lysates of a pLoxA deficient *loxA::Tn* (*PA1169* transposon deletion mutant, PW3111) strain which did not affect abiotic biofilm

formation compared to WT parent strain [22] (Figure 17C, SEM images F & I and Figure 19B). To assess the oxygenase enzymatic activity, we performed liquid chromatography mass spectrometry (LC-MS)-based analysis of the products generated by WT,  $\Delta wspF$  mutant and  $loxA::Tn$  mutant (Figure 17D). We employed two substrates, free AA (Figure 17D, left panel and Figure 19C) and AA esterified into PE (AA-PE) (Figure 17D, right panel and Figure 19D) and determined that the oxygenation activity of the  $\Delta wspF$  mutant was more than an order of magnitude greater than that of the  $loxA::Tn$  mutant. Given that, the mutant devoid of pLoxA induced necroptotic but not ferroptotic cell death (Figure 17A and Figure 19E), we concluded that the presence of pLoxA is indispensable for generating pro-ferroptotic signals.

To examine whether exogenous pLoxA in *P. aeruginosa* supernatants is the major contributor to ferroptosis in HBE cells, we studied the effects of two specific small-molecule inhibitors of mammalian 15LOX, PD146176 and ML351 [105, 255]. In agreement with previous reports [225], ferroptosis induced in HBE cells by an inhibitor of GPX4, RSL3, was markedly suppressed by both inhibitors (Figure 17E, left panel). In contrast, both mammalian 15LOX specific inhibitors, which do not target pLoxA, were inept in protecting against *P. aeruginosa* induced ferroptosis (Figure 17E, right panel). However, baicalein, a non-specific lipoxygenase inhibitor, suppressed cell death induced by both RSL3 and *P. aeruginosa* (Figure 19F).

To further scrutinize the role of pLoxA in ferroptosis we used two genetic approaches. First, we generated a  $loxA::Tn$  complemented strain (PW3111 Tn7::*loxA*) expressing pLoxA. Bacterial cell lysates prepared from complemented PW3111 Tn7::*loxA* and pLoxA-deficient  $loxA::Tn$  (PW3111) strains grown in biofilm conditions were incubated with the pLoxA substrate – stearoyl-arachidonoyl-PE (SA/AA-PE) to generate the pro-ferroptotic signal 15-HOO-SA/AA-PE. We added this reaction mixture to HBE cells pre-treated with RSL3 in the presence or

absence of ferrostatin-1. Cell lysate from pLoxA expressing complemented strain induced cell death which was rescued by ferrostatin-1 while lysate from pLoxA deficient strain (*loxA::Tn*) did not induce ferroptosis (Figure 17F and Figures 19G and 19H). Second we used a PAO1 isogenic strain - rugose small colony variant MJK8 and its *loxA* deleted strain MJK8 $\Delta$ PA1169 [230] (herein referred to as MJK8 $\Delta$ *loxA*). Supernatants from MJK8 strain induced cell death prevented by ferrostatin-1 while the MJK8 $\Delta$ *loxA* supernatant did not induce ferroptotic cell death of target HBE cells (Figure 17G and Figure 19I).

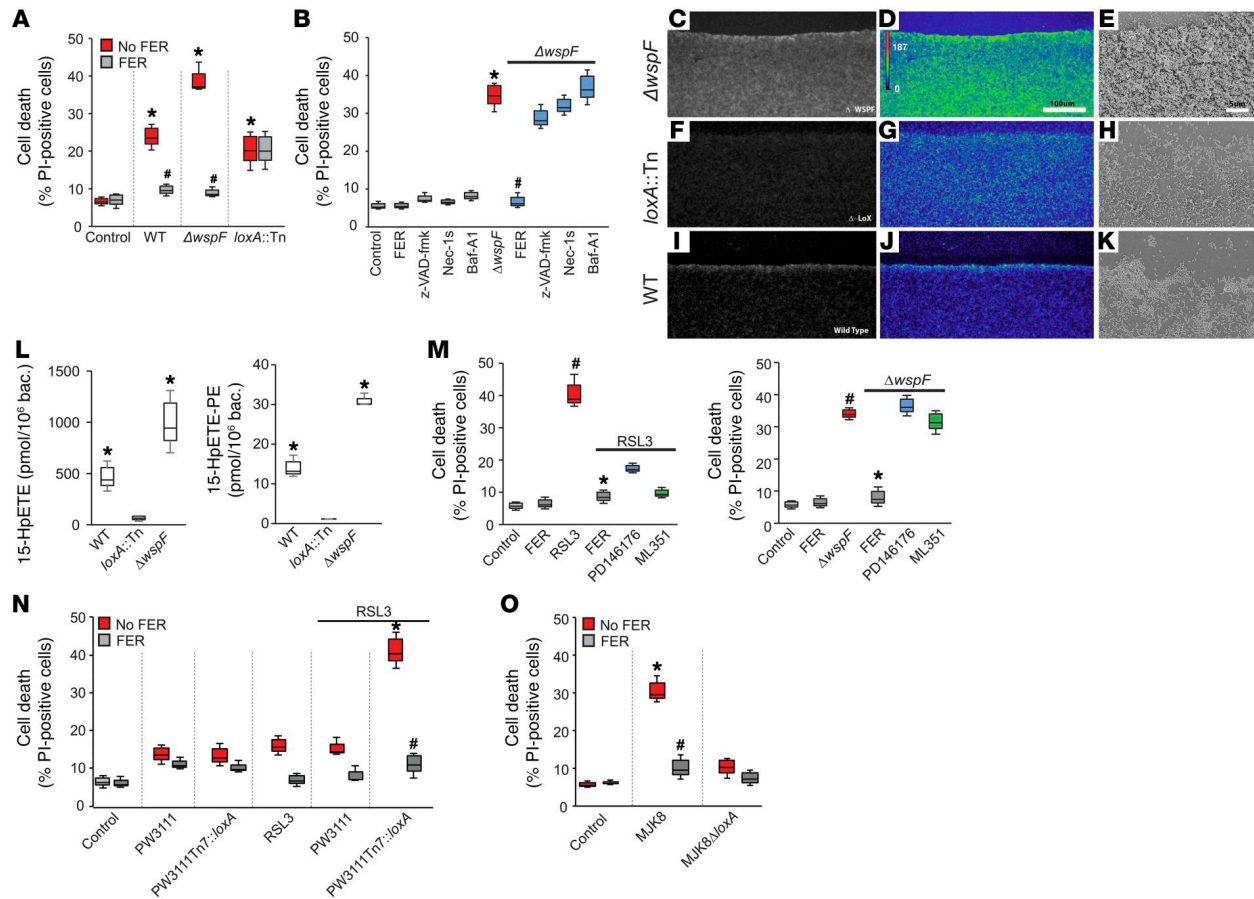


**Figure 17. pLoxA is required for *P. aeruginosa* supernatant induced ferroptosis.**

(A) HBE cells were treated with supernatants (10  $\mu$ g each) from WT,  $\Delta$ wspF or pLoxA deficient mutant *loxA::Tn* (PW3111) with or without ferrostatin-1 (FER, 0.2  $\mu$ M). Cell death (20h) assessed by propidium iodide (PI); means $\pm$ s.d., \*p<0.05 vs. control (untreated HBE cells); #p<0.05 vs. corresponding no FER treatment, N=3. (B)  $\Delta$ wspF supernatant alone or with z-

VAD-fmk (20  $\mu$ M), Nec-1s (20  $\mu$ M), Baf-A1 (1 nM). FER, positive control; means $\pm$ s.d., \* $p$ <0.05 vs. control (untreated); <sup>#</sup>  $p$ <0.05 vs.  $\Delta$ *wspF* only, N=3. **(C)** Representative fixed Biofilms on glass cover-slips stained with anti-pLoxA antibodies (Green) (B, E & H) or analyzed by SEM (C, F & I) (out of 3 performed) **(D)** Dioxygenase activity: WT,  $\Delta$ *wspF* or *loxA*::Tn supernatants were incubated with DOPC/AA (1:10) or DOPC/SAPE (1:1) liposomes (10 min, 37°C). AA oxidation product, 15-HpETE (Left panel), or HpETE-PE from AA-PE (Right panel) assessed by LC-MS; normalized to bacteria/ml of supernatant; \* $p$ <0.05 vs. *loxA*::Tn supernatant, N=3. **(E)** Effect of 15LOX specific inhibitors (PD146176 and ML351; 1.0  $\mu$ M) on  $\Delta$ *wspF*-ferroptosis. RSL3 (200 nM, left panel) was a positive control (both inhibitors were effective against host 15LOX); means $\pm$ s.d., <sup>#</sup>  $p$ <0.05 vs. control (untreated); \* $p$ <0.05 vs. RSL3 or  $\Delta$ *wspF*-supernatant, N=3. **(F)** Bacterial cell-lysates (pLoxA deficient or complemented, 100  $\mu$ g each) were incubated with SAPE (100  $\mu$ M, 30 min) and then added to RSL3 (20 nM) pre-treated HBE cells with or without FER (0.2  $\mu$ M). Means $\pm$ s.d., \* $p$ <0.05 vs. RSL3; <sup>#</sup>  $p$ <0.05 vs. no FER PW3111 Tn7-*loxA*, N=3. **(G)** HBE cells were incubated with supernatant from MJK8 or its *loxA*-knock out strain (MJK8 $\Delta$ *loxA*) in the presence or absence of FER (0.2  $\mu$ M). means $\pm$ s.d., \* $p$ <0.05 vs. control (untreated HBE cells); <sup>#</sup>  $p$ <0.05 vs. no FER MJK8 supernatant, N=3. (1-way ANOVA for **A**, **B**, **D**, **E**, **F** and **G**)

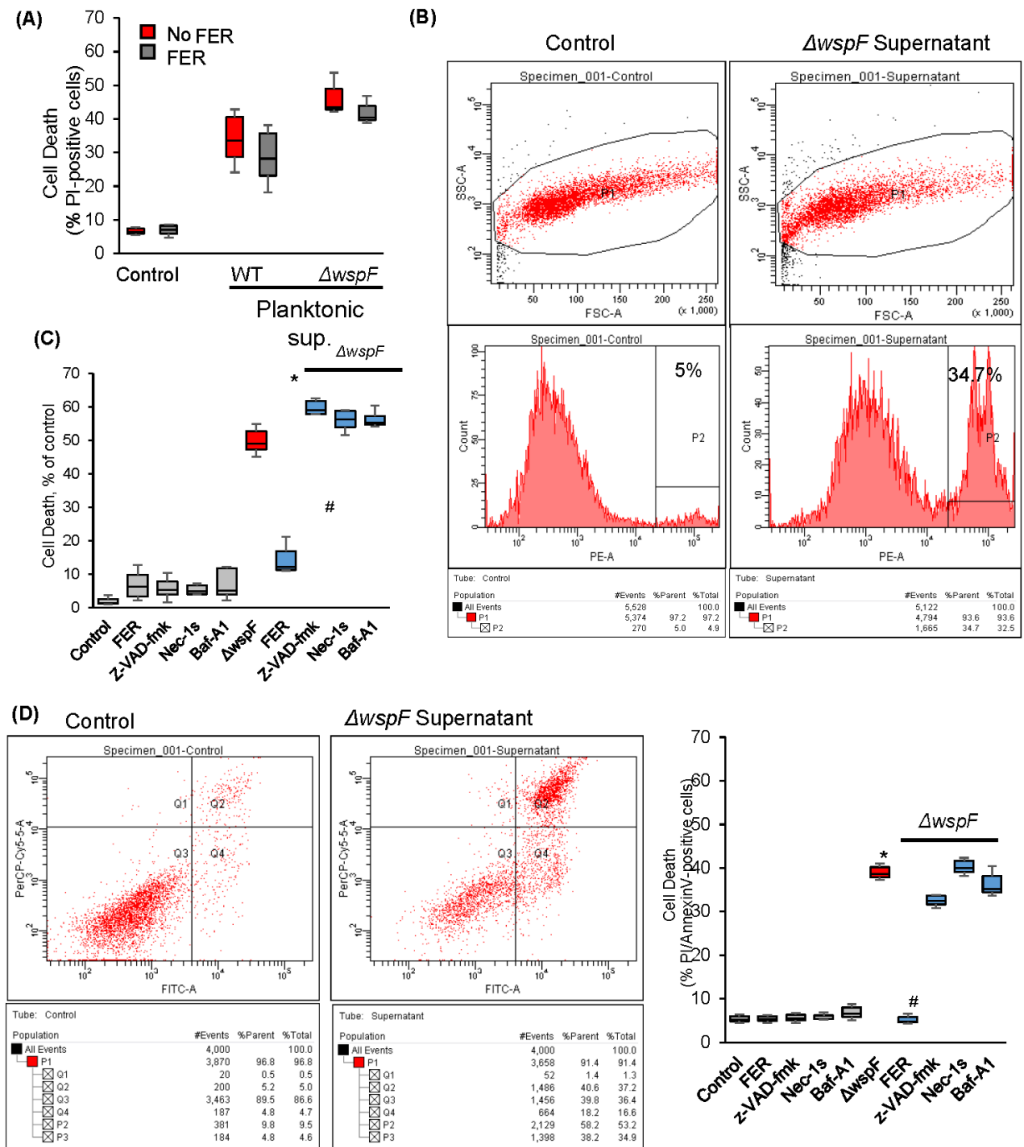


**Figure 18. *P. aeruginosa* supernatant induced cell death is rescued by ferrostatin-1.**

(A) HBE cells were treated with *P. aeruginosa* WT or  $\Delta wspF$  mutant supernatants (Sup.) collected in planktonic growth conditions in the presence or absence of a ferroptosis inhibitor, ferrostatin-1 (FER, 0.2  $\mu$ M) for 20h at 37°C. Cell death was monitored after PI-staining by flow-cytometry. Data represent means $\pm$ s.d., N=3. (B) Representative FACS plots showing the settings of gating used for cell death analysis using PI-staining. Control (Left panel) and  $\Delta wspF$  supernatant (Right panel). (C & D) HBE cells were incubated with  $\Delta wspF$  supernatants alone or with z-VAD-fmk (20  $\mu$ M), Nec-1s (necrostatin-1s, 20  $\mu$ M) or Baf-A1 (bafilomycin-A1, 1 nM). FER was used for comparative assessments of ferroptotic cell death (“positive control”). Cell death was assessed by MTT assay (C) or PI/Annexin V double-staining (D) (Right panel). Data represent mean $\pm$ s.d., \*p<0.05 vs. control (untreated); #p<0.05 vs.  $\Delta wspF$  only N=3. (D) Representative PI/Annexin V double staining FACS plots for control and  $\Delta wspF$  supernatant (Left panel).

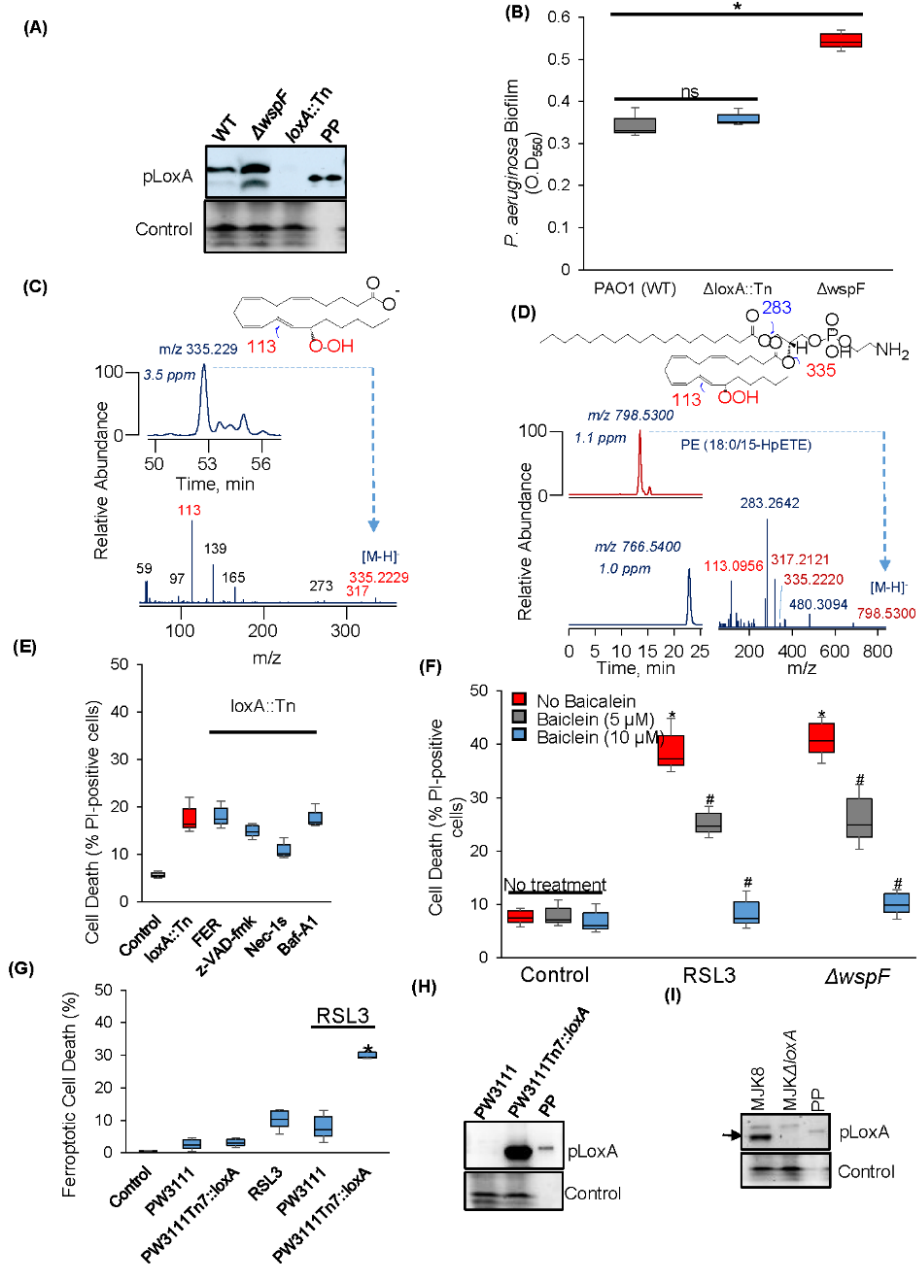


**Figure 19. pLoxA is required for *P. aeruginosa* supernatant induced ferroptosis.**

(A) Expression of pLoxA in the  $\Delta wspF$  mutant. Western blots of pLoxA in lysates of WT,  $\Delta wspF$  and  $loxA::Tn$  strains from biofilm cultures (Upper panel), PP is purified pLoxA protein. Control is loading control PA-I lectin. (B) *P. aeruginosa* wild type (WT),  $\Delta wspF$  mutant or  $\Delta loxA::Tn$  (PW3111) mutant were grown in LB broth for 12-14 h at 37°C, diluted ( $OD_{600} = 0.05$ ) in MEM and plated in 96-well vinyl microtiter plates (100  $\mu$ l per well). Bacteria were grown for 24 h at 37°C without agitation, the supernatants were removed and the biofilms were washed with water, stained with crystal violet (41%), and quantified at  $OD_{550}$ . Data represent mean  $\pm$  s.d., \*p < 0.05 vs. WT, N = 3. (C and D) Typical LC-MS profiles of oxidized (Upper panel) and non-oxidized (Lower panel) AA (C) and AA-PE (D). (E) HBE cells were treated with  $loxA::Tn$  supernatants alone or with FER (0.2  $\mu$ M), or with z-VAD-fmk (20  $\mu$ M) or Nec-1s (necrostatin-

1s, 20  $\mu$ M) or Baf-A1 (bafilomycin-A1, 1 nM). Data presented are means $\pm$ s.d., \* $p$ <0.05 vs. *loxA::Tn*, N=3 (F) HBE cells were treated with  $\Delta$ *wspF* supernatants or RSL3 in the absence or presence of Baicalein (5.0 and 10.0  $\mu$ M) for 20 h at 37°C. Cell death was estimated by flow cytometry. Data represent means  $\pm$  s.d., \* $p$ <0.05 vs untreated control; # $p$ <0.05 vs. RSL3 or  $\Delta$ *wspF* supernatant, N = 3. (G) Bacterial cell-lysates (pLoxA deficient or complemented, 100  $\mu$ g each) were incubated with SAPE (100  $\mu$ M) for 30 min and then added to RSL3 (20 nM) pre-treated HBE cells with or without FER (0.2  $\mu$ M). Ferroptotic cell death = Cell death induced in the absence of ferrostatin-1 – cell death protected by ferrostatin-1. Data represent means  $\pm$  s.d., \* $p$ <0.05 vs. RSL3 + *loxA::Tn*, N = 3. (H) Western blot shows expression of pLoxA in complemented strain (Upper panel). PP is purified pLoxA. Control is loading control PA-I lectin (Lower panel). (I) Western blot of pLoxA in lysates of MJK8 WT and MJK $\Delta$ *loxA* using antibody against pLoxA. PP is recombinant pLoxA. Lower panel: Loading control PA-I-lectin.

### 2.2.7.2 pLoxA generated 15-HOO-AA-PE act as pro-ferroptotic signals in HBE cells

To interrogate the role of lipid hydroperoxides as pro-ferroptotic signals, we employed a fluorogenic probe, Liperfluo, which, similar to GPX4, selectively reduces hydroperoxy-lipids to respective alcohols to yield a fluorescent product [256, 257]. Incubation with the *ΔwspF* mutant supernatant induced a time-dependent increase in the fluorescent signal in HBE cells, which was fully protected by ferrostatin-1 (Figure 20A, left and right panels). This response was similar to the one elicited by the treatment of HBE cells with a GPX4 inhibitor, RSL3, as a positive control [225]. Notably, Liperfluo fluorescence originated in a single cell, over time was spreading and detectable in clusters of many surrounding cells (i.e., in a non-cell autonomous fashion) (Figure 20B). Assuming that Liperfluo fluorescence responses ~~were~~ report the early generation and propagation of pro-ferroptotic lipid peroxidation products, we monitored the dissemination of cell death using Sytox Green labeling of HBEs. Similar to previously reported results [97, 258, 259], *P. aeruginosa ΔwspF* supernatant induced cell death was also associated with the appearance of clusters of dying cells (Figure 21). Expectedly, this clonal loss of plasma membrane integrity revealed by Sytox Green occurred at later time points than Liperfluo-positivity of cells.

To determine the molecular identity of lipid oxidation products generated by *P. aeruginosa ΔwspF* supernatant in HBE cells, we performed quantitative phospholipidomics analysis (Figure 20C-E). We established that PE contained 15 oxidized species (Figure 20D and Table 3). Importantly, treatment of HBE cells with ferrostatin-1 selectively reduced the levels of four oxidized PE (PEox) species (Figure 20E) that have been identified as PE containing either 15-HOO-AA-PE or 12-HOO-AA-PE in *sn*-2 position (Figures 22 and 23) and were previously reported as predictive biomarkers of RSL3-induced ferroptosis [225].

To further explore the role of phospholipid peroxidation in *P. aeruginosa* induced cell death, we manipulated the content and molecular speciation of lipids in target cells. Our previous work showed that AA-supplementation sensitizes cells to ferroptosis via increased synthesis of AA-PE as a pro-ferroptotic oxidation substrate for 15LOX [225]. Exogenous AA significantly enhanced ferroptosis induced by WT and  $\Delta wspF$  supernatants but had no effect on pLoxA deficient *loxA::Tn* (PW3111) supernatant (Figure 24A).

Additional testing was performed by genetic manipulations of phospholipid biosynthetic (Acyl-CoA synthetase Long-Chain Family Member 4, *ACSL4*) or remodeling (Lysophosphatidylcholine Acyltransferase 3, *LPCAT3*) pathways. HBE cells with knock-down (KD) of *ACSL4*, which catalyzes the formation of long-chain PUFA-CoA (AA-CoA) [260], completely prevented *P. aeruginosa*-induced ferroptosis (Figure 24B). Similarly, KD of *LPCAT3*, involved in re-acylation (Lands cycle) of lysophospholipids [261], also markedly suppressed ferroptosis in HBE cells (Figure 24B and Figure 25A). Intriguingly, pLoxA-dependent biofilm formation [22] and epithelial cell death are interconnected as inhibition of ferroptosis by ferrostatin-1 was accompanied by a two-fold growth decrease in a biotic model (Figure 24C).

GPX4 can directly reduce *hydroperoxy*-PLs to non-pro-ferroptotic *hydroxy*-PLs [84, 257, 262]. Depletion of GPX4 - critical for the development of ferroptotic response - has been observed in a variety of cells treated with RSL3 [84, 225, 263]. *P. aeruginosa*  $\Delta wspF$  supernatant induced substantial loss of GPX4 protein in HBE cells (Figure 24D) thus eliminating this anti-ferroptotic regulator. Due to the reduction of 15-HOO-AA-PE to 15-HO-AA-PE by endogenous GPX4 in HBE cells, recombinant pLoxA was unable to induce ferroptotic cell death (Figure 25B), even though it generated 15-HOO-AA-PE in a model system (Figure 25C). However,

inactivation of GPX4 by RSL3, facilitated ferroptosis induced by WT but not pLoxA deficient *loxA::Tn* supernatant in 15-HOO-AA-PE-sensitized HBE cells, thus signifying the role of pLoxA (Figure 24E).

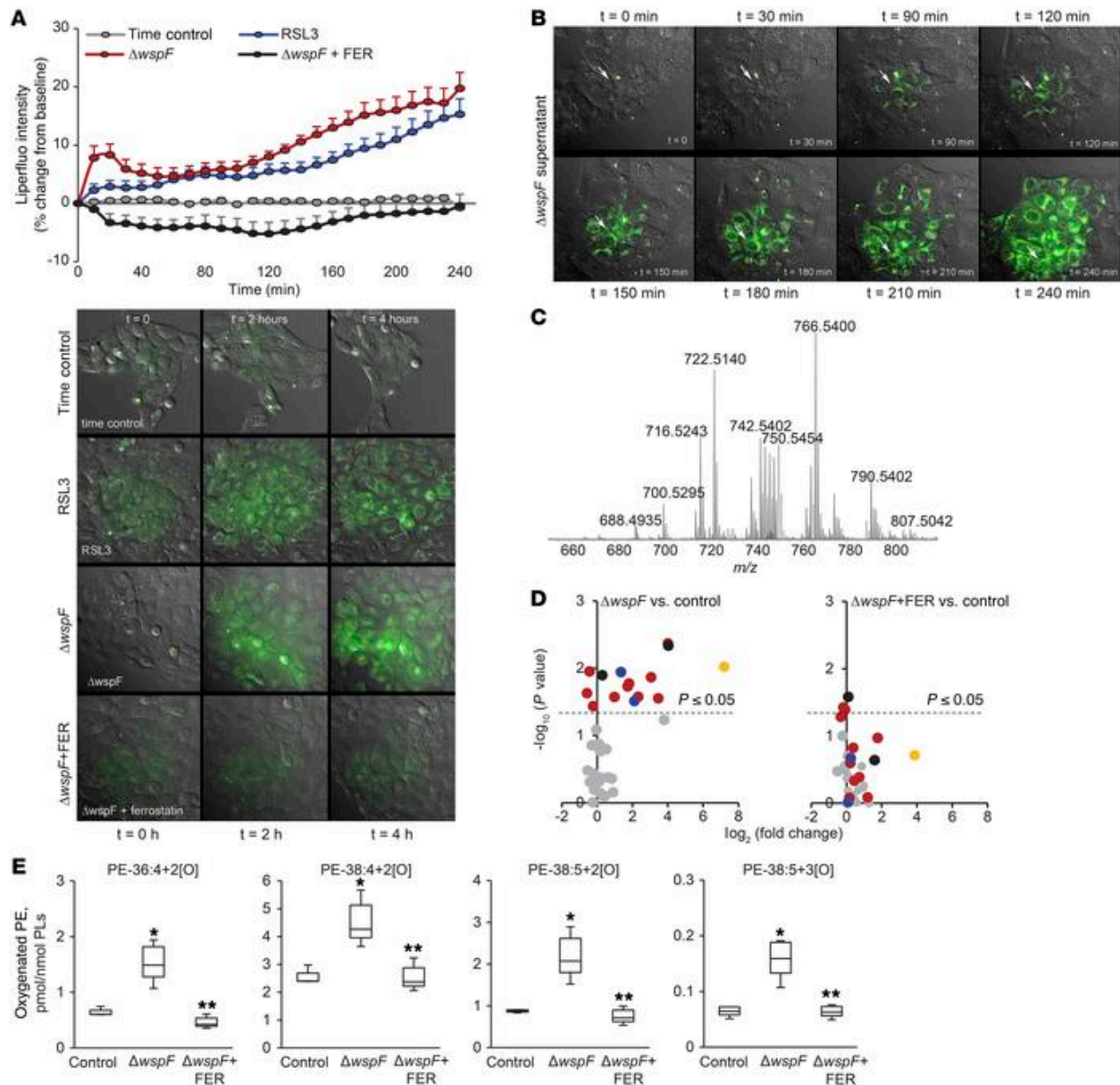


**Figure 20. *P. aeruginosa* supernatants generate pro-ferroptotic hydroperoxy-lipid signals in HBE cells.**

(A) Detection of lipid hydroperoxides by live cell fluorescence imaging of Liperfluo in HBE cells treated with RSL3 (200 nM) or  $\Delta wspF$  supernatant for 4h. Left panel shows time-course of changes in the fluorescence intensity from baseline. Right panel shows typical changes in fluorescence (out of 4 performed) in one stage position (out of 10) at three-time points (0, 2 and 4h). Time control used as background fluorescence changes and RSL3 as a positive control for ferroptosis. For statistical analysis, each stage position was counted as one data entry. (B) Typical Liperfluo response (out of 4 performed) to  $\Delta wspF$  showing synchronized spreading of the oxidized lipid signal within cells. The seed point for the signaling is indicated by an arrow in the t=0 image, the subsequent time course shows that the signals expanded in a clonal way to

include multiple surrounding cells (C) Typical mass spectrum of PE molecular species in lipid extracts from HBE cells (out of 3 performed). (D) Volcano plots of  $\Delta wspF$  biofilm supernatant induced changes in the levels of oxygenated PEs ( $\log_2$  (fold-change), vs. significance ( $-\log_{10}$  ( $p$ -value) by  $t$ -test) in HBE cells in the absence (left panel) and presence (right panel) of ferrostatin-1 (FER, 0.2  $\mu$ M). Yellow, red, blue and black circles represent PE plus one, two, three and four oxygens, respectively. N=3. (E) Quantitative assessments of four oxygenated PE species (previously identified as pro-ferroptotic signals) generated in HBE cells exposed to  $\Delta wspF$  supernatants. \* $p < 0.05$  vs. control; \*\* $p < 0.05$  vs.  $\Delta wspF$ , (1-way ANOVA), N=3.

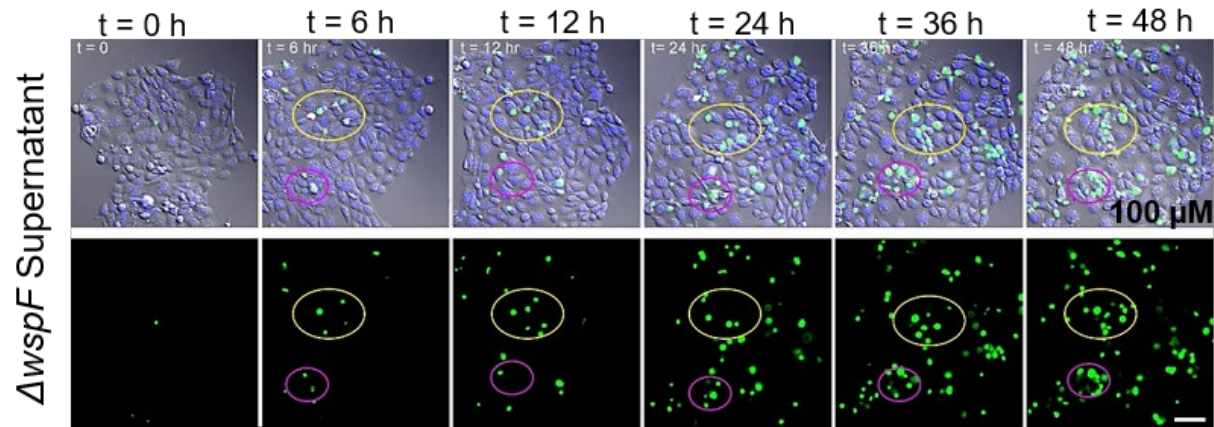


**Figure 21. Cell death induced by  $\Delta wspF$  supernatants.**

HBE cells were treated with  $\Delta wspF$  supernatants in the presence of Sytox Green and monitored for 48h by live-cell imaging. Sytox Green is a membrane impermeant nuclear dye that will only be seen in cells with permeable plasma membranes (which is indicative of the early stages of cell death processes). Two areas in the image are selected (yellow and magenta circles) in each case over a 48h imaging cycle (imaging every 30 minutes) the evident cell death expands in a clonal way to include multiple cells within the delineated areas. Bar=100 microns.

**Table 3. PE-OX species identified in Human Bronchial Epithelial (HBE) cells treated with *P. aeruginosa* hyper-biofilm mutant ( $\Delta wspF$ ) supernatant.**

Plus 1 Oxygen	Plus 2 Oxygen	Plus 3 Oxygen	Plus 4 Oxygen
PE(34:2)+1O	PE(34:4)+2O	PE(38:4)+3O	PE(38:2)+4O
	PE(38:4)+2O	PE(36:5)+3O	PE(40:6)+4O
	PE(36:5)+2O		
	PE(38:5)+2O		
	PE(36:4)+2O		
	PE(34:3)+2O		
	PE(36:3)+2O		
	PE(44:5)+2O		
	PE(38:6)+2O		
	PE(40:6)+2O		

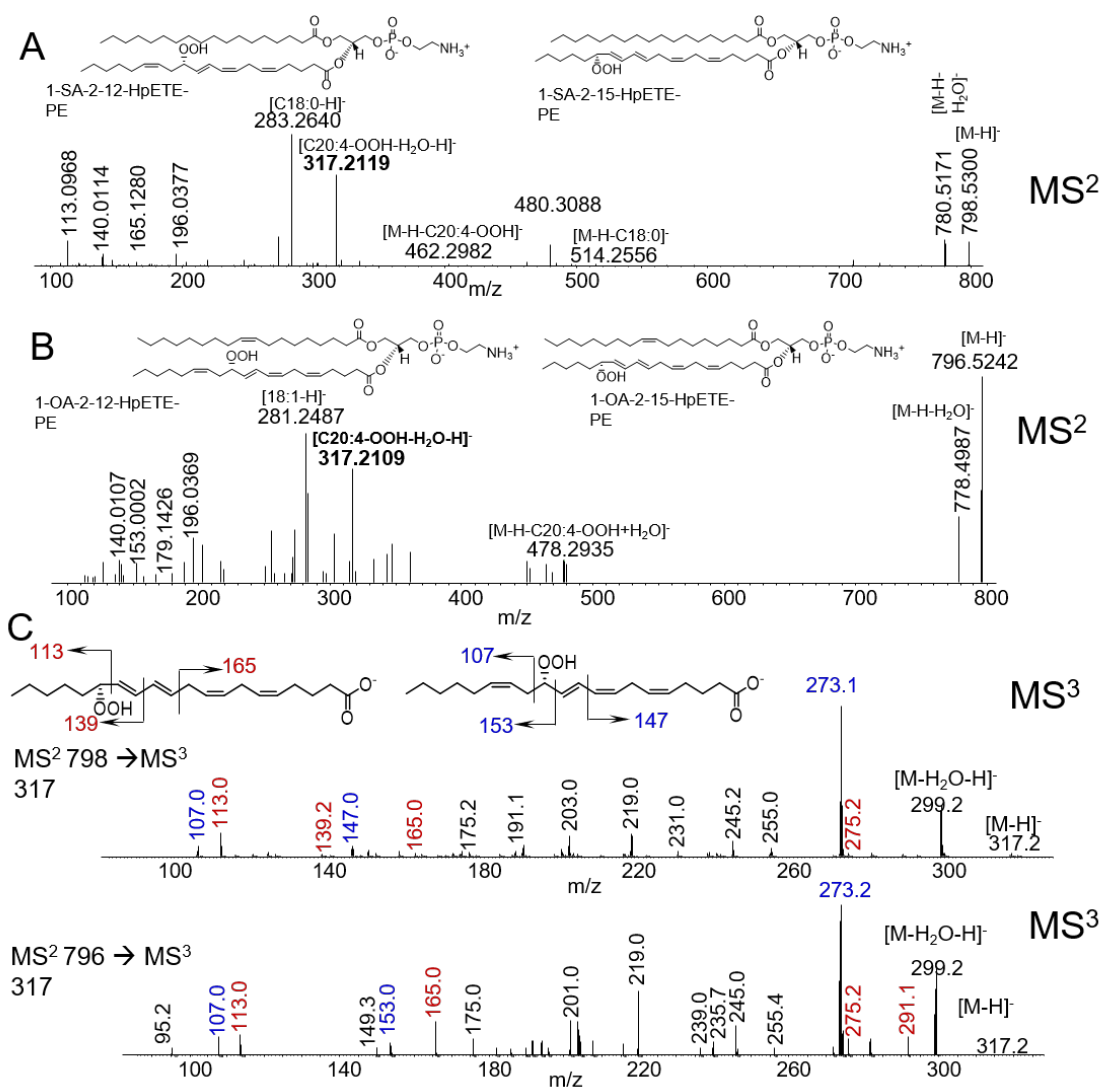


**Figure 22. Identification of di-oxygenated PE species in HBE cells exposed to supernatants obtained from  $\Delta wspF$  mutants.**

MS<sup>2</sup> profiles of di-oxygenated PE species (15-HOO-AA-PE and 12-HOO-AA-PE): (A) with m/z 798.5300 identified as 1-stearoyl-2-12-HpETE-*sn*-glycero-3-phosphoethanolamine (1-SA-2-12-HpETE-PE,) and 1-stearoyl-2-15-HpETE-*sn*-glycero-3-phosphoethanolamine (1-SA-2-15-HpETE-PE,) and (B) with m/z 796.5242 identified as 1-oleoyl-2-12-HpETE-*sn*-glycero-3-phosphoethanolamine (1-OA-2-12-HpETE-PE) and 1-oleoyl-2-15-HpETE-*sn*-glycero-3-phosphoethanolamine (1-OA-2-15-HpETE-PE). Inserts: Structural formulae of identified species; (C) MS<sup>3</sup> profiles of molecular ion with m/z 317.23 (m/z 335-H<sub>2</sub>O) formed during MS<sup>2</sup> fragmentation of di-oxygenated PE species with m/z 798.5300 (upper panel), m/z 796.5242 (Lower panel). Insert: Structural formulae of identified di-oxygenated AA metabolites: 12-HOO-arachidonic acid (12-HpETE) and 15-HOO-arachidonic acid (15-HpETE). Characteristic fragments used for identification of 12-HpETE and 15-HOO-AA are shown in blue and red, respectively. Identification was performed based on MS<sup>2</sup> and MS<sup>3</sup> fragmentation analysis using a Tribrid™ Ion-trap/Orbitrap™ Fusion-Lumos™ mass spectrometer, (Thermo-Fisher Scientific, NJ).

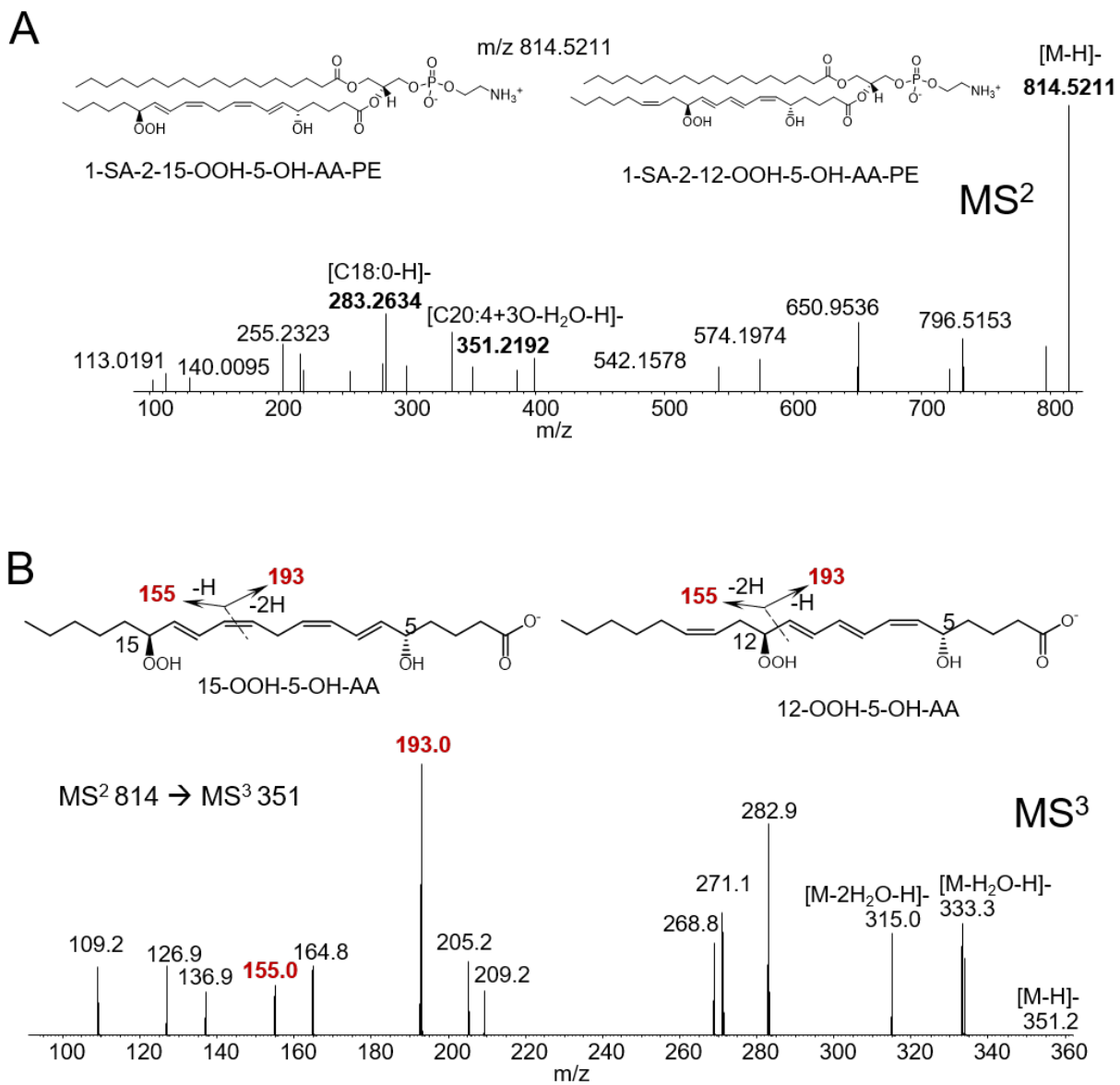


**Figure 23. Identification of tri-oxygenated PE species in HBE cells exposed to supernatants obtained from  $\Delta wspF$  mutants.**

(A) MS<sup>2</sup> profiles of tri-oxygenated PE species (1-stearoyl-2-12-hydroperoxy-5-hydroxy-arachidonoyl-*sn*-glycero-3-phosphoethanolamine (1-SA-2-15-OOH-5-OH-AA-PE) and 1-stearoyl-2-15-hydroperoxy-5-hydroxy-arachidonoyl-*sn*-glycero-3-phosphoethanolamine (1-SA-2-12-OOH-5-OH-AA-PE) with  $m/z$  814.5211. Insert: (A) Structural formulae of identified PE species. (B) MS<sup>3</sup> profiles of molecular ion with  $m/z$  351.23 formed during MS<sup>2</sup> fragmentation of di-oxygenated PE species with  $m/z$  814.5211. Insert: Structural formulae of 12-hydroperoxy-5-hydroxy-arachidonic acid (12-OOH-5-OH-AA) and 15-hydroperoxy-5-hydroxy-arachidonic acid (15-OOH-5-OH-AA). Identification was performed based on both MS<sup>2</sup> and MS<sup>3</sup> fragmentation analysis using a Tribrid™ Ion-trap/Orbitrap™ Fusion-Lumos™ mass spectro-meter.

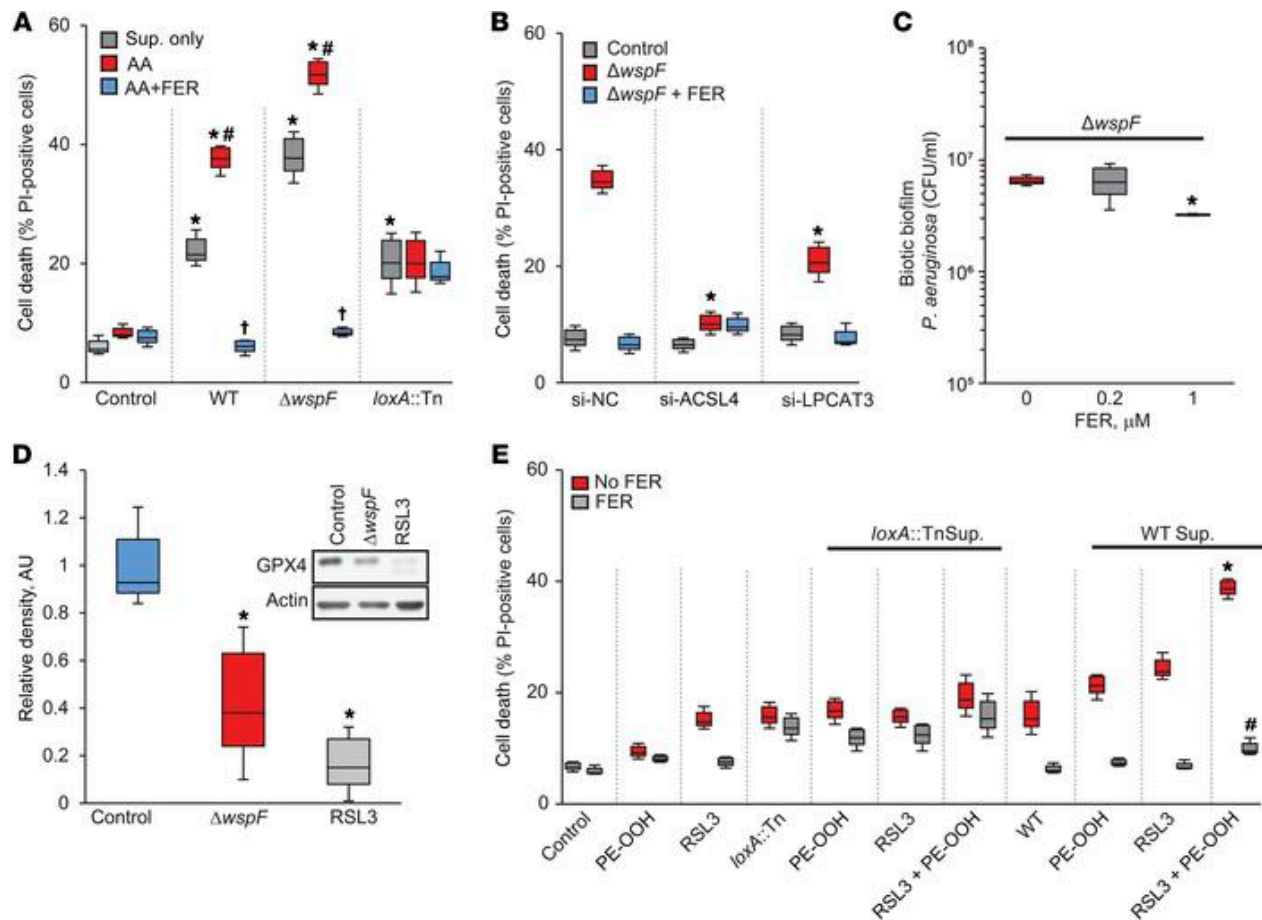
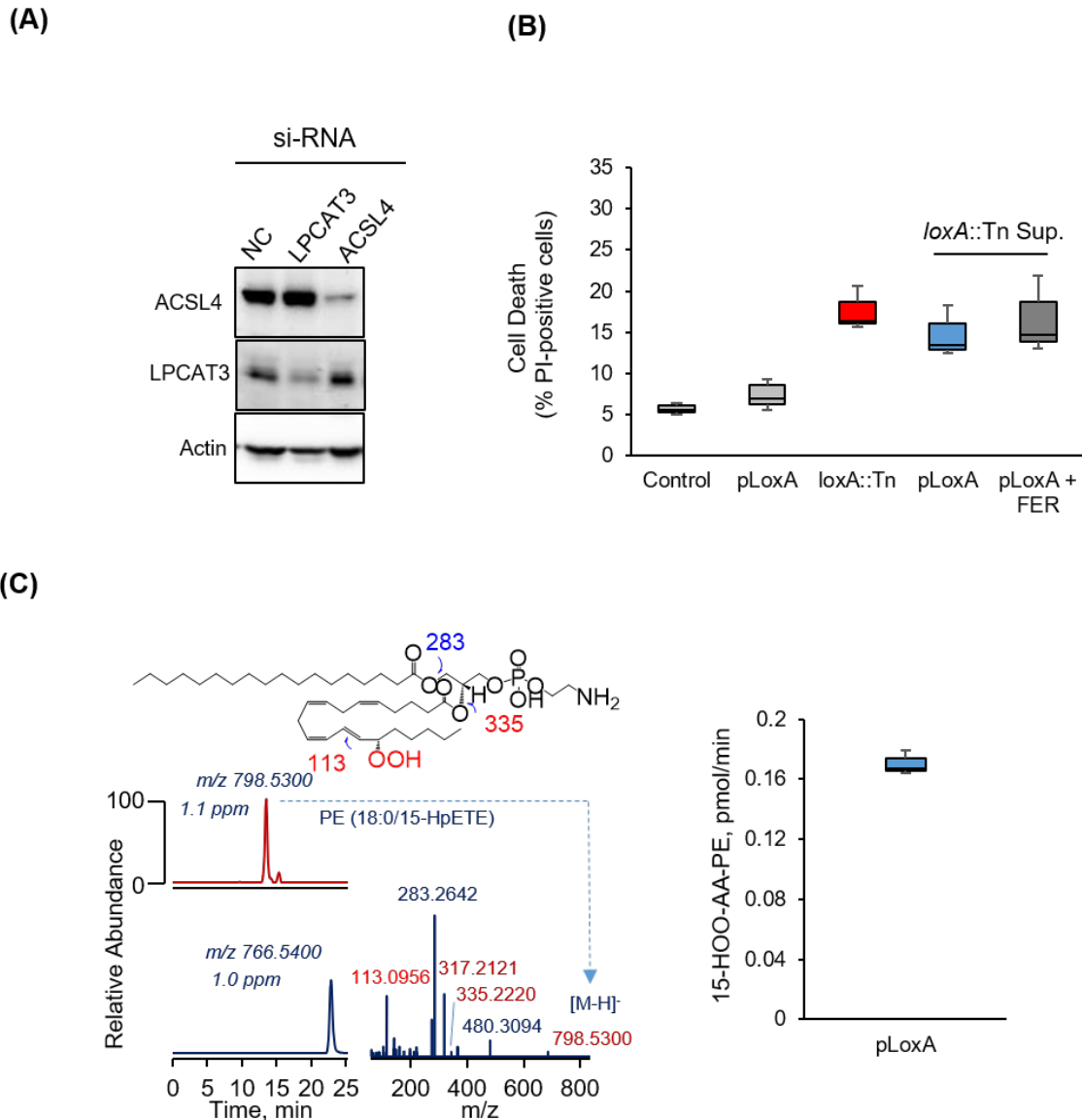


**Figure 24. *P. aeruginosa* induced ferroptosis is affected by manipulations of phospholipids in HBE cells.**

(A) Exogenous AA enhances PA induced ferroptosis. HBE cells were treated with WT,  $\Delta wspF$  or *loxA::Tn* supernatant (Sup.) alone or in combination with arachidonic acid (AA, 2.5  $\mu\text{M}$ ) for 20h at 37°C. Cell death was estimated as mentioned before. Data are presented as means $\pm$ s.d.; \* $p < 0.05$  vs. control (untreated); #  $p < 0.05$  vs. corresponding supernatant only;  $^{\$} p < 0.05$  vs. corresponding AA treatment. N=3. (B) HBE cells were transfected with scrambled si-RNA (si-NC) or si-RNA against *ACSL4* or *LPCAT3*. Transfected cells were treated with  $\Delta wspF$  supernatants with or without ferrostatin-1 (FER 0.2  $\mu\text{M}$ ) for 20h at 37°C before estimating cell death. Data are presented as means $\pm$ s.d.; \* $p < 0.05$  vs. si-NC  $\Delta wspF$ , N=3. (C) Ferrostatin-1 inhibits *P. aeruginosa* induced biofilm formation on HBE cells. Polarized HBE cells were incubated with  $\Delta wspF$  *P. aeruginosa* (MOI of 25) for 1h. After washing unattached bacteria, HBE cells in the absence or presence of ferrostatin-1 (0.2 and 1.0  $\mu\text{M}$ ) for 5h. Biofilms were removed, lysed with Triton X-100 (0.1%) and the number of bacteria in each sample was determined by CFU assay. Data are presented as means $\pm$ s.d.; \* $p < 0.05$  vs.  $\Delta wspF$  with no FER, N=3. (D) Treatment of HBE cells with  $\Delta wspF$  supernatant decreases the content of GPX4. Cells were treated with  $\Delta wspF$  supernatant and incubated for 20h at 37°C. Samples were collected and processed for Western blotting to determine the levels of GPX4. RSL3, a covalent GPX4 inhibitor, was used as a positive control. For quantification, the band intensity of GPx4 protein was normalized to respective band intensity of actin. Inset: Typical western blot (out of 3

performed). Data are presented as means±s.d.; \*p<0.05 vs. control (untreated) HBE cells, N=3. (E) Exogenous 15-HOO-AA-PE elevated WT, but not loxA deficient *loxA::Tn* supernatant induced cell death. HBE cells pre-treated with RSL3 (20 nM for 4h), were incubated with PEOOH alone or with supernatant from *loxA::Tn* or WT in presence or absence of ferrostatin-1 (FER, 0.2 μM). Data are presented as means±s.d.; \*p<0.05 vs. control (untreated) HBE cells, #p<0.05 vs. FER, N=3. (1-way ANOVA)



### **2.2.7.3 Computational analysis identifies evolutionarily conserved specific features of pLoxA required for AA-PE oxidation.**

Lipoxygenases are found in different domains of life where their activities are associated with vitally important functions such as differentiation, proliferation, contractility [19, 226]. Mammalian and bacterial lipoxygenases show little sequence identity. Alignment of pLoxA sequence against the structurally resolved mammalian sequences (15LOX1 from human and 15LOX2 human) (Figure 26A) yielded respective fractional sequence identities of 0.25 and 0.31 (note that 15LOX1 and 15LOX2 themselves also share only 36% sequence identity). Phylogenetic analysis of Pfam [239] family members revealed that bacterial LOXes diverged from those of animals and plants at approximately the same time as the animal and plant lipoxygenases diverged from each other (Figure 27A, left panel). The bacterial LOXes however seem to be more similar to animal and plant lipoxygenases than to lipoxygenases from other eukaryotes (e.g., fungi), suggesting that there might have been a gene transfer event since the prokaryote/eukaryote split and the development of multicellular organisms (Figure 27A, left panel). This is further illustrated by the phylogenetic tree which shows clustering of sequences from particular organisms. Bacteria are spread over the tree although there is a main group that includes pLoxA (Figure 26B). Alignment of the conserved structural core of pLoxA revealed 223 bacterial sequences (out of ~30,000 examined) sharing a sequence identity of 20% or more and out of these, 37 had greater than 55% sequence identity with pLoxA. Figure 28 displays their pairwise sequence identities (Figure 28A), and the corresponding phylogenetic tree (Figure 28B). The tree reveals discrete clusters of pathogenic bacteria, including a large cluster that groups the *Pseudomonas* (green) in close proximity to *Burkholderia* (blue), in accord with a previous analysis [227]. Further examination of the location of conserved residues on the LOX

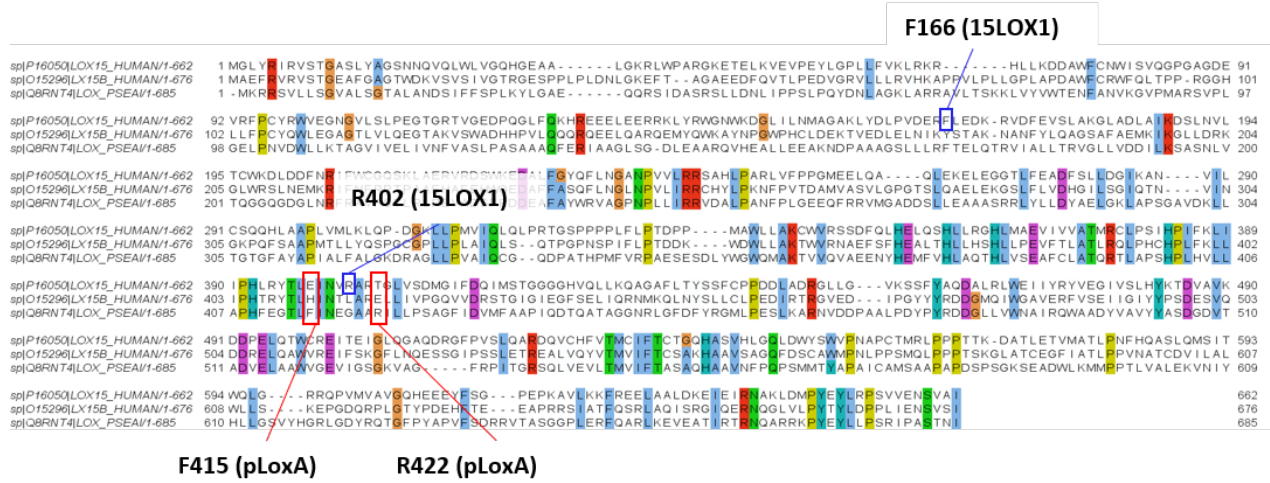
structure confirmed the tendency of core residues, near the catalytic site, to be conserved; whereas peripheral regions, including a helical hairpin that distinguishes *P. aeruginosa* from mammalian 15LOX1 and 15LOX2, exhibited significant sequence dissimilarity (or specificity) (Figure 28C).

Similar to other LOX enzymes, pLoxA employs non-heme coordinated iron (Fe) for the dioxygenase catalysis [162]. Therefore, we assessed the level of conservation of LOX amino acids, with peaks indicating the most conserved residues (Figure 27B). Expectedly, the catalytic site residues (H377, H382, H555, and N559 in pLoxA) were noted among the peaks. Examination of their evolutionary patterns across species confirmed their high level of conservation (Figure 27A, middle panel); whereas residues involved in substrate recognition exhibited a moderate level of conservation, with species-specific evolutionary trends (Figure 27A, right panel).

As an opportunistic bacterial pathogen, *P. aeruginosa* has acquired multiple adaptive genes favoring the highly adaptive phenotypes required to thrive and out-compete many other species in the highly pro-inflammatory environment of the host [160, 264, 265]. Among them is expression of pLoxA that facilitates the transition from planktonic to biofilm-forming state in the presence of the airway epithelium [22]. Utilization of secreted pLoxA to execute theft-ferroptosis via generation of 15-HOO-AA-PE signals not only destroys the epithelial barrier but may also compromise the immune-stimulating functions. To fulfill these important functions, *P. aeruginosa* has developed an enzyme with structural features distinct from mammalian (human) 15LOX1 [15] and 15LOX2 [16] (Figure 27C). pLoxA has two C-terminal  $\alpha$ -helical hairpin, composed of helices  $\alpha$ 2a and  $\alpha$ 2b, which are absent in the mammalian 15LOXs. The C-terminal helical hairpin modifies the organization of a ligand-binding pocket near the catalytic site

favoring the binding of bulky substrates, like AA-PE [162]. On the other hand, it lacks the N-terminal  $\beta$ -barrel domain typical of mammalian and human 15LOXs [15]. The remaining portions of the structure are closely superimposable between pLoxA and mammalian LOXs (Figure 27C). Dynamic motions of the two  $\alpha$ -helices modify the organization of the catalytic site favoring the binding of bulkier substrates, like AA-PE, vs. free AA in pLoxA (Figure 29A). Gaussian network model (GNM) analysis of pLoxA unveiled an additional regulatory mechanism whereby these helices act as a lid, regulating closed and opened states of the catalytic site for substrate binding (Figure 27D, upper panels). The mechanical role played by this extra lid is that it recruits the adjacent  $\alpha 2$  helix of pLoxA to enable a local hinge bending mechanism, which in turn facilitates the binding of PE-esterified AA to a site (Figure 29A and B) in the vicinity of the catalytic site, just like PEBP1 in PEBP1-15LOX complex (Figure 27D, lower panels).

(A)



(B)

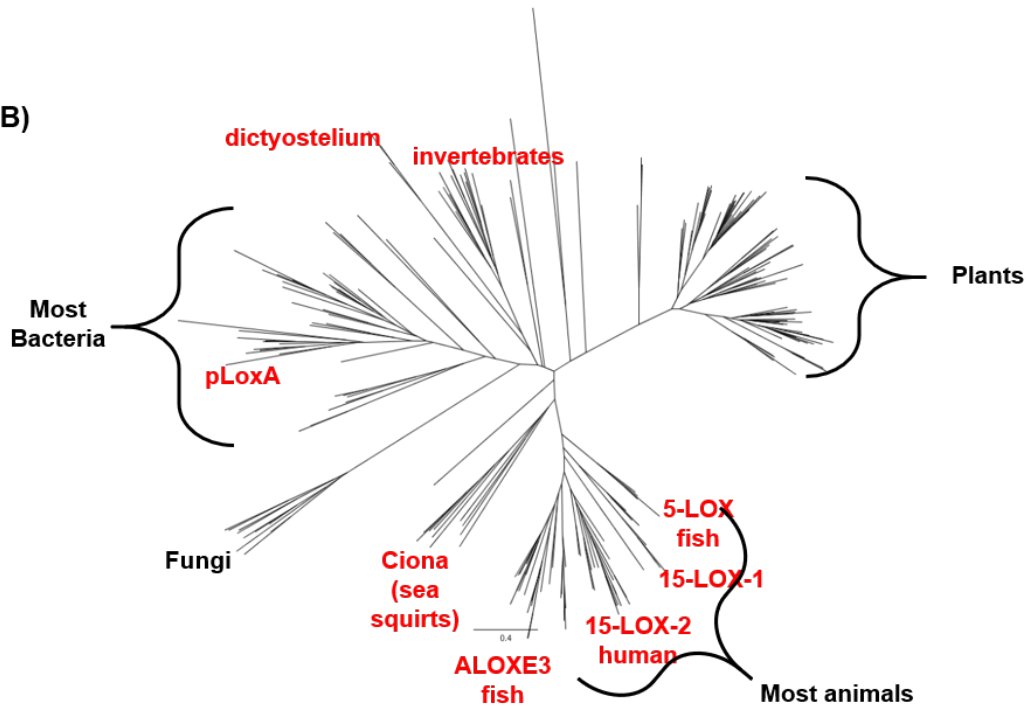


**Figure 26. Evolutionary analysis of LOX sequences.**

(A) Alignment of three sequences (two mammalian and the *P. aeruginosa*) obtained using Clustalx. Conserved residues are highlighted; those involved in AA binding are indicated. (B) Phylogenetic tree (undirected graph) obtained from the sequence-comparison map presented in Figure 27A.

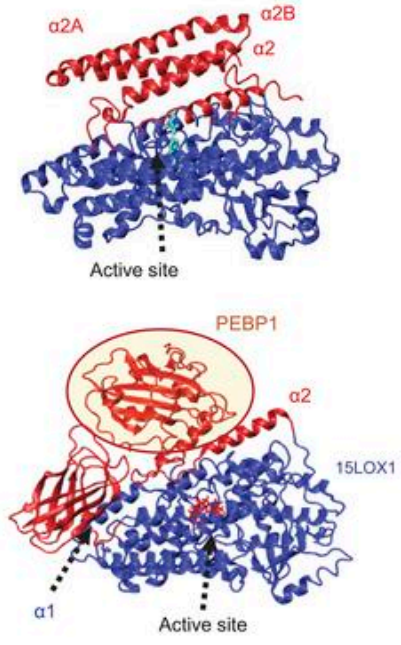
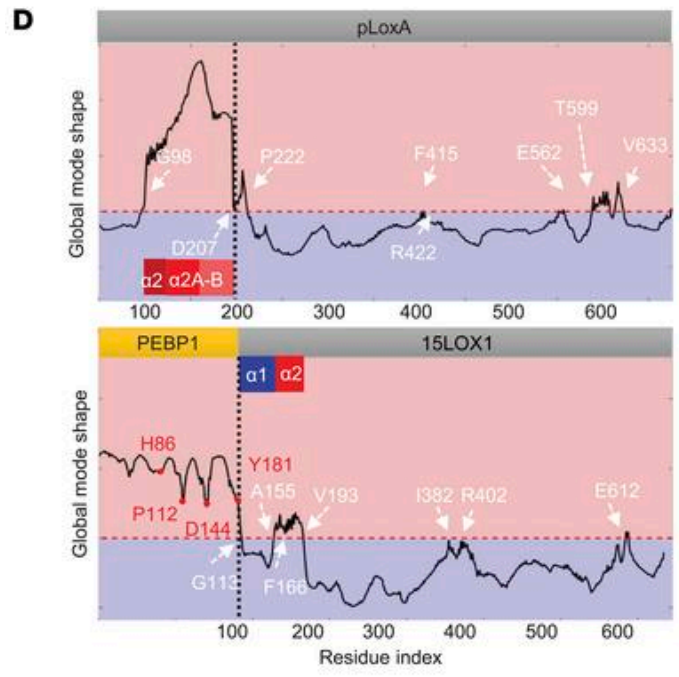
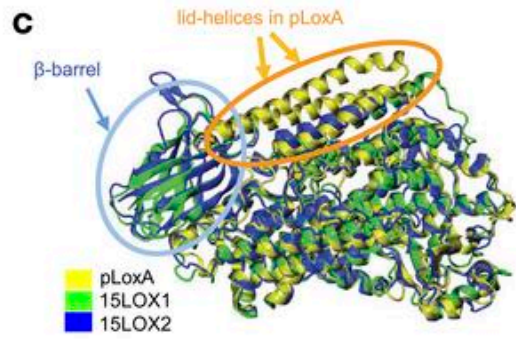
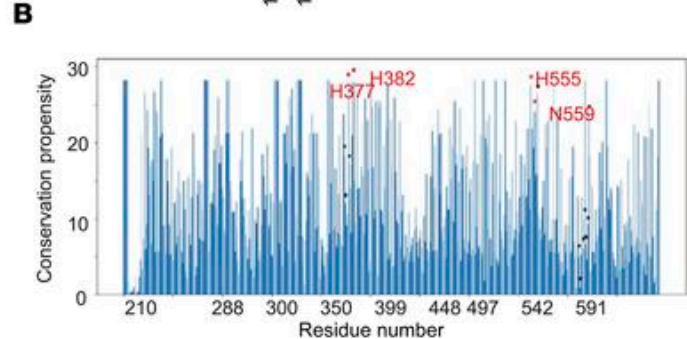
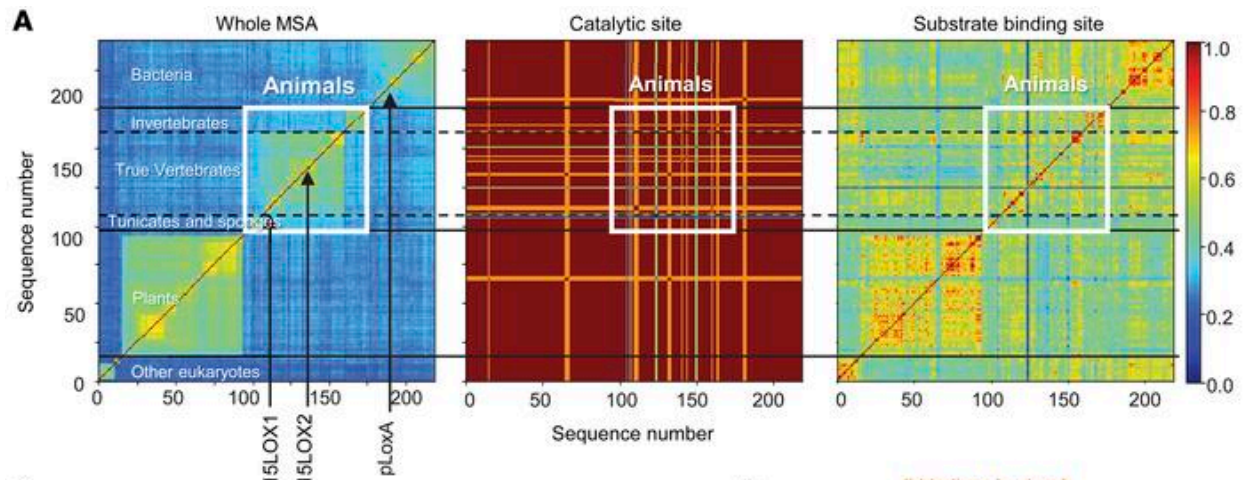


**Figure 27. Evolutionary analysis and computational modeling of pLoxA sequence and structure.**

(A) Comparing sequences of LOX homologs. The panels display sequence identity matrices obtained from 218 LOX sequences from all domains of life. High sequence similarity is in red, intermediate in yellow/green, and low in blue. Matrix generated for the entire LOX sequence (left panel) shows blocks evident for plants, animals and bacteria indicating their divergence a long time ago. Light blue shading between these blocks indicates a degree of sequence similarity higher than to the block of other eukaryotes at the bottom (dark blue off-diagonal). High conservation for the catalytic site is in the middle panel. Residues involved in substrate recognition (right panel) exhibit a moderate level of conservation and species-specific differentiation, evidenced by the blocks for plants, animals or bacteria. (B) Conservation propensity of LOX. The ordinate displays the Shannon entropy, subtracted from maximum entropy, plotted as a function of residue index; the peaks represent the most conserved residues. Note that catalytic residues (labeled) are among them. Residues involved in ligand coordination are indicated by the black dots. (C) Structural comparison of pLoxA and mammalian LOXs - 15LOX1 and 15LOX2. The structures resolved for pLoxA (yellow ribbon), 15LOX1 (green) and 15LOX2 (blue) are superimposed and display the missing  $\beta$ -barrel of the bacterial pLoxA and its additional  $\alpha$ -helical hairpin motif at the C-terminus. (D) Comparison of the global motions of pLoxA and 15LOX1 complexed with PEBP1. Displacements of residues along the global mode axis obtained from GNM analysis of pLoxA (left, top) and 15LOX1-PEBP1 complex (left, bottom) dividing the structure into two domains that exhibit anti-correlated motion (above and below the dashed line). Residues at the cross-over region (hinge centers or anchors) are labeled. The anti-correlated groups of residues are shown in red or blue (right top and bottom).

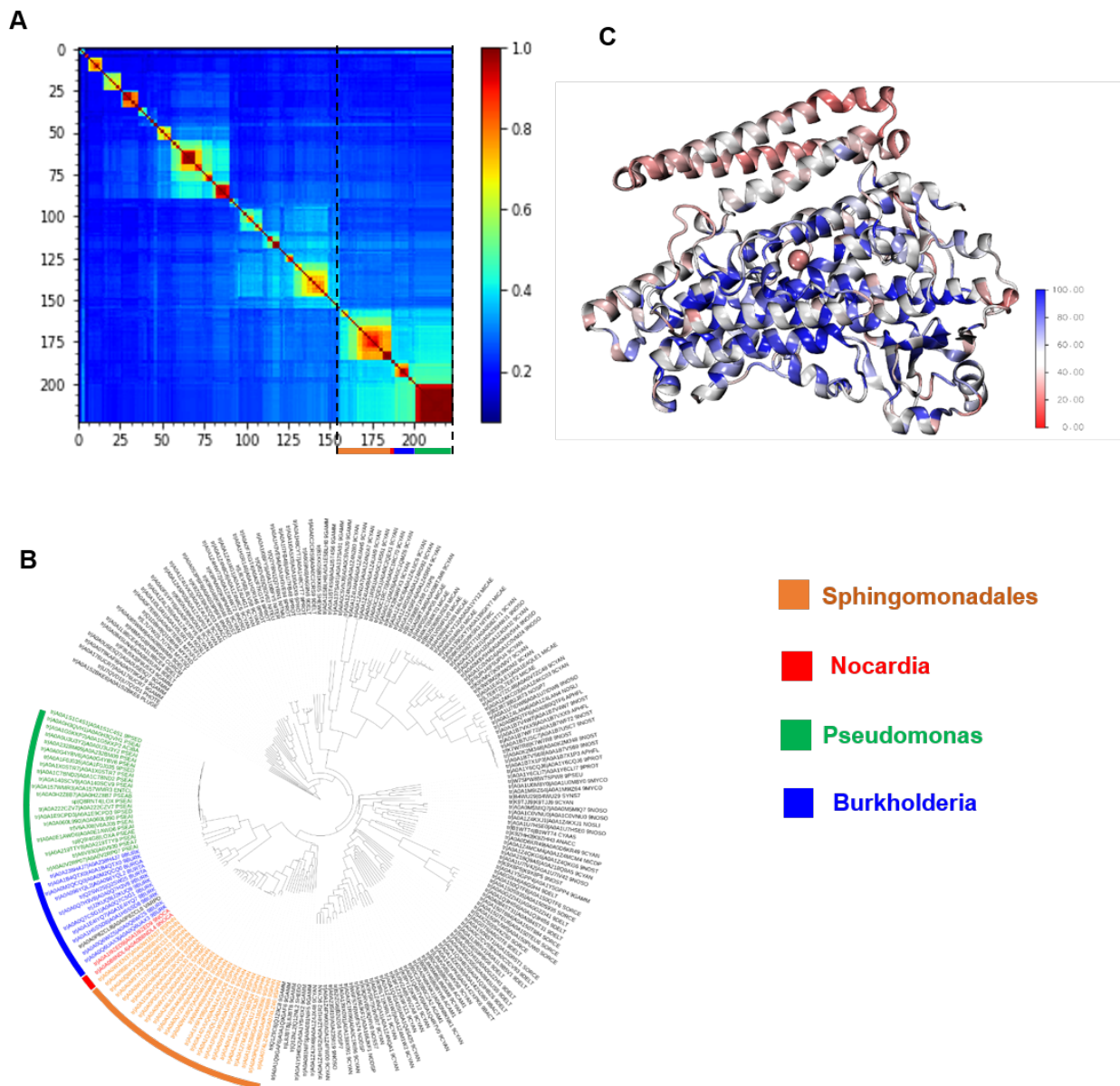


**Figure 28. Evolutionary analysis of lipoygenases (comparable to pLoxA) among bacteria.** (A) The panel displays the pairwise sequence identity matrix derived from the MSA of 223 bacterial lipoygenases. High sequence identity is shown in brown/red/orange, intermediate similarity in yellow/green, and low identity in blue. (B) Phylogenetic tree based on panel A. High sequence identity groups are colored: *Pseudomonas* (green), *Burkholderia* (blue), *Nocardia* (red) and *Spingomonadales* (orange). (C) pLoxA crystal structure color-coded by percent sequence similarity (using BLOSUM100) among bacterial sequences. Regions showing relatively conserved sequences are in blue, those with intermediate sequence similarity are white, and low sequence similarity, red.

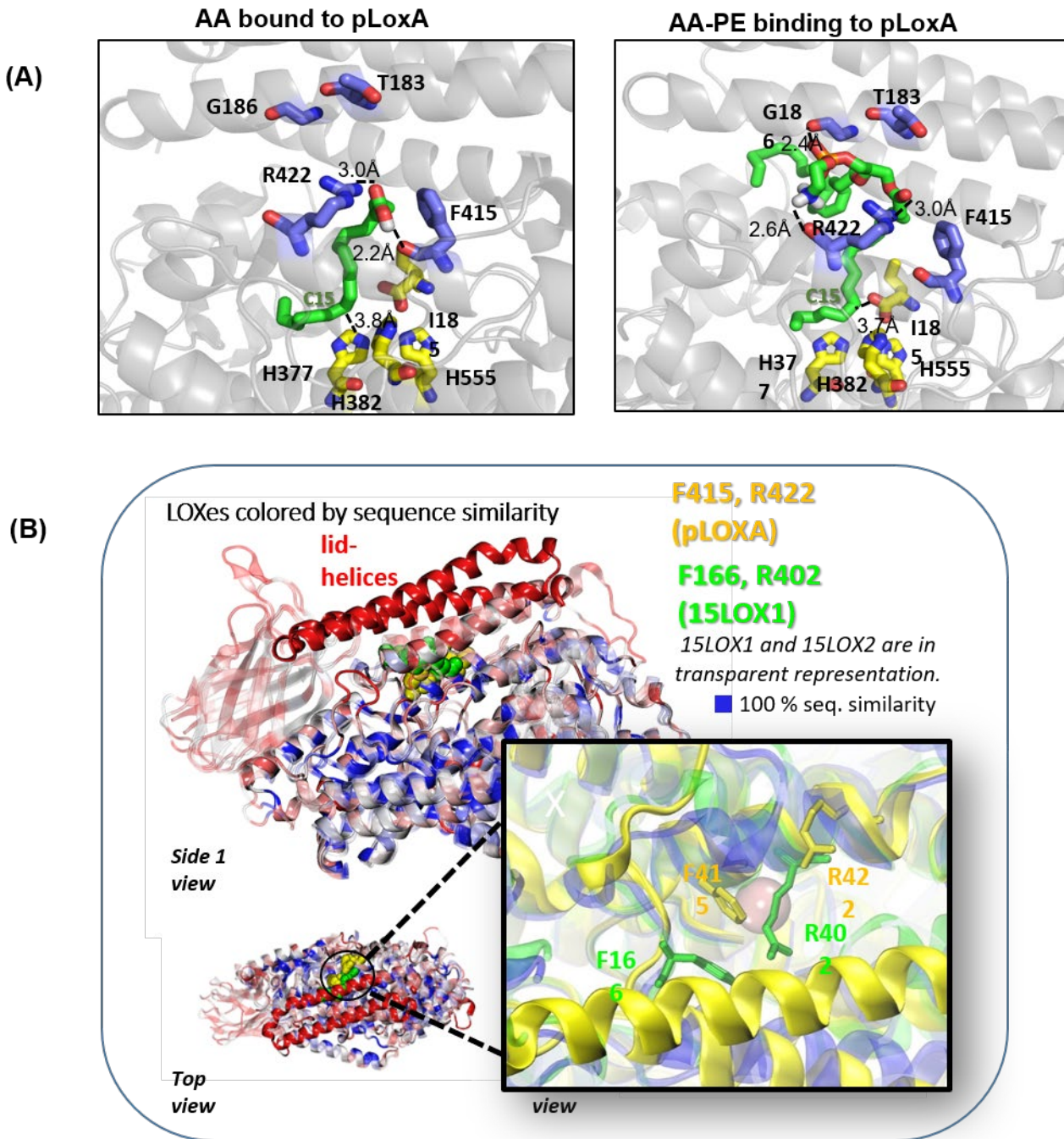


**Figure 29. Computational modeling of pLoxA structure and molecular dynamics.**

(A) Close up view of the binding pose and coordinating residues for the two ligands, Binding of AA (left) panel and AA-PE (right) panel illustrate the difference between the two poses. In the AA-PE binding more ligand-protein interactions are seen, especially between the PE head-group and the protein, which are not present in the AA binding. The average energies indicate AA-PE binding is more efficient than AA to PLoxA. The closest distances between some ligand and protein atoms are indicated and labeled. (B) Location of ligand-binding site in the structure, and comparison of a pair of Arg-Phe, represented by both bacterial and mammalian LOXes.

#### **2.2.7.4 Redox phospholipidomics reveals elevated levels of 15-HOO-AA-PE in airway tissues of *P. aeruginosa* infected patients with cystic fibrosis.**

Chronic biofilm-based infections of the airways with *P. aeruginosa* occur in 70–80% of patients with CF, representing the leading cause of morbidity and mortality in these patients [136, 137]. Assuming that *P. aeruginosa*-associated pathogenic mechanisms include pLoxA to regulate host-pathogen interactions at the airway mucosal surface via the induction of ferroptotic cell death as one of the virulence factors, we performed quantitative redox phospholipidomics studies of airway samples from CF and non-CF patients (Figure 30A). Several oxygenated PE species were elevated in CF vs. control samples (Figure 31A and Table 4). We identified three PEox species whose levels were significantly higher in CF patients vs. non-CF controls (Figure 31B). MS/MS fragmentation analysis identified PE(36:4) (Figure 31C) and PE(36:5) (Figure 31D) as precursors of the PE oxidation products (Figure 31E). These PEox species were also present in *P. aeruginosa* treated HBE cells (Figure 20E) and have been reported as predictive pro-ferroptotic biomarkers [225]. Microbiological testing revealed that out of 10 CF samples, 6 were infected with *P. aeruginosa* (Table 5). Remarkably, the content of these three PEox pro-ferroptotic signals were specifically elevated in *P. aeruginosa* infected CF lung samples but not in the samples infected with other pathogens such as *Burkholderia cenocepacia*, *Achromobacter xylosoxidans* or *Mycobacterium abscessus* (Figure 31B and Table 5).

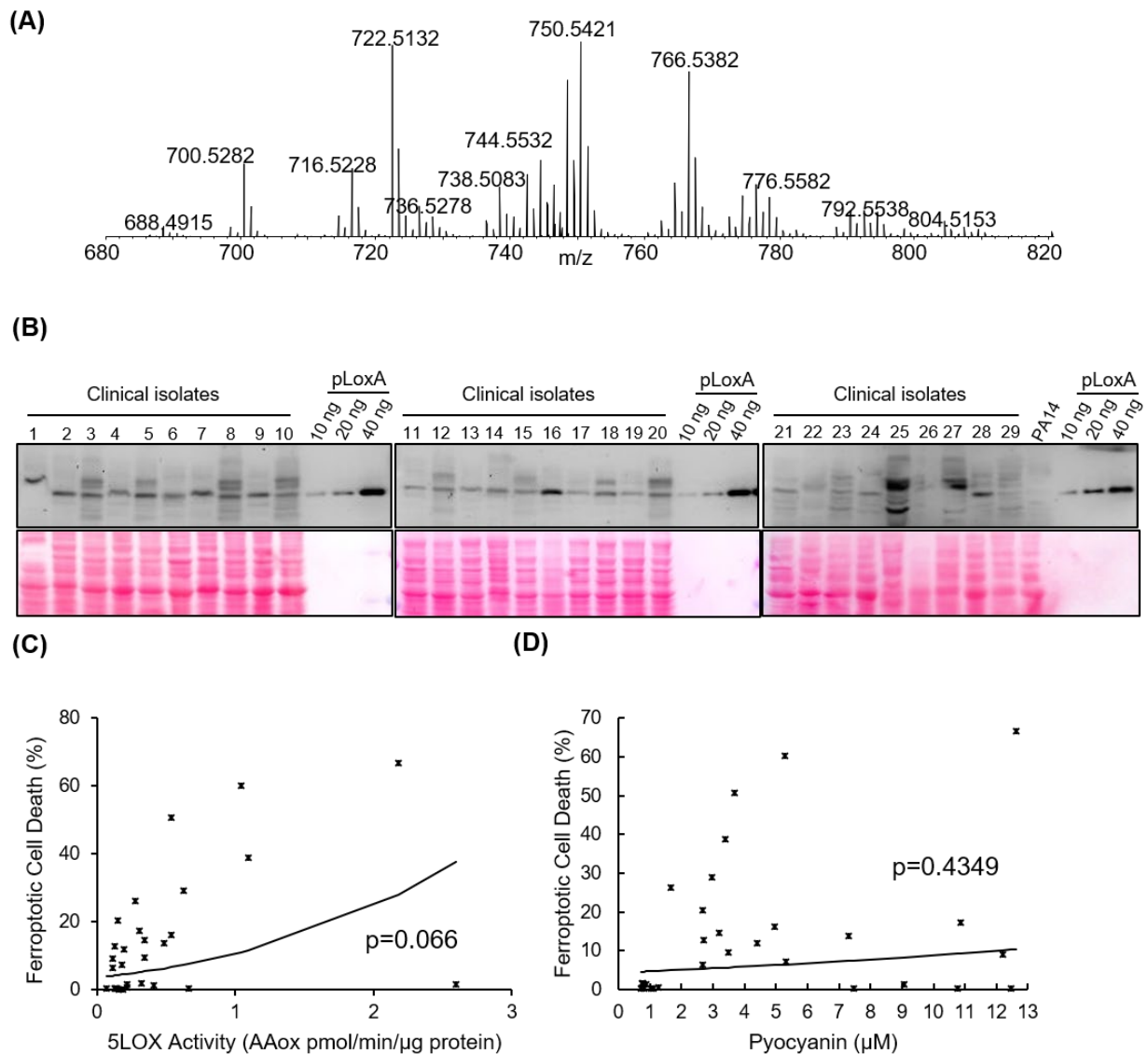


**Figure 30. *P. aeruginosa* clinical isolates from patients with persistent lower respiratory infection induce ferroptosis.**

**(A)** Typical mass spectrum of PE from a patient with CF. **(B)** Representative Western blot of clinical isolates. Samples were prepared from clinical isolates grown under biofilm conditions and probed with anti-pLoxA antibody (Upper panel) or stained with Ponceau S (Lower panel). **(C)** Dependence of the ferroptotic death of HBE cells on the 5LOX activity of clinical isolates (n=29) and **(D)** the contents of pyocyanin in the supernatants of clinical isolates (n=29).

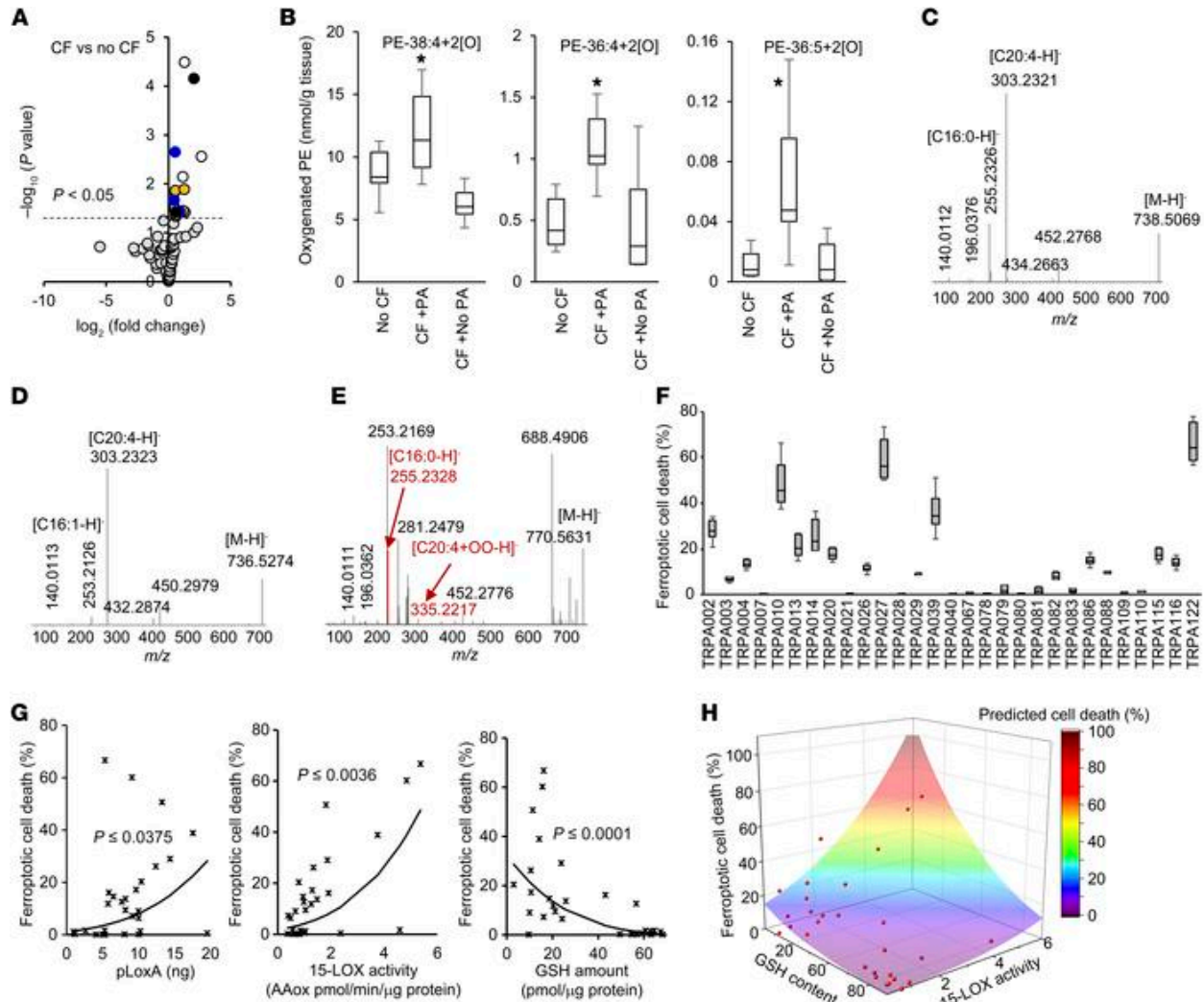


**Figure 31. Redox phospholipidomics reveals pro-ferroptotic oxygenated PE species in airway tissue samples from patients with cystic fibrosis (CF).**

(A) Volcano plot of differences in the levels of PEOx species in CF vs. non-CF patients - ( $\log_2$  (fold-difference) vs. significance ( $-\log_{10}$  ( $p$ -value))). Airway tissues from patients with emphysema were used as controls. Yellow, red, blue and black circles represent oxidized PE species containing one, two, three or four oxygens, respectively. N=10 (B) Quantitative assessments of PEOx species. Non-CF samples (N=10), CF samples with *P. aeruginosa* (N=6), CF samples with other bacterial pathogens (*B. cenocepacia* or *A. xylosoxidans* and *M. abscessus*, N=4). (C-E) MS/MS-based identification of PEOx molecular species in samples from patients with CF. Typical MS<sup>2</sup> spectra of PEOx precursors with m/z 738.5 (PE16:0/20:4) (C) and 736.5 (PE16:1/20:4) (D) containing arachidonic acid (C20:4 at m/z 303.2) at sn-2 positions. MS<sup>2</sup> spectra of PEOx with m/z 770.5 (PE16:0/20:4+2O) containing oxygenated arachidonic acid (C20:4+2O at m/z 335.2) (E) formed from the PE species with m/z 738.5 plus two oxygens (out of 3 performed). (F) Tobramycin resistant *P. aeruginosa* clinical isolates (TRPA002-0022) from patients with persistent lower respiratory infection induce ferroptosis. Biofilm supernatants from *P. aeruginosa* isolates incubated with HBE cells $\pm$ ferrostatin-1 (FER, 0.2  $\mu$ M). Ferroptosis was

calculated by subtracting from cell death induced by supernatants the cell death in the presence of ferrostatin-1. Ferroptotic activity of clinical isolates correlated significantly with pLoxA amounts (determined by Western (N=29) **(G)**), displayed strong positive dependence on 15LOX activity **(H)** ( $p=0.0036$ ) and correlated negatively with GSH level of HBE cells after treatment **(I)**. **(J)** 3D-plot illustrating jointly predicted ferroptotic activity of 15LOX activity and GSH (N=29). N is number of samples. (1-way ANOVA).

**Table 4. Identification of PE-OX species in CF lung samples infected with *P. aeruginosa*.**

Plus 1 Oxygen	Plus 2 Oxygen	Plus 3 Oxygen	Plus 4 Oxygen
PE(36:3)+1O	PE(34:3)+2O	PE(38:5)+3O	PE(40:2)+4O
PE(36:4)+1O	PE(36:4)+2O	PE(40:8)+3O	PE(40:7)+4O
PE(38:2)+1O	PE(36:5)+2O	PE(42:4)+3O	
PE(40:2)+1O	PE(38:4)+2O		
PE(42:4)+1O	PE(38:7)+2O		
PE(42:5)+1O	PE(40:7)+2O		

**Table 5. Identification of Pathogenic bacteria present in CF lung samples**

S. No.	Sample Name	Pathogenic bacteria
1	CF237	Achromobacter xylosoxidans
2	CF241	Pseudomonas aeruginosa
3	CF242	Pseudomonas aeruginosa, Stenotrophomas maltophilia
4	CF244	Burkholderia cenocepacia
5	CF245	Mycobacterium abscessus
6	CF246	Pseudomonas aeruginosa
7	CF247	Pseudomonas aeruginosa
8	CF248	Pseudomonas aeruginosa
9	CF249	Pseudomonas aeruginosa
10	CF250	Burkholderia cenocepacia

### **2.2.7.5 High prevalence of pLoxA in ferroptosis-inducing clinical isolates of *P. aeruginosa* from persistent lower respiratory tract infection patients.**

*P. aeruginosa* is one of the leading opportunistic pathogens that causes healthcare-associated lower respiratory tract infections including ventilator-associated pneumonia (VAP) [266]. Lower respiratory tract infections disproportionately affect the elderly, the immunocompromised and critically ill patients. High mortality rates associated with lower respiratory tract infections are further invigorated by increasing number of multi-drug and extensively-drug resistant strains of *P. aeruginosa* that leads to treatment failures and persistence of infection [267, 268]. To assess the significance of pLoxA in persistent lower respiratory tract infection, we examined the effectiveness of tobramycin-resistant *P. aeruginosa* respiratory isolates from 29 patients in the intensive care unit (ICU) to trigger ferroptosis in HBE cells (Figure 31F). We found that the ferroptotic cell death of *P. aeruginosa* clinical isolates correlated positively with the amounts of pLoxA (Figure 31G and Figure 30) and pLoxA enzymatic activity, particularly 12,15LOX activity (Figure 31H) and not significantly with 5LOX activity (Figure 30C). These data are compatible with our findings of 12- and 15-HOO-AA-PE dominating among the PE oxidation products generated by the *ΔwspF* mutant *P. aeruginosa* supernatants in HBE cells (Figures 22 and 23). We also found a strong negative correlation between the amounts of GSH in HBE cells (incubated with clinical isolate supernatants for 20h) and percent of ferroptotic cell death induced by clinical isolates ( $p < 0.0001$ ) (Figure 31I). This is compatible with the important role of GSH as the source of reducing equivalents for the GPX4-catalyzed reaction of elimination of pro-ferroptotic 15-HOO-AA-PE (via their reduction to 15-HO-AA-PE). Further, assessment of pyocyanin in the isolates revealed no correlation between its content and the effectiveness to cause ferroptosis in HBE cells (Figure 30D). Finally, we used the stepwise variable selection

method to generate a multivariate model and we found that 15LOX activity of pLoxA and the GSH amount of HBE cells jointly predicted the ferroptotic cell death with a R of 0.831 (Figure 31J).

### 2.2.8 Discussion

Execution of ferroptotic death program has been demonstrated in multiple normal and cancerous mammalian cells and different tissues where it has been implicated in pathogenesis of chronic and acute diseases such ischemia-reperfusion of liver [269], acute kidney injury [98], and Parkinson's disease [94]. Ferroptosis has been also documented in plants [270]. Here, we report for the first time, that ferroptotic death can be initiated by a common Gram-negative bacterial pathogen, *P. aeruginosa* that expresses and uses pLoxA to damage bronchial epithelial cells. The detection of pLoxA in *P. aeruginosa* in the early 2,000s created an apparent paradox: this organism does not contain PUFA lipids, the substrates of pLoxA catalyzed reactions. Overall, with the exception of several representatives of marine bacteria, mostly from the *Shewanella spp.* [140], the prokaryotic bacteria do not synthesize and usually do not contain PUFA lipids [140, 228]. This in turn justifies the lack of bacterial PUFA metabolizing enzymes and respective genes in their genomes [228]. Intriguingly, some bacteria – including *P. aeruginosa*, contain several genes/enzymes of PUFA metabolism [160] . These include enzymes of PUFA oxygenation and their subsequent strictly regulated conversion into different biologically active metabolites [160].

From phylogenetic studies of bacterial lipoxygenases, it can be assumed that nature selected *P. aeruginosa* to acquire lipoxygenase (pLoxA) to successfully assist its metabolic diversity (adapted to grow in partial or total lack of oxygen) [271] and ubiquitous presence (soil,

water, all man-made environments, plants, animals and humans) [272, 273]. This interpretation is compatible with the demonstrated enhanced expression and secretion of pLoxA during biofilm growth of the pathogen [22]. This facilitates the pLoxA's theft-ferroptotic mechanism as a virulence factor rather than membrane stabilizing enzyme [227, 228]. Transition to biofilm growth enables traits of multicellular lifestyle and "group behavior" which aid *P. aeruginosa* to thrive in hyper-inflammatory CF environment, resist antibiotic treatments and evade both arms of host immune responses [137, 274]. The switch from planktonic to biofilm growth is accompanied by multiple but critical changes like development of mucoid phenotype [275], auxotrophy [276], adapted metabolism, reduction of acute virulence factors and expression of new ones [136, 277], high mutation rate [278] and antibiotic resistance [274, 279, 280].

While pLoxA retains the major organizational principles essential for non-heme Fe-catalysis of dioxygenation of PUFA lipids present in many mammalian and human 15LOXes, it also acquired several specific features unique for the role of *P. aeruginosa* as a bacterial pathogen [21, 162]. pLoxA lacks the  $\alpha$ -barrel, which is typical of mammalian 15LOXes. The  $\beta$ -barrel is substituted in pLoxA by two  $\alpha$ -helices forming a lid, which presumably participates in substrate binding to the catalytic site via regulatory open and closed states of the protein. This function of the lid helices may be akin to the proposed role of a separate regulatory protein, PEBP1[33], in human 15LOXs. This helical hairpin region exhibits low sequence identity among bacterial LOXes, suggesting that the observed pathogenic (or pro-ferroptotic) behavior may be specific to *P. aeruginosa*. Consistently, our LC-MS analysis of clinical samples revealed elevated levels of pro-ferroptotic 15-HOO-AA-PE products only in cystic fibrosis patients infected with *P. aeruginosa* but not by other pathogens having similar to pLoxA sequences in their genomes.

The ability of *P. aeruginosa* pLoxA to act as a generator of signals for programmed death to host lung epithelial cells is in line with our previous data on the capacity of exogenous mammalian 15LOX2 + PEBP1 to trigger ferroptosis in GPX4-deficient target cells [33]. Combined, these results provide evidence for the importance of 15LOX-driven PE oxidation as pro-ferroptotic mechanism. We demonstrate that pLoxA can selectively and specifically oxidize membrane phospholipids, particularly AA-PE, of host epithelial cells and produce 15-HOO-AA-PE acting as pro-ferroptotic signals which, in the absence of GPX4 activity, cause ferroptosis. We demonstrate that pLoxA can selectively and specifically oxidize membrane phospholipids, particularly AA-PE, of host epithelial cells and produce 15-HOO-AA-PE acting as pro-ferroptotic signals. We also show that expression of pLoxA and pro-ferroptotic activity are associated with the pro-biofilm growth conditions of *P. aeruginosa*, the major pathogen in CF. It is plausible to envisage the secretion of pLoxA in vesicles as a pathogenic strategy adopted by *P. aeruginosa* to deliver pLoxA into host cells [250]. Once inside, it initiates lipid oxidation and generation of pro-ferroptotic phospholipid hydroperoxide signals. It is also possible that accessible AA-PE of ferroptotically dying cells may be utilized by secreted pLoxA as the substrate for the production of the pro-ferroptotic signals. Therefore, once formed, the signals can propagate from cell to cell in a non-cell-autonomous fashion.

In the lung of CF patients, once *P. aeruginosa* biofilm-based chronic infection is established, it is virtually impossible to eradicate it, and the infection is associated with increased mortality and morbidity [281]. Similarly, in *P. aeruginosa* nosocomial infections, a current worldwide healthcare issue [267], it can grow as biofilms on abiotic and biotic surfaces, resist antibiotic treatments and favor emergence of multi-drug resistant strains. Here we show that the role of pLoxA in the pathogenesis of *P. aeruginosa* during more persistent biofilm growth is

critical. pLoxA-driven oxidation of accessible AA-PE (inside or outside of injured target cells) yielding 15-HOO-AA-PEs as cell death signals propagates in non-cell autonomous fashion spreading among the neighboring cells and allowing for enhanced lung colonization. It is possible that this phenomenon of *P. aeruginosa* induced synchronized death of host epithelial cells may produce: i) essential building blocks for the biofilm formation, hence enhanced colonization by the pathogen; ii) clusters of dying epithelial cells may impair its barrier functions thus causing increased vulnerability of host tissues to other injurious factors (e.g., in cystic fibrosis, sepsis). Collectively, the clinical data from CF-patients and *P. aeruginosa* ICU respiratory isolates strongly suggest ferroptosis as vital feature of *P. aeruginosa* pathogenesis and that pLoxA is indispensable for this process. Based on these findings, we propose that the development of new specific small molecule pLoxA inhibitors may lead to novel therapies against CF and persistent lower respiratory tract infections. This is particularly important as we demonstrated inefficiency of selective mammalian 15LOX inhibitors in protecting against *P. aeruginosa* induced ferroptosis.

### 3.0 SUMMARY AND FUTURE DIRECTIONS

In the first part of the thesis, we established a genetic model of the yeast *S. cerevisiae*, which expresses *H. brasiliensis*  $\Delta^{12}$ -desaturase allowing it to generate PUFAs. Utilizing this model, we tested the hypothesis that the function of CL remodeling is to eliminate CLox species. We quantified CL and CLox in wild-type and *cld1* $\Delta$  yeast expressing the desaturase by redox phospholipidomics. CLox was found in both desaturase-expressing yeasts without the presence of exogenous oxidants. We also suggested that the major oxidation events occurred in mitochondria. The knockout of *cld1* resulted in an increase in mono-hydroperoxy-CLs, and a decrease in oxidizable CLs, along with a decrease of their chronological life span, respiratory capacity, and mitochondrial membrane potential. In addition, the expression of *cld1* was increased by H<sub>2</sub>O<sub>2</sub> treatment, and *in vitro* experiments showed that Cld1 preferably deacylates the oxidized aliphatic chains in CLs. To summarize, this study suggested that the function of CL remodeling is to mitigate CL peroxidation and the potential adverse effects of CLox products in the yeast *S. cerevisiae*.

Lipid peroxidation and its secondary metabolites have been reported to be involved in the cell death in mammalian cells. Indeed, CL oxidation and its oxidizing enzyme cyt C have been shown to be essential initiators of the early onset of apoptosis [71]. Furthermore, higher concentration of 4-HNE have been shown to induce apoptotic cell death and necrotic cell death[14]. Recently, hydroperoxy-PE has been identified as death signals for ferroptotic cell

death [90]. However, only a few studies have been conducted on the lipid peroxidation in yeast cell death. Lipid peroxidation was reported in yeast cells undergoing rapamycin-induced autophagy and H<sub>2</sub>O<sub>2</sub> treatment [282, 283]. Lipid peroxide and 4-HNE are toxic to yeast and the latter induces cell cycle arrest [284, 285]. Notably, Bax-induced cell death in the yeast is dependent on mitochondrial lipid peroxidation, and the lipid peroxidation is poorly related to superoxide and H<sub>2</sub>O<sub>2</sub> accumulation. These results suggest that possible oxidants are either oxygenases or secondary lipid peroxidation products [286]. Therefore, one of the future directions will be focused on the identification of the main contributor of lipid peroxidation in the desaturase-expressing yeast. Additionally, the deletion of *yca1*, a gene which encodes metacaspase that regulates yeast apoptotic cell death, can decrease the oxidative stress and prolong the yeast lifespan but not fully. These results suggest that PUFA-induced cell death occurs via both caspase-dependent and -independent mechanisms [126]. As an extension of these findings, one future study would be to investigate whether a caspase-dependent or -independent form of cell death is involved in the desaturase-expressing yeast, and to further explore the role of *yca1*. Finally, the role of CL remodeling in mitigating CL peroxidation could be further investigated in the study of CL remodeling defects in Barth syndrome.

In the second part of the thesis, we studied “theft-ferroptosis” induced by *P. aeruginosa* pLoxA in human bronchial epithelium cells, and further evaluated its clinical significance. We found pLoxA is required for *P. aeruginosa* supernatant-induced ferroptosis. By applying redox phospholipidomics we quantified and identified pro-ferroptotic lipid signals of 15-hydroperoxy-AA-PE in *P. aeruginosa* supernatant-induced ferroptotic HBE cells. Manipulation of host PL biosynthetic and remodeling pathways and supplementation of AA affected *P. aeruginosa* supernatant-induced ferroptosis. Evolutionary and computational analysis of pLoxA and other

LOX homologs showed that the catalytic core is highly conserved in all domains of life. In advance, the mechanism of pLoxA utilizing the  $\alpha$ -helical-lid interaction to control the accessibility of PL substrates is similar to the mammalian PEBP-15LOX complex. Redox phospholipidomic analysis revealed pro-ferroptotic lipid signals in airway tissue samples from CF patients with *P. aeruginosa* infection but not with other pathogens. *P. aeruginosa* clinical isolate-induced ferroptosis in HBE cells was correlated with pLoxA amount and its 15LOX activity. Taken together, our study showed that *P. aeruginosa* utilizes host polyunsaturated PE to trigger ferroptosis in the human bronchial epithelium.

The understanding of the advantages of pLoxA in *P. aeruginosa* infection is still not complete. Previous studies showed that pLoxA converts AA into 15-H(p)ETE [20-22]. It has been known that 15-HETE can be readily transformed into lipoxins by infiltrating polymorphonuclear cells expressing 5LOX [287]. Another study also showed the existence of lipoxin synthase activity in pLoxA [21]. These studies pointed out that one of the biological significances of pLoxA in *P. aeruginosa* infection is to downregulate host inflammatory responses, which could increase the chance of *P. aeruginosa* colonization. However, unlike other airway pathogens, *P. aeruginosa* survives in hyperinflammation state in CF airways [288]. In contrast to the potential anti-inflammatory role of pLoxA, *P. aeruginosa* secretes epoxide hydrolase Cif to impair the resolution of inflammation and promotes pulmonary inflammation in CF patients [160]. Therefore, it is suggested that *P. aeruginosa* distinctly possesses both pro-inflammatory and anti-inflammatory strategies to interfere host inflammation and to increase its survival in host airway.

pLoxA was found to be required for the biofilm formation on human airway epithelial cells but not on an abiotic surface [22]. Given the fact that the biofilm formation increases the virulence and antibiotic resistance of *P. aeruginosa* [289], pLoxA is a potential strategic enzyme of *P. aeruginosa* for better invasion of the host. This hypothesis is also supported by the observation that pLoxA is able to induce hemolysis of human red blood cells *in vitro* [34]. Our findings suggest that pLoxA-induced ferroptosis is another invasion strategy of *P. aeruginosa*, possibly by damaging the epithelial barrier of the host, or by providing the essential building blocks to facilitate biofilm formation. Defining how ferroptosis benefits the colonization and invasion of *P. aeruginosa* in the host *in vitro* and *in vivo* will be a potential future study.

To conclude, the first part of the thesis expanded our knowledge of CL remodeling via its role in removing CL peroxidation products and suggested the potential adverse effect of CLox species in the yeast *S. cerevisiae*. The study also provided a powerful genetic model for future studies of CL metabolism and CL peroxidation. The second part of the thesis revealed that *P. aeruginosa* hijacks and oxidizes host PUFA-lipids by pLoxA, and induces “theft-ferroptosis” in human bronchial epithelium. The results also emphasized the biological significance of pLoxA in host-pathogen interactions. Moreover, we identified a potential target for the future therapeutic development against *P. aeruginosa*-related diseases. Overall, combined with quantitative redox phospholipidomics, genetic, pharmacological, and computational approaches, our studies provide a deeper understanding of how organisms lacking PUFA synthesis utilize lipid peroxidation as signals. Finally, our studies also showed how an organism’s evolution and adaptation to the environment allowed them to further survival and propagate.

## BIBLIOGRAPHY

1. Reinhard, C.T., et al., *Earth's oxygen cycle and the evolution of animal life*. Proc Natl Acad Sci U S A, 2016. **113**(32): p. 8933-8.
2. Halliwell, B. and J.M.C. Gutteridge, *Free radicals in biology and medicine*. Fifth edition. ed. 2015, Oxford, United Kingdom ;: Oxford University Press. xxxviii, 905 pages.
3. Li, R., Z. Jia, and M.A. Trush, *Defining ROS in Biology and Medicine*. React Oxyg Species (Apex), 2016. **1**(1): p. 9-21.
4. Covarrubias, L., et al., *Function of reactive oxygen species during animal development: passive or active?* Dev Biol, 2008. **320**(1): p. 1-11.
5. Turrens, J.F., *Mitochondrial formation of reactive oxygen species*. J Physiol, 2003. **552**(Pt 2): p. 335-44.
6. Cadet, J. and J.R. Wagner, *DNA base damage by reactive oxygen species, oxidizing agents, and UV radiation*. Cold Spring Harb Perspect Biol, 2013. **5**(2).
7. Stadtman, E.R. and R.L. Levine, *Protein oxidation*. Ann N Y Acad Sci, 2000. **899**: p. 191-208.
8. Gaschler, M.M. and B.R. Stockwell, *Lipid peroxidation in cell death*. Biochem Biophys Res Commun, 2017. **482**(3): p. 419-425.
9. *Polyunsaturated fatty acid metabolism*. 1st edition. ed. 2018, Waltham, MA: Elsevier. pages cm.
10. Stubbs, C.D. and A.D. Smith, *The modification of mammalian membrane polyunsaturated fatty acid composition in relation to membrane fluidity and function*. Biochim Biophys Acta, 1984. **779**(1): p. 89-137.
11. Wymann, M.P. and R. Schneiter, *Lipid signalling in disease*. Nat Rev Mol Cell Biol, 2008. **9**(2): p. 162-76.
12. Repetto, M.G., N.F. Ferrarotti, and A. Boveris, *The involvement of transition metal ions on iron-dependent lipid peroxidation*. Arch Toxicol, 2010. **84**(4): p. 255-62.
13. Porter, N.A., S.E. Caldwell, and K.A. Mills, *Mechanisms of free radical oxidation of unsaturated lipids*. Lipids, 1995. **30**(4): p. 277-90.
14. Ayala, A., M.F. Munoz, and S. Arguelles, *Lipid peroxidation: production, metabolism, and signaling mechanisms of malondialdehyde and 4-hydroxy-2-nonenal*. Oxid Med Cell Longev, 2014. **2014**: p. 360438.
15. Gillmor, S.A., et al., *The structure of mammalian 15-lipoxygenase reveals similarity to the lipases and the determinants of substrate specificity*. Nat Struct Biol, 1997. **4**(12): p. 1003-9.
16. Kobe, M.J., et al., *The structure of human 15-lipoxygenase-2 with a substrate mimic*. J Biol Chem, 2014. **289**(12): p. 8562-9.
17. Ivanov, I., et al., *Molecular enzymology of lipoxygenases*. Arch Biochem Biophys, 2010. **503**(2): p. 161-74.

18. Haeggstrom, J.Z. and C.D. Funk, *Lipoxygenase and leukotriene pathways: biochemistry, biology, and roles in disease*. Chem Rev, 2011. **111**(10): p. 5866-98.
19. Oliw, E.H., *Plant and fungal lipoxygenases*. Prostaglandins Other Lipid Mediat, 2002. **68-69**: p. 313-23.
20. Vance, R.E., et al., *The opportunistic pathogen Pseudomonas aeruginosa carries a secretable arachidonate 15-lipoxygenase*. Proc Natl Acad Sci U S A, 2004. **101**(7): p. 2135-9.
21. Banthiya, S., et al., *Structural and functional basis of phospholipid oxygenase activity of bacterial lipoxygenase from Pseudomonas aeruginosa*. Biochim Biophys Acta, 2016. **1861**(11): p. 1681-1692.
22. Deschamps, J.D., et al., *Biochemical and Cellular Characterization and Inhibitor Discovery of Pseudomonas aeruginosa 15-Lipoxygenase*. Biochemistry, 2016. **55**(23): p. 3329-40.
23. Clark, S.R., et al., *Esterified eicosanoids are acutely generated by 5-lipoxygenase in primary human neutrophils and in human and murine infection*. Blood, 2011. **117**(6): p. 2033-43.
24. Arai, M., et al., *Preferential esterification of endogenously formed 5-hydroxyeicosatetraenoic acid to phospholipids in activated polymorphonuclear leukocytes*. Eur J Biochem, 1997. **244**(2): p. 513-9.
25. Birkle, D.L. and N.G. Bazan, *Effect of K<sup>+</sup> depolarization on the synthesis of prostaglandins and hydroxyeicosatetra(5,8,11,14)enoic acids (HETE) in the rat retina. Evidence for esterification of 12-HETE in lipids*. Biochim Biophys Acta, 1984. **795**(3): p. 564-73.
26. Stenson, W.F. and C.W. Parker, *Metabolism of arachidonic acid in ionophore-stimulated neutrophils. Esterification of a hydroxylated metabolite into phospholipids*. J Clin Invest, 1979. **64**(5): p. 1457-65.
27. Schewe, T., et al., *A lipoxygenase in rabbit reticulocytes which attacks phospholipids and intact mitochondria*. FEBS Lett, 1975. **60**(1): p. 149-52.
28. Murray, J.J. and A.R. Brash, *Rabbit reticulocyte lipoxygenase catalyzes specific 12(S) and 15(S) oxygenation of arachidonoyl-phosphatidylcholine*. Arch Biochem Biophys, 1988. **265**(2): p. 514-23.
29. Jung, G., D.C. Yang, and A. Nakao, *Oxygenation of phosphatidylcholine by human polymorphonuclear leukocyte 15-lipoxygenase*. Biochem Biophys Res Commun, 1985. **130**(2): p. 559-66.
30. Maskrey, B.H., et al., *Activated platelets and monocytes generate four hydroxyphosphatidylethanolamines via lipoxygenase*. J Biol Chem, 2007. **282**(28): p. 20151-63.
31. Bender, G., et al., *Membrane-dependent Activities of Human 15-LOX-2 and Its Murine Counterpart: IMPLICATIONS FOR MURINE MODELS OF ATHEROSCLEROSIS*. J Biol Chem, 2016. **291**(37): p. 19413-24.
32. Coffa, G. and A.R. Brash, *A single active site residue directs oxygenation stereospecificity in lipoxygenases: stereocontrol is linked to the position of oxygenation*. Proc Natl Acad Sci U S A, 2004. **101**(44): p. 15579-84.
33. Wenzel, S.E., et al., *PEBP1 Wardens Ferroptosis by Enabling Lipoxygenase Generation of Lipid Death Signals*. Cell, 2017. **171**(Oct. 19): p. 628-641.

34. Banthiya, S., et al., *Secreted lipoxygenase from Pseudomonas aeruginosa exhibits biomembrane oxygenase activity and induces hemolysis in human red blood cells*. Arch Biochem Biophys, 2015. **584**: p. 116-24.
35. Aldrovandi, M., et al., *Specific oxygenation of plasma membrane phospholipids by Pseudomonas aeruginosa lipoxygenase induces structural and functional alterations in mammalian cells*. Biochim Biophys Acta Mol Cell Biol Lipids, 2018. **1863**(2): p. 152-164.
36. Bochkov, V.N., et al., *Generation and biological activities of oxidized phospholipids*. Antioxid Redox Signal, 2010. **12**(8): p. 1009-59.
37. Fruhwirth, G.O., A. Loidl, and A. Hermetter, *Oxidized phospholipids: from molecular properties to disease*. Biochim Biophys Acta, 2007. **1772**(7): p. 718-36.
38. Dennis, E.A. and P.C. Norris, *Eicosanoid storm in infection and inflammation*. Nat Rev Immunol, 2015. **15**(8): p. 511-23.
39. Bochkov, V., et al., *Pleiotropic effects of oxidized phospholipids*. Free Radic Biol Med, 2017. **111**: p. 6-24.
40. Raja, V. and M.L. Greenberg, *The functions of cardiolipin in cellular metabolism-potential modifiers of the Barth syndrome phenotype*. Chem Phys Lipids, 2014. **179**: p. 49-56.
41. Schlame, M., et al., *Molecular symmetry in mitochondrial cardiolipins*. Chem Phys Lipids, 2005. **138**(1-2): p. 38-49.
42. Cheng, H., et al., *Shotgun lipidomics reveals the temporally dependent, highly diversified cardiolipin profile in the mammalian brain: temporally coordinated postnatal diversification of cardiolipin molecular species with neuronal remodeling*. Biochemistry, 2008. **47**(21): p. 5869-80.
43. Kiebish, M.A., et al., *Lipidomic analysis and electron transport chain activities in C57BL/6J mouse brain mitochondria*. J Neurochem, 2008. **106**(1): p. 299-312.
44. Tyurina, Y.Y., et al., *A mitochondrial pathway for biosynthesis of lipid mediators*. Nat Chem, 2014. **6**(6): p. 542-52.
45. Kagan, V.E., et al., *Cardiolipin signaling mechanisms: collapse of asymmetry and oxidation*. Antioxid Redox Signal, 2015. **22**(18): p. 1667-80.
46. Paradies, G., et al., *Functional role of cardiolipin in mitochondrial bioenergetics*. Biochim Biophys Acta, 2014. **1837**(4): p. 408-17.
47. Kameoka, S., et al., *Phosphatidic Acid and Cardiolipin Coordinate Mitochondrial Dynamics*. Trends Cell Biol, 2018. **28**(1): p. 67-76.
48. Chen, S., et al., *Loss of mitochondrial DNA in the yeast cardiolipin synthase *crd1* mutant leads to up-regulation of the protein kinase Swe1p that regulates the G2/M transition*. J Biol Chem, 2010. **285**(14): p. 10397-407.
49. Zhou, J., et al., *Loss of cardiolipin leads to longevity defects that are alleviated by alterations in stress response signaling*. J Biol Chem, 2009. **284**(27): p. 18106-14.
50. Chu, C.T., et al., *Cardiolipin externalization to the outer mitochondrial membrane acts as an elimination signal for mitophagy in neuronal cells*. Nat Cell Biol, 2013. **15**(10): p. 1197-1205.
51. Shen, Z., et al., *Cardiolipin Regulates Mitophagy through the Protein Kinase C Pathway*. J Biol Chem, 2017. **292**(7): p. 2916-2923.
52. Schug, Z.T. and E. Gottlieb, *Cardiolipin acts as a mitochondrial signalling platform to launch apoptosis*. Biochim Biophys Acta, 2009. **1788**(10): p. 2022-31.

53. Kagan, V.E., et al., *Cytochrome c acts as a cardiolipin oxygenase required for release of proapoptotic factors*. Nat Chem Biol, 2005. **1**(4): p. 223-32.
54. Kutik, S., et al., *The translocator maintenance protein Tam41 is required for mitochondrial cardiolipin biosynthesis*. J Cell Biol, 2008. **183**(7): p. 1213-21.
55. Tamura, Y., et al., *Tam41 is a CDP-diacylglycerol synthase required for cardiolipin biosynthesis in mitochondria*. Cell Metab, 2013. **17**(5): p. 709-18.
56. Schlame, M. and M.L. Greenberg, *Biosynthesis, remodeling and turnover of mitochondrial cardiolipin*. Biochim Biophys Acta Mol Cell Biol Lipids, 2017. **1862**(1): p. 3-7.
57. Tyurina, Y.Y., et al., *Lipidomics Characterization of Biosynthetic and Remodeling Pathways of Cardiolipins in Genetically and Nutritionally Manipulated Yeast Cells*. ACS Chem Biol, 2017. **12**(1): p. 265-281.
58. Xu, Y., et al., *The enzymatic function of tafazzin*. J Biol Chem, 2006. **281**(51): p. 39217-24.
59. Ren, M., C.K. Phoon, and M. Schlame, *Metabolism and function of mitochondrial cardiolipin*. Prog Lipid Res, 2014. **55**: p. 1-16.
60. Beranek, A., et al., *Identification of a cardiolipin-specific phospholipase encoded by the gene CLD1 (YGR110W) in yeast*. J Biol Chem, 2009. **284**(17): p. 11572-8.
61. Mancuso, D.J., et al., *Genetic ablation of calcium-independent phospholipase A2 $\gamma$  leads to alterations in hippocampal cardiolipin content and molecular species distribution, mitochondrial degeneration, autophagy, and cognitive dysfunction*. J Biol Chem, 2009. **284**(51): p. 35632-44.
62. Baile, M.G., K. Whited, and S.M. Claypool, *Deacylation on the matrix side of the mitochondrial inner membrane regulates cardiolipin remodeling*. Mol Biol Cell, 2013. **24**(12): p. 2008-20.
63. Baile, M.G., et al., *Unremodeled and remodeled cardiolipin are functionally indistinguishable in yeast*. J Biol Chem, 2014. **289**(3): p. 1768-78.
64. Schlame, M., et al., *Deficiency of tetralinoleoyl-cardiolipin in Barth syndrome*. Ann Neurol, 2002. **51**(5): p. 634-7.
65. Barth, P.G., et al., *An X-linked mitochondrial disease affecting cardiac muscle, skeletal muscle and neutrophil leucocytes*. J Neurol Sci, 1983. **62**(1-3): p. 327-55.
66. Aprikyan, A.A. and Z. Khuchua, *Advances in the understanding of Barth syndrome*. Br J Haematol, 2013. **161**(3): p. 330-8.
67. Valianpour, F., et al., *Monolysocardiolipins accumulate in Barth syndrome but do not lead to enhanced apoptosis*. J Lipid Res, 2005. **46**(6): p. 1182-95.
68. Ikon, N. and R.O. Ryan, *Barth Syndrome: Connecting Cardiolipin to Cardiomyopathy*. Lipids, 2017. **52**(2): p. 99-108.
69. van Werkhoven, M.A., et al., *Monolysocardiolipin in cultured fibroblasts is a sensitive and specific marker for Barth Syndrome*. J Lipid Res, 2006. **47**(10): p. 2346-51.
70. Ye, C., et al., *Deletion of the cardiolipin-specific phospholipase Cld1 rescues growth and life span defects in the tafazzin mutant: implications for Barth syndrome*. J Biol Chem, 2014. **289**(6): p. 3114-25.
71. Kagan, V.E., et al., *Cytochrome c acts as a cardiolipin oxygenase required for release of proapoptotic factors*. Nature chemical biology, 2005. **1**(4): p. 223-232.
72. Kagan, V.E., et al., *Cytochrome c/cardiolipin relations in mitochondria: a kiss of death*. Free Radic Biol Med, 2009. **46**(11): p. 1439-53.

73. Huang, Z., et al., *Cardiolipin deficiency leads to decreased cardiolipin peroxidation and increased resistance of cells to apoptosis*. Free Radic Biol Med, 2008. **44**(11): p. 1935-44.
74. Tyurin, V.A., et al., *Mass-spectrometric characterization of phospholipids and their primary peroxidation products in rat cortical neurons during staurosporine-induced apoptosis*. J Neurochem, 2008. **107**(6): p. 1614-33.
75. Bayir, H., et al., *Selective early cardiolipin peroxidation after traumatic brain injury: an oxidative lipidomics analysis*. Ann Neurol, 2007. **62**(2): p. 154-69.
76. Tyurina, Y.Y., et al., *Oxidative lipidomics of gamma-irradiation-induced intestinal injury*. Free Radic Biol Med, 2008. **44**(3): p. 299-314.
77. Verkleij, A.J. and J.A. Post, *Membrane phospholipid asymmetry and signal transduction*. J Membr Biol, 2000. **178**(1): p. 1-10.
78. Fadok, V.A., et al., *Loss of phospholipid asymmetry and surface exposure of phosphatidylserine is required for phagocytosis of apoptotic cells by macrophages and fibroblasts*. J Biol Chem, 2001. **276**(2): p. 1071-7.
79. Fadok, V.A., et al., *Exposure of phosphatidylserine on the surface of apoptotic lymphocytes triggers specific recognition and removal by macrophages*. J Immunol, 1992. **148**(7): p. 2207-16.
80. Tyurin, V.A., et al., *Oxidatively modified phosphatidylserines on the surface of apoptotic cells are essential phagocytic 'eat-me' signals: cleavage and inhibition of phagocytosis by Lp-PLA2*. Cell Death Differ, 2014. **21**(5): p. 825-35.
81. Kagan, V.E., et al., *Oxidative lipidomics of apoptosis: redox catalytic interactions of cytochrome c with cardiolipin and phosphatidylserine*. Free Radic Biol Med, 2004. **37**(12): p. 1963-85.
82. Matura, T., *Oxidized phosphatidylserine: production and bioactivities*. Yonago Acta Med, 2014. **57**(4): p. 119-27.
83. Dixon, S.J., et al., *Ferroptosis: an iron-dependent form of nonapoptotic cell death*. Cell, 2012. **149**(5): p. 1060-72.
84. Yang, W.S., et al., *Regulation of ferroptotic cancer cell death by GPX4*. Cell, 2014. **156**(1-2): p. 317-331.
85. Ingold, I., et al., *Selenium Utilization by GPX4 Is Required to Prevent Hydroperoxide-Induced Ferroptosis*. Cell, 2018. **172**(3): p. 409-422 e21.
86. Mao, G.W., et al., *Tocopherols and tocotrienols prevent lipoxygenase-driven phospholipid oxidation in ferroptosis*. Faseb Journal, 2017. **31**.
87. Hinman, A., et al., *Vitamin E hydroquinone is an endogenous regulator of ferroptosis via redox control of 15-lipoxygenase*. PLoS One, 2018. **13**(8): p. e0201369.
88. Doll, S., et al., *ACSL4 dictates ferroptosis sensitivity by shaping cellular lipid composition*. Nat Chem Biol, 2017. **13**(1): p. 91-98.
89. Dixon, S.J., et al., *Human Haploid Cell Genetics Reveals Roles for Lipid Metabolism Genes in Nonapoptotic Cell Death*. ACS Chem Biol, 2015. **10**(7): p. 1604-9.
90. Kagan, V.E., et al., *Oxidized arachidonic and adrenic PEs navigate cells to ferroptosis*. Nat Chem Biol, 2017. **13**(1): p. 81-90.
91. Wenzel, S.E., et al., *PEBP1 Wardens Ferroptosis by Enabling Lipoxygenase Generation of Lipid Death Signals*. Cell, 2017. **171**(3): p. 628-641 e26.
92. Skouta, R., et al., *Ferostatins inhibit oxidative lipid damage and cell death in diverse disease models*. J Am Chem Soc, 2014. **136**(12): p. 4551-6.

93. Do Van, B., et al., *Ferroptosis, a newly characterized form of cell death in Parkinson's disease that is regulated by PKC*. Neurobiol Dis, 2016. **94**: p. 169-78.
94. Hambright, W.S., et al., *Ablation of ferroptosis regulator glutathione peroxidase 4 in forebrain neurons promotes cognitive impairment and neurodegeneration*. Redox Biol, 2017. **12**: p. 8-17.
95. Anthonymuthu, T.S., et al., *Oxidized phospholipid signaling in traumatic brain injury*. Free Radic Biol Med, 2018. **124**: p. 493-503.
96. Li, Q., et al., *Inhibition of neuronal ferroptosis protects hemorrhagic brain*. JCI Insight, 2017. **2**(7): p. e90777.
97. Linkermann, A., et al., *Synchronized renal tubular cell death involves ferroptosis*. Proc Natl Acad Sci U S A, 2014. **111**(47): p. 16836-41.
98. Friedmann Angeli, J.P., et al., *Inactivation of the ferroptosis regulator Gpx4 triggers acute renal failure in mice*. Nat Cell Biol, 2014. **16**(12): p. 1180-91.
99. Lorincz, T., et al., *Ferroptosis is Involved in Acetaminophen Induced Cell Death*. Pathol Oncol Res, 2015. **21**(4): p. 1115-21.
100. Wang, H., et al., *Characterization of ferroptosis in murine models of hemochromatosis*. Hepatology, 2017. **66**(2): p. 449-465.
101. Kang, Y., et al., *Cellular protection using Flt3 and PI3Kalpha inhibitors demonstrates multiple mechanisms of oxidative glutamate toxicity*. Nat Commun, 2014. **5**: p. 3672.
102. Fan, Z., et al., *Nrf2-Keap1 pathway promotes cell proliferation and diminishes ferroptosis*. Oncogenesis, 2017. **6**(8): p. e371.
103. Jiang, L., et al., *Ferroptosis as a p53-mediated activity during tumour suppression*. Nature, 2015. **520**(7545): p. 57-62.
104. Wang, S.J., et al., *Acetylation Is Crucial for p53-Mediated Ferroptosis and Tumor Suppression*. Cell Rep, 2016. **17**(2): p. 366-373.
105. Ou, Y., et al., *Activation of SAT1 engages polyamine metabolism with p53-mediated ferroptotic responses*. Proc Natl Acad Sci U S A, 2016. **113**(44): p. E6806-E6812.
106. Tarangelo, A., et al., *p53 Suppresses Metabolic Stress-Induced Ferroptosis in Cancer Cells*. Cell Rep, 2018. **22**(3): p. 569-575.
107. Shimada, K., et al., *Global survey of cell death mechanisms reveals metabolic regulation of ferroptosis*. Nat Chem Biol, 2016. **12**(7): p. 497-503.
108. Zhang, Y., et al., *BAP1 links metabolic regulation of ferroptosis to tumour suppression*. Nat Cell Biol, 2018. **20**(10): p. 1181-1192.
109. Ejsing, C.S., et al., *Global analysis of the yeast lipidome by quantitative shotgun mass spectrometry*. Proc Natl Acad Sci U S A, 2009. **106**(7): p. 2136-41.
110. Klose, C., et al., *Flexibility of a eukaryotic lipidome--insights from yeast lipidomics*. PLoS One, 2012. **7**(4): p. e35063.
111. Stukey, J.E., V.M. McDonough, and C.E. Martin, *The OLE1 gene of Saccharomyces cerevisiae encodes the delta 9 fatty acid desaturase and can be functionally replaced by the rat stearyl-CoA desaturase gene*. J Biol Chem, 1990. **265**(33): p. 20144-9.
112. Krasowska, A., et al., *Spontaneous and radical-induced plasma membrane lipid peroxidation in differently oxidant-sensitive yeast species and its suppression by antioxidants*. Folia Microbiol (Praha), 2000. **45**(6): p. 509-14.
113. Hein, E.M. and H. Hayen, *Comparative Lipidomic Profiling of S. cerevisiae and Four Other Hemiascomycetous Yeasts*. Metabolites, 2012. **2**(1): p. 254-67.

114. Rockenfeller, P., et al., *Fatty acids trigger mitochondrion-dependent necrosis*. Cell Cycle, 2010. **9**(14): p. 2836-42.
115. Ferreira, T.C., L.M. de Moraes, and E.G. Campos, *Cell density-dependent linoleic acid toxicity to Saccharomyces cerevisiae*. FEMS Yeast Res, 2011. **11**(5): p. 408-17.
116. Masia, A., et al., *Enrichment with a polyunsaturated fatty acid enhances the survival of Saccharomyces cerevisiae in the presence of tributyltin*. FEMS Microbiol Lett, 1998. **167**(2): p. 321-6.
117. Yazawa, H., et al., *Production of polyunsaturated fatty acids in yeast Saccharomyces cerevisiae and its relation to alkaline pH tolerance*. Yeast, 2009. **26**(3): p. 167-84.
118. Avery, S.V., N.G. Howlett, and S. Radice, *Copper toxicity towards Saccharomyces cerevisiae: dependence on plasma membrane fatty acid composition*. Appl Environ Microbiol, 1996. **62**(11): p. 3960-6.
119. Howlett, N.G. and S.V. Avery, *Induction of lipid peroxidation during heavy metal stress in Saccharomyces cerevisiae and influence of plasma membrane fatty acid unsaturation*. Appl Environ Microbiol, 1997. **63**(8): p. 2971-6.
120. Tanomman, S., et al., *Characterization of fatty acid delta-6 desaturase gene in Nile tilapia and heterogenous expression in Saccharomyces cerevisiae*. Comp Biochem Physiol B Biochem Mol Biol, 2013. **166**(2): p. 148-56.
121. Tavares, S., et al., *Metabolic engineering of Saccharomyces cerevisiae for production of Eicosapentaenoic Acid, using a novel {Delta}5-Desaturase from Paramecium tetraurelia*. Appl Environ Microbiol, 2011. **77**(5): p. 1854-61.
122. Sakuradani, E., et al., *Identification of Delta12-fatty acid desaturase from arachidonic acid-producing mortierella fungus by heterologous expression in the yeast Saccharomyces cerevisiae and the fungus Aspergillus oryzae*. Eur J Biochem, 1999. **261**(3): p. 812-20.
123. Napier, J.A., et al., *Identification of a Caenorhabditis elegans Delta6-fatty-acid-desaturase by heterologous expression in Saccharomyces cerevisiae*. Biochem J, 1998. **330 ( Pt 2)**: p. 611-4.
124. Bucek, A., et al., *Delta12-Fatty acid desaturase from Candida parapsilosis is a multifunctional desaturase producing a range of polyunsaturated and hydroxylated fatty acids*. PLoS One, 2014. **9**(3): p. e93322.
125. Cipak, A., et al., *Saccharomyces cerevisiae strain expressing a plant fatty acid desaturase produces polyunsaturated fatty acids and is susceptible to oxidative stress induced by lipid peroxidation*. Free Radic Biol Med, 2006. **40**(5): p. 897-906.
126. Johansson, M., et al., *PUFA-induced cell death is mediated by Yca1p-dependent and -independent pathways, and is reduced by vitamin C in yeast*. FEMS Yeast Res, 2016. **16**(2): p. fow007.
127. *Classics in infectious diseases. On the blue and green coloration that appears on bandages. By Carle Gessard (1850-1925)*. Rev Infect Dis, 1984. **6 Suppl 3**: p. S775-6.
128. Cross, A., et al., *Nosocomial infections due to Pseudomonas aeruginosa: review of recent trends*. Rev Infect Dis, 1983. **5 Suppl 5**: p. S837-45.
129. Driscoll, J.A., S.L. Brody, and M.H. Kollef, *The epidemiology, pathogenesis and treatment of Pseudomonas aeruginosa infections*. Drugs, 2007. **67**(3): p. 351-68.
130. Weiner, L.M., et al., *Antimicrobial-Resistant Pathogens Associated With Healthcare-Associated Infections: Summary of Data Reported to the National Healthcare Safety*

- Network at the Centers for Disease Control and Prevention, 2011-2014. Infect Control Hosp Epidemiol*, 2016. **37**(11): p. 1288-1301.
131. Gellatly, S.L. and R.E. Hancock, *Pseudomonas aeruginosa: new insights into pathogenesis and host defenses*. *Pathog Dis*, 2013. **67**(3): p. 159-73.
  132. Williams, B.J., J. Dehnbostel, and T.S. Blackwell, *Pseudomonas aeruginosa: host defence in lung diseases*. *Respirology*, 2010. **15**(7): p. 1037-56.
  133. Rhodes, N.J., et al., *Resistance Trends and Treatment Options in Gram-Negative Ventilator-Associated Pneumonia*. *Curr Infect Dis Rep*, 2018. **20**(2): p. 3.
  134. Davies, J.C., *Pseudomonas aeruginosa in cystic fibrosis: pathogenesis and persistence*. *Paediatr Respir Rev*, 2002. **3**(2): p. 128-34.
  135. Bhagirath, A.Y., et al., *Cystic fibrosis lung environment and Pseudomonas aeruginosa infection*. *BMC Pulm Med*, 2016. **16**(1): p. 174.
  136. Bragonzi, A., et al., *Pseudomonas aeruginosa microevolution during cystic fibrosis lung infection establishes clones with adapted virulence*. *Am J Respir Crit Care Med*, 2009. **180**(2): p. 138-45.
  137. Moradali, M.F., S. Ghods, and B.H. Rehm, *Pseudomonas aeruginosa Lifestyle: A Paradigm for Adaptation, Survival, and Persistence*. *Front Cell Infect Microbiol*, 2017. **7**: p. 39.
  138. Epanand, R.M. and R.F. Epanand, *Domains in bacterial membranes and the action of antimicrobial agents*. *Mol Biosyst*, 2009. **5**(6): p. 580-7.
  139. Benamara, H., et al., *Characterization of membrane lipidome changes in Pseudomonas aeruginosa during biofilm growth on glass wool*. *PLoS One*, 2014. **9**(9): p. e108478.
  140. Russell, N.J. and D.S. Nichols, *Polyunsaturated fatty acids in marine bacteria--a dogma rewritten*. *Microbiology*, 1999. **145** ( Pt 4): p. 767-79.
  141. Yazawa, K., *Production of eicosapentaenoic acid from marine bacteria*. *Lipids*, 1996. **31** **Suppl**: p. S297-300.
  142. Baker, L.Y., et al., *Pseudomonas aeruginosa responds to exogenous polyunsaturated fatty acids (PUFAs) by modifying phospholipid composition, membrane permeability, and phenotypes associated with virulence*. *BMC Microbiol*, 2018. **18**(1): p. 117.
  143. Moravec, A.R., et al., *Exogenous Polyunsaturated Fatty Acids Impact Membrane Remodeling and Affect Virulence Phenotypes among Pathogenic Vibrio Species*. *Appl Environ Microbiol*, 2017. **83**(22).
  144. Kang, Y., et al., *The Pseudomonas aeruginosa PsaA responds to long-chain fatty acid signals to regulate the fadBA5 beta-oxidation operon*. *Microbiology*, 2008. **154**(Pt 6): p. 1584-98.
  145. Liaw, S.J., H.C. Lai, and W.B. Wang, *Modulation of swarming and virulence by fatty acids through the RsbA protein in Proteus mirabilis*. *Infect Immun*, 2004. **72**(12): p. 6836-45.
  146. Kenny, J.G., et al., *The Staphylococcus aureus response to unsaturated long chain free fatty acids: survival mechanisms and virulence implications*. *PLoS One*, 2009. **4**(2): p. e4344.
  147. Sun, Y., et al., *Fatty acids regulate stress resistance and virulence factor production for Listeria monocytogenes*. *J Bacteriol*, 2012. **194**(19): p. 5274-84.
  148. Thompson, L., A. Cockayne, and R.C. Spiller, *Inhibitory effect of polyunsaturated fatty acids on the growth of Helicobacter pylori: a possible explanation of the effect of diet on peptic ulceration*. *Gut*, 1994. **35**(11): p. 1557-61.

149. Giamarellos-Bourboulis, E.J., et al., *In vitro influence of polyunsaturated fatty acids on nosocomial Pseudomonas aeruginosa: a preliminary report*. Int J Antimicrob Agents, 1995. **6**(1): p. 47-50.
150. Miller, R.D., K.E. Brown, and S.A. Morse, *Inhibitory action of fatty acids on the growth of Neisseria gonorrhoeae*. Infect Immun, 1977. **17**(2): p. 303-12.
151. Conde-Alvarez, R., et al., *Synthesis of phosphatidylcholine, a typical eukaryotic phospholipid, is necessary for full virulence of the intracellular bacterial parasite Brucella abortus*. Cell Microbiol, 2006. **8**(8): p. 1322-35.
152. Rossi, R.M., et al., *Cardiolipin Synthesis and Outer Membrane Localization Are Required for Shigella flexneri Virulence*. MBio, 2017. **8**(4).
153. Dalebroux, Z.D., et al., *Delivery of cardiolipins to the Salmonella outer membrane is necessary for survival within host tissues and virulence*. Cell Host Microbe, 2015. **17**(4): p. 441-51.
154. Panjwani, N., et al., *Pathogenesis of corneal infection: binding of Pseudomonas aeruginosa to specific phospholipids*. Infect Immun, 1996. **64**(5): p. 1819-25.
155. Slavetinsky, C., S. Kuhn, and A. Peschel, *Bacterial aminoacyl phospholipids - Biosynthesis and role in basic cellular processes and pathogenicity*. Biochim Biophys Acta Mol Cell Biol Lipids, 2017. **1862**(11): p. 1310-1318.
156. Rashid, R., et al., *Comprehensive analysis of phospholipids and glycolipids in the opportunistic pathogen Enterococcus faecalis*. PLoS One, 2017. **12**(4): p. e0175886.
157. Giamarellos-Bourboulis, E.J., et al., *Lipid peroxidation by Pseudomonas aeruginosa in the pathogenesis of nosocomial sepsis*. J Postgrad Med, 2003. **49**(1): p. 11-6; discussion 16.
158. Toufekoula, C., et al., *Compartmentalization of lipid peroxidation in sepsis by multidrug-resistant gram-negative bacteria: experimental and clinical evidence*. Crit Care, 2013. **17**(1): p. R6.
159. Sorrell, T.C., M. Muller, and K. Sztelma, *Bacterial metabolism of human polymorphonuclear leukocyte-derived arachidonic acid*. Infect Immun, 1992. **60**(5): p. 1779-85.
160. Flitter, B.A., et al., *Pseudomonas aeruginosa sabotages the generation of host proresolving lipid mediators*. Proc Natl Acad Sci U S A, 2017. **114**(1): p. 136-141.
161. Alegria, T.G., et al., *Ohr plays a central role in bacterial responses against fatty acid hydroperoxides and peroxyxynitrite*. Proc Natl Acad Sci U S A, 2017. **114**(2): p. E132-E141.
162. Garreta, A., et al., *Structure and interaction with phospholipids of a prokaryotic lipoxygenase from Pseudomonas aeruginosa*. FASEB J, 2013. **27**(12): p. 4811-21.
163. Pangborn, M.C., *Isolation and purification of a serologically active phospholipid from beef heart*. Journal of Biological Chemistry, 1942. **143**(1): p. 247-256.
164. Schlame, M., D. Rua, and M.L. Greenberg, *The biosynthesis and functional role of cardiolipin*. Progress in lipid research, 2000. **39**(3): p. 257-88.
165. Schlame, M. and M.L. Greenberg, *Biosynthesis, remodeling and turnover of mitochondrial cardiolipin*. Biochim Biophys Acta, 2017. **1862**(1): p. 3-7.
166. Joshi, A.S., et al., *Cellular functions of cardiolipin in yeast*. Biochimica et biophysica acta, 2009. **1793**(1): p. 212-8.
167. Claypool, S.M., et al., *Cardiolipin defines the interactome of the major ADP/ATP carrier protein of the mitochondrial inner membrane*. J Cell Biol, 2008. **182**(5): p. 937-50.

168. Jiang, F., et al., *Absence of cardiolipin in the crd1 null mutant results in decreased mitochondrial membrane potential and reduced mitochondrial function*. J Biol Chem, 2000. **275**(29): p. 22387-94.
169. Gohil, V.M., et al., *Cardiolipin biosynthesis and mitochondrial respiratory chain function are interdependent*. J Biol Chem, 2004. **279**(41): p. 42612-8.
170. Raja, V., et al., *Loss of Cardiolipin Leads to Perturbation of Acetyl-CoA Synthesis*. J Biol Chem, 2017. **292**(3): p. 1092-1102.
171. Patil, V.A., et al., *Loss of cardiolipin leads to perturbation of mitochondrial and cellular iron homeostasis*. J Biol Chem, 2013. **288**(3): p. 1696-705.
172. Gebert, N., et al., *Mitochondrial cardiolipin involved in outer-membrane protein biogenesis: implications for Barth syndrome*. Curr Biol, 2009. **19**(24): p. 2133-9.
173. Joshi, A.S., N. Fei, and M.L. Greenberg, *Get1p and Get2p are required for maintenance of mitochondrial morphology and normal cardiolipin levels*. FEMS Yeast Res, 2016. **16**(3).
174. Joshi, A.S., et al., *Cardiolipin and mitochondrial phosphatidylethanolamine have overlapping functions in mitochondrial fusion in Saccharomyces cerevisiae*. J Biol Chem, 2012. **287**(21): p. 17589-97.
175. Bione, S., et al., *A novel X-linked gene, G4.5. is responsible for Barth syndrome*. Nat Genet, 1996. **12**(4): p. 385-9.
176. Shen, Z., et al., *The Role of Cardiolipin in Cardiovascular Health*. Biomed Res Int, 2015. **2015**: p. 891707.
177. Jiang, J., et al., *Interplay between bax, reactive oxygen species production, and cardiolipin oxidation during apoptosis*. Biochem Biophys Res Commun, 2008. **368**(1): p. 145-50.
178. Tyurina, Y.Y., et al., *Mechanisms of cardiolipin oxidation by cytochrome c: relevance to pro- and antiapoptotic functions of etoposide*. Mol Pharmacol, 2006. **70**(2): p. 706-17.
179. Kriska, T., W. Korytowski, and A.W. Girotti, *Role of mitochondrial cardiolipin peroxidation in apoptotic photokilling of 5-aminolevulinic acid-treated tumor cells*. Arch Biochem Biophys, 2005. **433**(2): p. 435-46.
180. Petrosillo, G., et al., *Reactive oxygen species generated from the mitochondrial electron transport chain induce cytochrome c dissociation from beef-heart submitochondrial particles via cardiolipin peroxidation. Possible role in the apoptosis*. FEBS Lett, 2001. **509**(3): p. 435-8.
181. Vadkertiova, R., et al., *Yeasts and yeast-like organisms associated with fruits and blossoms of different fruit trees*. Can J Microbiol, 2012. **58**(12): p. 1344-52.
182. Spencer, J.F.T. and D.M. Spencer, *Ecology: Where Yeasts Live*, in *Yeasts in Natural and Artificial Habitats*, J.F.T. Spencer and D.M. Spencer, Editors. 1997, Springer Berlin Heidelberg: Berlin, Heidelberg. p. 33-58.
183. Spencer, J.F. and D.M. Spencer, *Yeasts in natural and artificial habitats*. 2013: Springer Science & Business Media.
184. Huffnagle, G.B. and M.C. Noverr, *The emerging world of the fungal microbiome*. Trends in microbiology, 2013. **21**(7): p. 334-341.
185. Andrisic, L., et al., *Transcriptional and antioxidative responses to endogenous polyunsaturated fatty acid accumulation in yeast*. Mol Cell Biochem, 2015. **399**(1-2): p. 27-37.

186. Kim, J. and C.L. Hoppel, *Monolysocardiolipin: improved preparation with high yield*. J Lipid Res, 2011. **52**(2): p. 389-92.
187. Fabrizio, P. and V.D. Longo, *The chronological life span of Saccharomyces cerevisiae*. Aging Cell, 2003. **2**(2): p. 73-81.
188. Hu, J., et al., *Assessing chronological aging in Saccharomyces cerevisiae*. Methods Mol Biol, 2013. **965**: p. 463-72.
189. Chang, S.C., et al., *Isolation and characterization of the gene (CLS1) encoding cardiolipin synthase in Saccharomyces cerevisiae*. J Biol Chem, 1998. **273**(24): p. 14933-41.
190. Tuller, G., et al., *YDL142c encodes cardiolipin synthase (Cls1p) and is non-essential for aerobic growth of Saccharomyces cerevisiae*. FEBS Lett, 1998. **421**(1): p. 15-8.
191. Tamai, K.T. and M.L. Greenberg, *Biochemical characterization and regulation of cardiolipin synthase in Saccharomyces cerevisiae*. Biochim Biophys Acta, 1990. **1046**(2): p. 214-22.
192. Jiang, F., H.S. Rizavi, and M.L. Greenberg, *Cardiolipin is not essential for the growth of Saccharomyces cerevisiae on fermentable or non-fermentable carbon sources*. Mol Microbiol, 1997. **26**(3): p. 481-91.
193. Xu, Y., et al., *Remodeling of cardiolipin by phospholipid transacylation*. J Biol Chem, 2003. **278**(51): p. 51380-5.
194. Losito, I., et al., *Improved specificity of cardiolipin peroxidation by soybean lipoxigenase: a liquid chromatography - electrospray ionization mass spectrometry investigation*. J Mass Spectrom, 2011. **46**(12): p. 1255-62.
195. Chen, Z., et al., *Profiling of cardiolipins and their hydroperoxides in HepG2 cells by LC/MS*. Anal Bioanal Chem, 2017. **409**(24): p. 5735-5745.
196. Wright, M.M. and C.R. McMaster, *PC and PE synthesis: mixed micellar analysis of the cholinephosphotransferase and ethanolaminephosphotransferase activities of human choline/ethanolamine phosphotransferase 1 (CEPT1)*. Lipids, 2002. **37**(7): p. 663-72.
197. Carman, G.M. and G.M. Zeimet, *Regulation of phospholipid biosynthesis in the yeast Saccharomyces cerevisiae*. J Biol Chem, 1996. **271**(23): p. 13293-6.
198. Niki, E., *Free radical initiators as source of water- or lipid-soluble peroxy radicals*. Methods Enzymol, 1990. **186**: p. 100-8.
199. Musatov, A., *Contribution of peroxidized cardiolipin to inactivation of bovine heart cytochrome c oxidase*. Free Radic Biol Med, 2006. **41**(2): p. 238-46.
200. Grivennikova, V.G. and A.D. Vinogradov, *Generation of superoxide by the mitochondrial Complex I*. Biochim Biophys Acta, 2006. **1757**(5-6): p. 553-61.
201. Minners, J., et al., *Diazoxide-induced respiratory inhibition - a putative mitochondrial K(ATP) channel independent mechanism of pharmacological preconditioning*. Mol Cell Biochem, 2007. **294**(1-2): p. 11-8.
202. Liu, G.Y., et al., *The phospholipase iPLA2gamma is a major mediator releasing oxidized aliphatic chains from cardiolipin, integrating mitochondrial bioenergetics and signaling*. J Biol Chem, 2017. **292**(25): p. 10672-10684.
203. Zinser, E., et al., *Phospholipid synthesis and lipid composition of subcellular membranes in the unicellular eukaryote Saccharomyces cerevisiae*. J Bacteriol, 1991. **173**(6): p. 2026-34.
204. Atkinson, K., S. Fogel, and S.A. Henry, *Yeast mutant defective in phosphatidylserine synthesis*. J Biol Chem, 1980. **255**(14): p. 6653-61.

205. Carman, G.M. and S.A. Henry, *Phospholipid biosynthesis in yeast*. *Annu Rev Biochem*, 1989. **58**: p. 635-69.
206. Simbeni, R., et al., *Import of phosphatidylserine into isolated yeast mitochondria*. *Biochim Biophys Acta*, 1993. **1145**(1): p. 1-7.
207. Pascual-Ahuir, A., S. Manzanares-Estredor, and M. Proft, *Pro- and Antioxidant Functions of the Peroxisome-Mitochondria Connection and Its Impact on Aging and Disease*. *Oxid Med Cell Longev*, 2017. **2017**: p. 9860841.
208. Luttkik, M.A., et al., *The Saccharomyces cerevisiae NDE1 and NDE2 genes encode separate mitochondrial NADH dehydrogenases catalyzing the oxidation of cytosolic NADH*. *J Biol Chem*, 1998. **273**(38): p. 24529-34.
209. de Vries, S. and L.A. Grivell, *Purification and characterization of a rotenone-insensitive NADH:Q6 oxidoreductase from mitochondria of Saccharomyces cerevisiae*. *Eur J Biochem*, 1988. **176**(2): p. 377-84.
210. Mesquita, A., et al., *Caloric restriction or catalase inactivation extends yeast chronological lifespan by inducing H<sub>2</sub>O<sub>2</sub> and superoxide dismutase activity*. *Proc Natl Acad Sci U S A*, 2010. **107**(34): p. 15123-8.
211. McClelland, L.J., et al., *Structure of a mitochondrial cytochrome c conformer competent for peroxidase activity*. *Proc Natl Acad Sci U S A*, 2014. **111**(18): p. 6648-53.
212. Elmer-Dixon, M.M. and B.E. Bowler, *Site A-Mediated Partial Unfolding of Cytochrome c on Cardiolipin Vesicles Is Species-Dependent and Does Not Require Lys72*. *Biochemistry*, 2017. **56**(36): p. 4830-4839.
213. Kagan, V.E., et al., *Cardiolipin asymmetry, oxidation and signaling*. *Chem Phys Lipids*, 2014. **179**: p. 64-9.
214. Imai, H., et al., *Lipid Peroxidation-Dependent Cell Death Regulated by GPx4 and Ferroptosis*. *Curr Top Microbiol Immunol*, 2017. **403**: p. 143-170.
215. Maiorino, M., M. Conrad, and F. Ursini, *GPx4, Lipid Peroxidation, and Cell Death: Discoveries, Rediscoveries, and Open Issues*. *Antioxid Redox Signal*, 2017.
216. Avery, A.M., S.A. Willetts, and S.V. Avery, *Genetic dissection of the phospholipid hydroperoxidase activity of yeast gpx3 reveals its functional importance*. *J Biol Chem*, 2004. **279**(45): p. 46652-8.
217. Avery, A.M. and S.V. Avery, *Saccharomyces cerevisiae expresses three phospholipid hydroperoxide glutathione peroxidases*. *J Biol Chem*, 2001. **276**(36): p. 33730-5.
218. Yang, W.S., et al., *Peroxidation of polyunsaturated fatty acids by lipoxygenases drives ferroptosis*. *Proc Natl Acad Sci U S A*, 2016. **113**(34): p. E4966-75.
219. Mao, G., et al., *Mitochondrial Redox Opto-Lipidomics Reveals Mono-Oxygenated Cardiolipins as Pro-Apoptotic Death Signals*. *ACS Chem Biol*, 2016. **11**(2): p. 530-40.
220. Nakagawa, Y., *Initiation of apoptotic signal by the peroxidation of cardiolipin of mitochondria*. *Ann N Y Acad Sci*, 2004. **1011**: p. 177-84.
221. Zhong, H., et al., *Mitochondrial control of apoptosis through modulation of cardiolipin oxidation in hepatocellular carcinoma: A novel link between oxidative stress and cancer*. *Free Radic Biol Med*, 2017. **102**: p. 67-76.
222. Jiang, J., et al., *Designing inhibitors of cytochrome c/cardiolipin peroxidase complexes: mitochondria-targeted imidazole-substituted fatty acids*. *Free Radic Biol Med*, 2014. **71**: p. 221-30.
223. Maddalena, L.A., et al., *The mitochondria-targeted imidazole substituted oleic acid 'TPP-IOA' affects mitochondrial bioenergetics and its protective efficacy in cells is influenced*

- by cellular dependence on aerobic metabolism. *Biochim Biophys Acta*, 2017. **1858**(1): p. 73-85.
224. Cipak, A., et al., *Adaptation to oxidative stress induced by polyunsaturated fatty acids in yeast*. *Biochim Biophys Acta*, 2008. **1781**(6-7): p. 283-7.
  225. Kagan, V.E., et al., *Oxidized arachidonic and adrenic PEs navigate cells to ferroptosis*. *Nat Chem Biol*, 2017. **13**(1): p. 81-90.
  226. Kuhn, H., M. Walther, and R.J. Kuban, *Mammalian arachidonate 15-lipoxygenases structure, function, and biological implications*. *Prostaglandins Other Lipid Mediat*, 2002. **68-69**: p. 263-90.
  227. Hansen, J., et al., *Bacterial lipoxygenases, a new subfamily of enzymes? A phylogenetic approach*. *Appl Microbiol Biotechnol*, 2013. **97**(11): p. 4737-47.
  228. Horn, T., et al., *Evolutionary aspects of lipoxygenases and genetic diversity of human leukotriene signaling*. *Prog Lipid Res*, 2015. **57**: p. 13-39.
  229. Jacobs, M.A., et al., *Comprehensive transposon mutant library of Pseudomonas aeruginosa*. *Proc Natl Acad Sci U S A*, 2003. **100**(24): p. 14339-44.
  230. Starkey, M., et al., *Pseudomonas aeruginosa rugose small-colony variants have adaptations that likely promote persistence in the cystic fibrosis lung*. *J Bacteriol*, 2009. **191**(11): p. 3492-503.
  231. Lee, D.G., et al., *Genomic analysis reveals that Pseudomonas aeruginosa virulence is combinatorial*. *Genome Biol*, 2006. **7**(10): p. R90.
  232. Choi, K.H. and H.P. Schweizer, *mini-Tn7 insertion in bacteria with single attTn7 sites: example Pseudomonas aeruginosa*. *Nat Protoc*, 2006. **1**(1): p. 153-61.
  233. Choi, K.H., et al., *Genetic tools for select-agent-compliant manipulation of Burkholderia pseudomallei*. *Appl Environ Microbiol*, 2008. **74**(4): p. 1064-75.
  234. Khakimova, M., et al., *The stringent response controls catalases in Pseudomonas aeruginosa and is required for hydrogen peroxide and antibiotic tolerance*. *J Bacteriol*, 2013. **195**(9): p. 2011-20.
  235. O'Toole, G.A. and R. Kolter, *Initiation of biofilm formation in Pseudomonas fluorescens WCS365 proceeds via multiple, convergent signalling pathways: a genetic analysis*. *Mol Microbiol*, 1998. **28**(3): p. 449-61.
  236. Zemke, A.C., et al., *Nitrite modulates bacterial antibiotic susceptibility and biofilm formation in association with airway epithelial cells*. *Free Radic Biol Med*, 2014. **77**: p. 307-16.
  237. Muller, M. and N.D. Merrett, *Mechanism for glutathione-mediated protection against the Pseudomonas aeruginosa redox toxin, pyocyanin*. *Chem Biol Interact*, 2015. **232**: p. 30-7.
  238. Koes, D.R., M.P. Baumgartner, and C.J. Camacho, *Lessons Learned in Empirical Scoring with smina from the CSAR 2011 Benchmarking Exercise*. *Journal of chemical information and modeling*, 2013. **53**(8): p. 1893-1904.
  239. Finn, R.D., et al., *The Pfam protein families database: towards a more sustainable future*. *Nucleic Acids Res*, 2016. **44**(D1): p. D279-85.
  240. Bakan, A., et al., *Evol and ProDy for bridging protein sequence evolution and structural dynamics*. *Bioinformatics*, 2014. **30**(18): p. 2681-3.
  241. Edgar, R.C., *MUSCLE: a multiple sequence alignment method with reduced time and space complexity*. *BMC Bioinformatics*, 2004. **5**: p. 113.
  242. Edgar, R.C., *MUSCLE: multiple sequence alignment with high accuracy and high throughput*. *Nucleic Acids Res*, 2004. **32**(5): p. 1792-7.

243. Okonechnikov, K., O. Golosova, and M. Fursov, *Unipro UGENE: a unified bioinformatics toolkit*. Bioinformatics, 2012. **28**(8): p. 1166-7.
244. Eyal, E., G. Lum, and I. Bahar, *The anisotropic network model web server at 2015 (ANM 2.0)*. Bioinformatics, 2015. **31**(9): p. 1487-9.
245. Li, H., et al., *iGNM 2.0: the Gaussian network model database for biomolecular structural dynamics*. Nucleic Acids Res, 2016. **44**(D1): p. D415-22.
246. Li, H., et al., *DynOmics: dynamics of structural proteome and beyond*. Nucleic Acids Res, 2017.
247. Folch, J., M. Lees, and G.H. Sloane Stanley, *A simple method for the isolation and purification of total lipides from animal tissues*. J Biol Chem, 1957. **226**(1): p. 497-509.
248. Box, G.E.P. and D.R. Cox, *An Analysis of Transformations*. Journal of the Royal Statistical Society. Series B (Methodological), 1964. **26**(2): p. 211-252.
249. Ballok, A.E., et al., *Epoxide-mediated differential packaging of Cif and other virulence factors into outer membrane vesicles*. J Bacteriol, 2014. **196**(20): p. 3633-42.
250. Bomberger, J.M., et al., *Long-distance delivery of bacterial virulence factors by Pseudomonas aeruginosa outer membrane vesicles*. PLoS Pathog, 2009. **5**(4): p. e1000382.
251. Smith, E.E., et al., *Genetic adaptation by Pseudomonas aeruginosa to the airways of cystic fibrosis patients*. Proc Natl Acad Sci U S A, 2006. **103**(22): p. 8487-92.
252. Traverse, C.C., et al., *Tangled bank of experimentally evolved Burkholderia biofilms reflects selection during chronic infections*. Proc Natl Acad Sci U S A, 2013. **110**(3): p. E250-9.
253. Ousingsawat, J., et al., *Ca(2+) signals, cell membrane disintegration, and activation of TMEM16F during necroptosis*. Cell Mol Life Sci, 2017. **74**(1): p. 173-181.
254. Redmann, M., et al., *Inhibition of autophagy with bafilomycin and chloroquine decreases mitochondrial quality and bioenergetic function in primary neurons*. Redox Biol, 2017. **11**: p. 73-81.
255. Rai, G., et al., *Discovery of ML351, a Potent and Selective Inhibitor of Human 15-Lipoxygenase-1*, in *Probe Reports from the NIH Molecular Libraries Program*. 2010, National Center for Biotechnology Information (US): Bethesda (MD).
256. Yamanaka, K.e.a., *A novel fluorescent probe with high sensitivity and selective detection of lipid hydroperoxides in cells*. RSC Advances, 2012. **2**: p. 7894-7900.
257. Cozza, G., et al., *Glutathione peroxidase 4-catalyzed reduction of lipid hydroperoxides in membranes: The polar head of membrane phospholipids binds the enzyme and addresses the fatty acid hydroperoxide group toward the redox center*. Free Radic Biol Med, 2017. **112**: p. 1-11.
258. Kim, S.E., et al., *Ultrasml nanoparticles induce ferroptosis in nutrient-deprived cancer cells and suppress tumour growth*. Nat Nanotechnol, 2016. **11**(11): p. 977-985.
259. Poursaitidis, I., et al., *Oncogene-Selective Sensitivity to Synchronous Cell Death following Modulation of the Amino Acid Nutrient Cystine*. Cell Rep, 2017. **18**(11): p. 2547-2556.
260. Kuch, E.M., et al., *Differentially localized acyl-CoA synthetase 4 isoenzymes mediate the metabolic channeling of fatty acids towards phosphatidylinositol*. Biochim Biophys Acta, 2014. **1841**(2): p. 227-39.
261. Li, L.O., E.L. Klett, and R.A. Coleman, *Acyl-CoA synthesis, lipid metabolism and lipotoxicity*. Biochim Biophys Acta, 2010. **1801**(3): p. 246-51.

262. Thomas, J.P., et al., *Protective action of phospholipid hydroperoxide glutathione peroxidase against membrane-damaging lipid peroxidation. In situ reduction of phospholipid and cholesterol hydroperoxides.* J Biol Chem, 1990. **265**(1): p. 454-61.
263. Gaschler, M.M., et al., *FINO2 initiates ferroptosis through GPX4 inactivation and iron oxidation.* Nat Chem Biol, 2018. **14**(5): p. 507-515.
264. Marvig, R.L., et al., *Convergent evolution and adaptation of Pseudomonas aeruginosa within patients with cystic fibrosis.* Nat Genet, 2015. **47**(1): p. 57-64.
265. Folkesson, A., et al., *Adaptation of Pseudomonas aeruginosa to the cystic fibrosis airway: an evolutionary perspective.* Nat Rev Microbiol, 2012. **10**(12): p. 841-51.
266. Vincent, J.L., et al., *Sepsis in European intensive care units: results of the SOAP study.* Crit Care Med, 2006. **34**(2): p. 344-53.
267. Vincent, J.L., et al., *International study of the prevalence and outcomes of infection in intensive care units.* JAMA, 2009. **302**(21): p. 2323-9.
268. Davies, J.C. and D. Bilton, *Bugs, biofilms, and resistance in cystic fibrosis.* Respir Care, 2009. **54**(5): p. 628-40.
269. Hofmans, S., et al., *Novel Ferroptosis Inhibitors with Improved Potency and ADME Properties.* J Med Chem, 2016. **59**(5): p. 2041-53.
270. Distefano, A.M., et al., *Heat stress induces ferroptosis-like cell death in plants.* J Cell Biol, 2017. **216**(2): p. 463-476.
271. Silby, M.W., et al., *Pseudomonas genomes: diverse and adaptable.* FEMS Microbiol Rev, 2011. **35**(4): p. 652-80.
272. Frimmersdorf, E., et al., *How Pseudomonas aeruginosa adapts to various environments: a metabolomic approach.* Environ Microbiol, 2010. **12**(6): p. 1734-47.
273. Lyczak, J.B., C.L. Cannon, and G.B. Pier, *Establishment of Pseudomonas aeruginosa infection: lessons from a versatile opportunist.* Microbes Infect, 2000. **2**(9): p. 1051-60.
274. Hogardt, M. and J. Heesemann, *Microevolution of Pseudomonas aeruginosa to a chronic pathogen of the cystic fibrosis lung.* Curr Top Microbiol Immunol, 2013. **358**: p. 91-118.
275. Govan, J.R. and V. Deretic, *Microbial pathogenesis in cystic fibrosis: mucoid Pseudomonas aeruginosa and Burkholderia cepacia.* Microbiol Rev, 1996. **60**(3): p. 539-74.
276. Barth, A.L. and T.L. Pitt, *The high amino-acid content of sputum from cystic fibrosis patients promotes growth of auxotrophic Pseudomonas aeruginosa.* J Med Microbiol, 1996. **45**(2): p. 110-9.
277. Nguyen, D. and P.K. Singh, *Evolving stealth: Genetic adaptation of Pseudomonas aeruginosa during cystic fibrosis infections.* Proceedings of the National Academy of Sciences of the United States of America, 2006. **103**(22): p. 8305-8306.
278. Oliver, A., et al., *High frequency of hypermutable Pseudomonas aeruginosa in cystic fibrosis lung infection.* Science, 2000. **288**(5469): p. 1251-4.
279. Hogardt, M. and J. Heesemann, *Adaptation of Pseudomonas aeruginosa during persistence in the cystic fibrosis lung.* Int J Med Microbiol, 2010. **300**(8): p. 557-62.
280. Breidenstein, E.B., C. de la Fuente-Nunez, and R.E. Hancock, *Pseudomonas aeruginosa: all roads lead to resistance.* Trends Microbiol, 2011. **19**(8): p. 419-26.
281. Langton Hewer, S.C. and A.R. Smyth, *Antibiotic strategies for eradicating Pseudomonas aeruginosa in people with cystic fibrosis.* Cochrane Database Syst Rev, 2009(4): p. CD004197.

282. Reekmans, R., et al., *Old yellow enzyme interferes with Bax-induced NADPH loss and lipid peroxidation in yeast*. FEMS Yeast Res, 2005. **5**(8): p. 711-25.
283. Kissova, I., et al., *Lipid oxidation and autophagy in yeast*. Free Radic Biol Med, 2006. **41**(11): p. 1655-61.
284. Wonisch, W., et al., *Treatment of the budding yeast Saccharomyces cerevisiae with the lipid peroxidation product 4-HNE provokes a temporary cell cycle arrest in G1 phase*. Free Radic Biol Med, 1998. **25**(6): p. 682-7.
285. Evans, M.V., et al., *Toxicity of linoleic acid hydroperoxide to Saccharomyces cerevisiae: involvement of a respiration-related process for maximal sensitivity and adaptive response*. J Bacteriol, 1998. **180**(3): p. 483-90.
286. Priault, M., et al., *Bax-induced cell death in yeast depends on mitochondrial lipid oxidation*. Eur J Biochem, 2002. **269**(22): p. 5440-50.
287. Serhan, C.N. and E. Oliw, *Unorthodox routes to prostanoid formation: new twists in cyclooxygenase-initiated pathways*. J Clin Invest, 2001. **107**(12): p. 1481-9.
288. Cohen, T.S. and A. Prince, *Cystic fibrosis: a mucosal immunodeficiency syndrome*. Nat Med, 2012. **18**(4): p. 509-19.
289. Schroeder, M., B.D. Brooks, and A.E. Brooks, *The Complex Relationship between Virulence and Antibiotic Resistance*. Genes, 2017. **8**(1).